NORTHWESTERN UNIVERSITY

A DISSERTATION

The Ovary: Physical and Biochemical Properties Controlling Folliculogenesis

SUBMITTED TO THE GRADUATE SCHOOL

IN PARTIAL FULFILLMENT OF THE REQUIREMENTS

for the degree

DOCTOR OF PHILOSOPHY

Field of Life Sciences

By

Nathaniel Henning

EVANSTON, IL

June 2022

Abstract

The Ovary: Physical and Biochemical Properties Controlling Folliculogenesis

Nathaniel Henning

A prominent cause of premature ovarian insufficiency (POI) is gonadotoxic cancer therapies, which deplete the ovarian reserve of follicles, oocytes, and hormone-producing cells. Current fertility preservation methods include the removal and cryopreservation of ovarian tissue prior to gonadotoxic treatment. This cryopreserved tissue can be transplanted back and has been found to restore fertility in 20-40% of cases and restore ovarian hormone production for 2 months to 12 years. Our goal is to understand the physical properties and biochemical components of the ovarian microenvironment and their role in maintaining the ovarian reserve to restore fertility and ovarian hormones for patients using a bioprosthetic ovary. The extracellular matrix (ECM) is a network of proteins providing physical and biochemical support to organs. This thesis characterizes spatial maps of the porcine matrisome (ECM and ECM-associated proteins) identifying undiscovered proteins and potential modulators of follicle activation, mapping of the physical properties of ovaries, and the development of tools to dissect the mechanistic relationship between the matrisome and follicle activation.

First, we mapped the composition of the matrisome of porcine ovaries through the cortical compartment, where quiescent follicles reside and the medullary compartment, where the larger follicles grow and mature. To do this we sliced the ovaries, uniformly in two anatomical planes, enriched for matrisome proteins and performed bottom-up shotgun proteomic analyses. We identified 42 matrisome proteins that were significantly differentially expressed across depths, and 11 matrisome proteins that have not been identified in previous ovarian protein analyses. We validated these data for nine proteins and confirmed compartmental differences with a second

processing method. Here we describe a processing and proteomic analysis pipeline that revealed spatial differences and matrisome protein candidates that may influence folliculogenesis.

Second, using atomic force microscopy (AFM), we determined that the bovine ovarian cortex was significantly more rigid than the medulla, with a rigidity gradient showing a gradual decrease in rigidity across compartments. To determine if this difference in rigidity was maintained in isolated matrisome proteins from bovine ovarian compartments, we cast, and 3D printed hydrogels created from decellularized bovine ovarian cortex and medulla slices. The 3D printed scaffolds from the cortex were more rigid than those derived from the medulla. To expand our bioengineering toolbox that will aide in the investigation of how biochemical and physical cues may affect folliculogenesis, we sought to confirm the concentration of matrisome proteins in bovine ovarian compartments. The matrisome proteins, COL1, FN, EMILIN1 and AGRN were more abundant in the bovine ovarian cortex than the medulla. Whereas VTN was more abundant in the medulla than the cortex and COL4 was present in similar amounts within both compartments. Finally, we removed proteins of interest, EMILIN1 and AGRN, from decellularized bovine ovarian cortex materials and confirmed that this specifically depleted these proteins without affecting the rigidity of cast or 3D printed hydrogels. Culturing human mesenchymal stem cells (hMSCs) on EMILIN1 depleted materials we saw no change in proliferation or cell survival. However, we saw a significant difference in gene expression of candidate genes downstream of TGFβ that was reversed upon supplementation with EMILIN1. Taken together our results indicate the existence of a rigidity gradient in the bovine ovary, that this rigidity gradient is maintained in resulting engineered materials strongly implicating a role for matrisome proteins in contributing to the physical properties of the bovine ovary. By establishing additional engineering tools, we will continue to explore mechanisms behind matrisome-follicle interactions.

This work defines the physical and biochemical properties of the ovarian microenvironment across compartments and develops tools to further investigate the role of specific proteins in modulating follicle quiescence, follicle activation, and the progression of folliculogenesis. Additionally, these results feed our underlying knowledge and provides new tools for investigating mechanistic relationships towards creating an effective next generation bioprosthetic ovary by controlling primordial follicle activation to improves bioprosthetic longevity.

To my family, John, Cindy, Carole, Tim, Corinne, and Murphy. To Mariya. To my friends Charlene and Andy, Hana, Ariel, and Marquis. For your support, laughs, meals, games, and all the memories.

Acknowledgements

In 2007, I was sent a letter from the University I was attending telling me that I wouldn't be invited to return for the next Fall semester. I'd been struggling with depression, and instead after another aborted attempt at community college entered the workforce at Ecolab as a customer service representative. Later I would be promoted into a logistics role and hit the ceiling because I lacked a college degree. Initially, I did full-time online classes while working full-time. After receiving my associates degree and with a great deal of trepidation I decided to leave my job for full-time in person school so I could get my four-year degree at Hamline University. I was fortunate to find mentors like Dr. Rita Majerle, Dr. Nevin Young, Dr. Jodi Goldberg, and Dr. Martinez-Vaz who imbued in me a love of research and pushed me first to pursue an honors thesis and then to pursue graduate school to get my PhD. I wouldn't be here writing this thesis without them and the many hours I spent with them in the classroom, the lab, or in their offices after hours. Now I'm here at a top university ready to receive my PhD. It's been a long road since I was told not to come back.

This work couldn't have been completed without the support of my family, friends, and co-workers. First though, I want to thank Dr. Monica Laronda, whose guidance, patience, empathy, and reminders to be consistent are memories and lessons that I will always cherish. The supportive and enriching environment that you've created has been extremely important to my growth as a scientist. I will miss meetings that went far over their scheduled time where we outlined papers, grants, and years of research ideas. I left each of those meetings a better scientist and I don't think I'll forget about scale bars ever again. Your enthusiasm as well for every research idea, even wild ones like spatially mapping the matrisome of the ovary is something that was always appreciated.

Thank you to the members of the Laronda Lab both current and former for being intelligent, fun, and supportive community members through the roller coaster that is a PhD and research. Kelly Even (never Odd) thank you for teaching me to be a better lab steward and for providing years of company, jokes, and the drinks. Sofia Petukhova, for always asking hard questions, for years of assistance, and for the nerdy conversation Grace Schwartz, you provided endless support, guidance, and occasionally a sharp kick in the butt that I needed during the second half of my lab career. To my lab children, Hana and Elizabeth, thank you for your company, your troubleshooting, your cat watching, all the non-science and science chats, and your patience with somebody who didn't really have a way with words. Hana, I'm sorry you always dealt with the sprawl, and I could never have hoped to have a better person to share a workspace with or a better friend to make along the way. I never thought I'd have such wonderful lab-mates that I'd invite several of them to my wedding (sorry to those who joined after). Know that I will miss all of you dearly.

To my family, I owe you a debt that can never be repaid. Thank you to my Mom and Dad for your endless reservoirs of patience both during graduate school and before, for instilling me with my love of science, for saving my life. None of this would have been possible at all without your support. To my siblings, thank you for the times good and bad, for asking questions about my work, for being interested and for being there all the times I needed it most. To my grandmother, Nana you provided more to help me make it through my undergraduate degree than anyone ever could. Your long phone calls, your emotional support, helping me when times were hard, and making sure that no matter what I took time for myself and to try to enjoy the journey even when it was challenging. A simple acknowledgment is not enough but thank you.

For Charlene and Andy, thank you for everything but most definitely the daily memes, the support, and making sure I always was taking care of myself whether that was sleeping, drinking water, or any number of other basic things we take for granted. It will never be forgotten, and I can never thank you enough for it.

Finally, Mariya there is no acknowledgment that could summarize or suffice.

List of Abbreviations

2D – Two-dimensional

3D – Three-dimensional

3DP – Three-dimensional printing

AFM – Atomic Force Microscopy

AGC - automatic gain control

AGRN – Agrin

ANOVA – Analysis of Variance

BIRC - baculoviral inhibitors of apoptosis repeat containing apoptosis inhibitors

BSA – Bovine Serum Albumin

COL1 – Collagen 1

COL1A2 – Collagen 1 alpha 2

COL4 – Collagen 4

COL4A2 – Collagen 4 alpha 2

CTK – collagenase type IV, trypsin, and knockout serum replacement

DAG1 - α -Dystroglycan

dECM – decellularized Extracellular Matrix

DSD – Differences in Sexual Development

ECM – Extracellular Matrix

ECM1 – Extracellular Matrix 1

EGF – Epidermal Growth Factor

EMILIN1 – Elastin microfibrillar interface protein 1

FBS – Fetal Bovine Serum

FN1 – Fibronectin

FRESH – Freeform Reversible Embedding of Suspended Hydrogels

FSH – Follicle Stimulating Hormone

FST - Follistatin

FT-ICR – Fourier-transform ion cyclotron resonance

HCD – higher-energy collisional dissociation

HCl – Hydrochloric Acid

H&E - Hematoxylin and eosin

hMSC – Human Mesenchymal Stemcells

IF - Immunofluorescence

IHC – Immunohistochemistry

iPCR – immono polymerase chain reaction

LATS1/2 - Large Tumor Suppressor Kinase 1/2

LC-MS/MS – Liquid chromatography–mass spectrometry

LH – Luteinizing Hormone

>LIF – Leukemia inhibitory factor

LS-Means – Least Square Means

MAPF – Magnet Assisted Protein Filtration

MDF – Modified Davidson's Fixative

MST1/2 - mammalian STE20-like protein kinase 1/2

mTORC - mammalian target of rapamycin complex

OSE – Ovarian Surface Epithelium

OTC – Ovarian Tissue Cryopreservation

PBS – Phosphate Buffered Saline

PCOS – Polycystic Ovarian Syndrome

PI3K – Phosphoinositide 3-kinases

PLGA - poly (lactic-co-glycolic acid)

POI – Premature Ovarian Insufficiency

PTN – Pleiotrophin

qPCR – quantitative polymerase chain reaction

ROCK – Rho-associated protein kinase

SAV1 - Protein salvador homolog 1

SDS – Sodium Dodecyl Sulfate

SEM - Scanning Electron Microscopy

TAZ – transcriptional coactivator with PDZ-binding motif

TEAD - TEA/ATTS DNA binding domain

TGFB – Transforming Growth Factor Beta

VTN – Vitronectin

YAP - yes-associated protein

ZP3 – Zona Pellucida 3

Table of Contents

List of Tables

List of Figures

Chapter 1

General Introduction: Building an Ovary using Tissue-Specific Microenvironments

Significance

Ovarian follicles are the spherical cell aggregates that contain the immature oocyte/gamete and supportive hormone-producing cells. Quiescent primordial follicles make up the ovarian reserve, which marks out the overall fertility lifespan of an individual with ovaries. When the ovary is exposed to gonadotoxic treatments such as chemotherapy or radiation, the number of ovarian follicles that make up this reserve, or source of eggs and ovarian hormones, is depleted, and this depletion accelerates the onset of menopause. Premature ovarian insufficiency (POI), or early menopause, can occur as a result of numerous genetic, autoimmune, iatrogenic (such as chemotherapeutics), or idiopathic causes (1). Fertility preservation is an option for those with a known treatment or progressive disorder that may disrupt normal ovarian function and is a key quality-of-life concern for many cancer patients and survivors (2). In addition, 55% of surveyed patients with differences in sexual development (DSD) or intersex, or those with dysgenetic gonads, who can acquire POI, reported their desire to have biological children and that they wished they had explored fertility options (3). One option for fertility preservation in adults, and the only option for prepubertal children with ovaries, is ovarian tissue cryopreservation (OTC). In addition to considerations for fertility loss, the loss of ovarian hormones has detrimental systemic effects, and multiple cohorts have identified a life expectancy two years shorter in women with POI from various comorbidities that effect their cardiovascular system, metabolism, bone turnover, ability to heal wounds, and cognitive function (4,5).

There are more than 11,000 children between the ages of 0 to 14 who are diagnosed with cancer each year (1,2). Advances in treatments have dramatically increased five-year survival rates with seven patients out of eight surviving five or more years (1,2). However, current options to restore fertility and hormone function for these patients are limited to OTC followed by the auto-

transplantation of preserved tissue into the patient after treatment. To date, over 140 livebirths have been reported from transplantation of OTC tissue following eradication and recovery from cancer (6, 7, 8). However, only 20-40% of patients with transplants have live offspring and hormone restoration is highly variable, ranging from 2 months to 12 years with an average of 2-5 years of hormone restoration (9,10, 11). In addition, transplantation of this tissue is contraindicated in those with a moderate-to-high risk of metastatic or systemic disease within the ovaries due to the possibility of reintroducing disease via transplanted tissue (12). Addressing these concerns and improving upon current transplantation outcomes will require a structure that supports isolated ovarian follicles, free of cancer cells.

Current follicle isolation methods leverage both enzymatic and mechanical isolation. Processing steps that include a series of washing have been shown to remove cancer cells from primordial follicle preparations in murine ovaries that were seeded with breast cancer cells and in human ovaries from leukemia patients (13,14). Because oocytes have not yet been made from human stem cells, the gametes will need to be isolated from the patient to produce biological offspring. This transplant would be integrated into a patient care plan to enable full restoration of hormones and fertility in patients for decades. This transplant would feature an architectural design that supports isolated follicles through growth and ovulation, which was established for a murine bioprosthetic ovary transplant (15).

Further, recent research in tissue engineering and regenerative medicine has elucidated the importance of the matrisome. The matrisome, effectively the skeleton of an organ, provides physical and biochemical cues that drive important biological processes such as cellular differentiation, proliferation, migration, and cellular morphology. Leveraging the matrisome to control these and other tissue-specific processes will be key to developing transplantable

bioprosthetics. In the ovary, the physical and biological properties of the matrisome have been implicated in controlling the important processes of follicle quiescence and folliculogenesis. Improving upon the first iteration of a murine bioprosthetic ovary through investigations of how compartmentalization, biochemical and physical cues influence hormone production, follicle activation, and egg quality will inform an improved design and utilization for restorative therapies in the clinic.

Overview of the Ovary: Structure and Function

An Overview of Mammalian Folliculogenesis

The ovarian follicle is the fundamental functional unit of the ovary. Each ovarian follicle consists of the oocyte and its supporting steroidogenic somatic cells (granulosa cells and theca cells). The population of interest for this thesis is the quiescent primordial follicles which make up the ovarian reserve which is effectively the potential of the ovary to provide systemic hormone support and fertilizable eggs in a monthly cycle (3). Primordial follicles contain an oocyte, arrested in the first prophase of meiosis, which is surrounded by a single layer of flattened squamous granulosa cells. These primordial follicles are recruited and activated in a cyclical fashion to undergo the maturation process of folliculogenesis, a complex process regulated by endocrine, paracrine, autocrine, and juxtacrine factors, as well as cell-matrix interactions (31). The final fate of this cohort of activated follicles is either atresia or ovulation (31). Though cohorts of primordial follicles are recruited in waves the mechanism behind follicle activation is poorly understood though many of the downstream pathways after activation have been elucidated and several of these will be discussed later in this chapter (16-22). After activation, primordial follicles transition to the primary stage, which is characterized by granulosa cells undergoing a morphological change from squamous to cuboidal (23). As granulosa cells undergo proliferation and the oocyte grows

the primary follicle transitions to a secondary follicle, which is characterized by multiple layers of granulosa cells surrounding the oocyte. A basement membrane forms around the outermost layer of granulosa cells and an additional layer of support cells called theca cells surround the follicle outside of the basement membrane. These thecal cells will then differentiate further into two layers, the theca externa (connective and supportive tissue) and interna (androgen secreting). These layers have ultrastructural features, which allow them to function as the source of androgens that granulosa cells use to produce estrogens (24). The first three stages of folliculogenesis are considered gonadotropin independent and instead rely on complex networks of communication between the oocyte, its supporting cells, somatic cells, and the microenvironment (25,26). After the pubertal transition, and the onset of the production of follicle stimulating hormone (FSH) by the pituitary, gonadotropin dependent follicles beyond the first stages being to appear. As the follicle continues to develop, a fluid-cavity known as the antrum is formed and in addition to further oocyte growth and support cell proliferation the granulosa cells differentiate into two distinct populations, mural granulosa cells, responsible for steroidogenesis and cumulus cells, which maintain contact with the oocyte itself (26). At this stage antral follicles are dependent on FSH and luteinizing hormone (LH) for
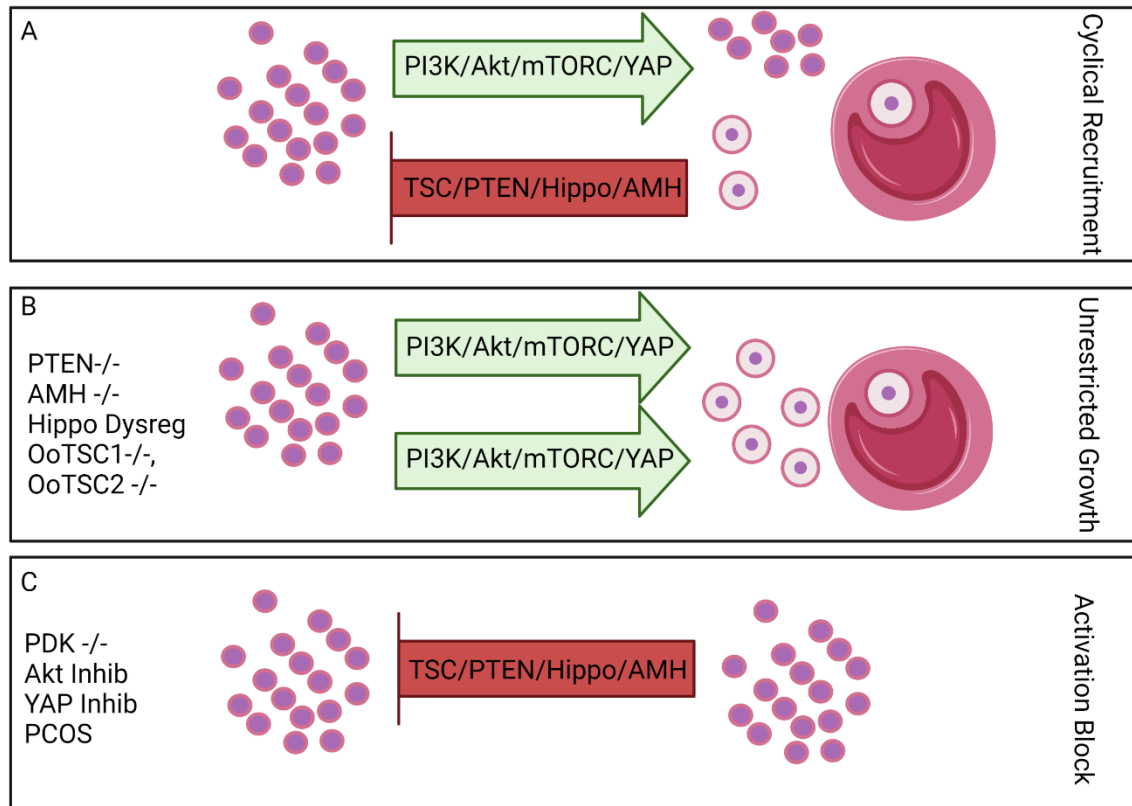
Figure 1. Activation, maintenance cues and dysregulation of follicle activation. A) PI3K/AKT and mTORC pathway activation, which promotes follicle activation and is regulated by PTEN, Hippo, and the Tsc1/2 pathways. Activated growing follicles also secrete AMH which acts to suppress follicle activation. A balance of activating and maintenance signals result in cyclic recruitment of primordial follicles throughout the reproductive lifespan until menopause B) Disruption of regulatory machinery leads to the unrestrained activation of the PI3K/AKT/mTORC pathways. The mass activation of primordial follicles results in the rapid depletion of the ovarian reserve and onset of premature ovarian insufficiency. C) Blocking activation signals through inhibitors, genetic models, or pathology results in no activation signal, which results in lack of follicle activation, growth, and development resulting in anovulation, infertility, and follicle atresia.

continued growth and maturation towards ovulation (25,26). The FSH receptor drives granulosa cell survival and proliferation, estradiol production, and LH receptor expression (26,27). Under the influence of LH the oocytes in antral follicles complete the first meiotic cell division and then arrest at the second meiotic phase. Follicles at this stage are referred to as an antral or Graafian follicle, which if chosen as the dominant follicle and will be undergo ovulation after LH stimulation, releasing the oocyte into the pelvic cavity for collection by the fallopian tube. Most follicles do not reach this stage and instead undergo the process of atresia during which the follicle is degenerated (28,29, 30).

Regulation of folliculogenesis is complex, and various factors will be detailed blow. In brief, follicle development is regulated by many extrinsic signals including endocrine and paracrine factors and there is a growing body of evidence that supports the involvement of the extracellular matrix both of the ovarian follicle itself and the ovarian microenvironment (31,32, 33, 34, 35). Signaling between the oocytes and its supporting cells (theca and granulosa cells) are essential for proper folliculogenesis to occur as gap junctions between granulosa cells and the oocyte allow for the transport of factors between these two cell types (36, 37, 38, 39, 40). Finally, the ECM composition surrounding these follicular compartments and also the microenvironment the follicle exists in has been implicated in regulating the function of these cells via cell-matrix interactions. Therefore, it is important to understand ovarian structure and the changes in the ovarian microenvironment and these cell-matrix interactions in order to understand the maintenance of the ovarian reserve, follicle activation, and the process of folliculogenesis.

The Ovary is Functionally Compartmentalized

Looking at the ovary as a whole, it is functionally compartmentalized into two major sub-anatomical compartments. The outermost compartment with a greater fibrous matrisome density

is the cortical region, also referred to as the cortex (**Figure 2**) (41,42). This region houses quiescent primordial follicles which make up the bank of follicles that produce cyclical hormones and eggs known as the ovarian reserve mentioned above. Both hormone production and the number of follicles in the reserve are controlled via the regulated activation of primordial follicles that grow and mature through the various stages of folliculogenesis. Further, it is the cortex of the ovary that is cryopreserved for future use because it contains this bank of potential eggs, the ovarian reserve, and is more resistant to potential damage during cryopreservation/freezing. In a healthy ovary, primordial follicles are cyclically activated to undergo folliculogenesis until the onset of menopause, when folliculogenesis and the hormones and eggs that are released ceases. Folliculogenesis requires significant tissue remodeling, and the medullary region, also referred to simply as the medulla, (where growing follicles reside) is less dense than the cortex (31). Once activated, the primordial follicles grow to >600-fold their original size, recruiting additional somatic cell differentiation and vessels that support this growth and provide an outlet for systemic distribution of additional hormones (4). Ovulation occurs through a process of ECM degradation and pressurized expulsion of the egg, and the remaining follicular cells form a temporary progesterone-producing gland that dissolves into a fibrous scar tissue. Each of these crucial follicular events is supported by, or remodels, the surrounding microenvironment.

Ovarian stromal cells, which have a similar morphology to fibroblasts, make up the connective tissue throughout the ovary and around follicles (298, 299). Stromal cells have been

(A)
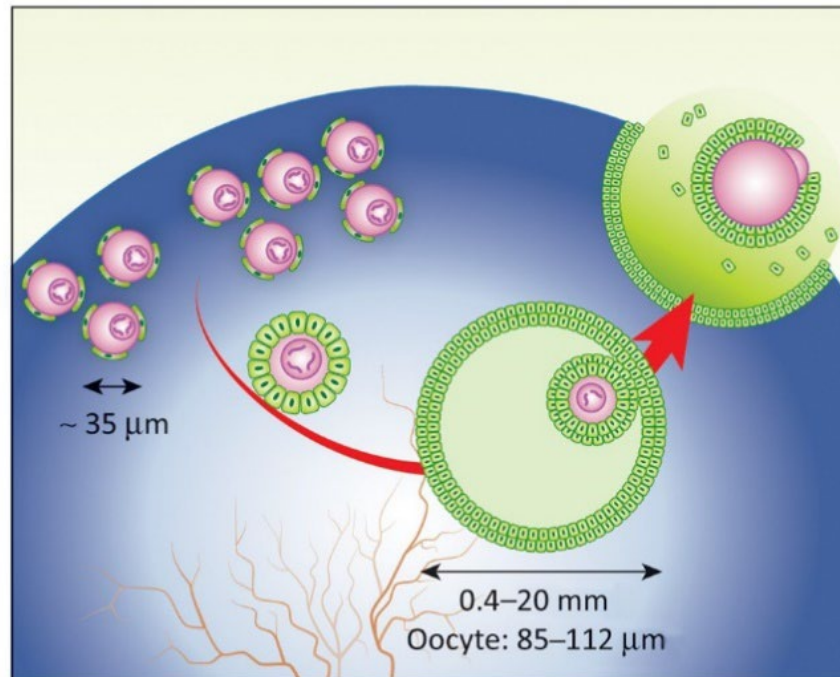
Figure 2. Schematic of Ovarian Compartmentalization. Primordial follicles (left, 35 μm) remain quiescent within the ovarian cortex until they are recruited to grow. Follicles grow, accumulate antral fluid, and recruit vessels within the ovarian medulla until they ovulate through the surface. The ovary contains a gradient of denser to less-dense matrisome as represented by the blue gradient.

implicated in having a role in folliculogenesis, primordial follicle activation and the differentiation of theca cells (298,299). Stromal cell differentiation into theca cells appears to be driven by insulin-like growth factor (IGF-1), kit ligand (KL) and basic fibroblastic growth factor (bFGF) activity (300, 301, 302). In primordial follicle activation, bone morphogenetic proteins 4 and 7 (BMP-4 and -7), secreted by stromal and/or theca cells have been identified as positive regulators of this process and the primordial-to-primary transition (303,304). Compartmentalization of the ovary can also be seen in the morphology of stromal cells (298,299). Stromal cells located in the cortex are organized parallel to the surface and have a rounded morphology (298,299). Stromal cells in the medulla, often referred to as interstitial or luteinized cells are less organized, have an elongated structure and are believed to differentiate into theca cells (300,301, 302). Single-cell analysis of human ovarian ovaries shows differential expression of genes in stromal cells across compartments and has also identified other distinct populations across ovarian compartments, specifically immune cells, endothelial cells, perivascular cells (305).

Like human ovaries, bovine and porcine ovaries have distinct cortical and medullary regions, as visualized by gross pathology or using scanning electron microscopy (SEM) (41,43). Organized collagen bundles make up the tightly packed, uniform pore walls of the cortex. The medulla has larger pores made by the larger ovarian follicles and vessels, as well as more-permeable walls that include fibronectin fibers among less-uniform collagen bundles (41). The density of collagen fibers is also greater around primordial follicles than around growing follicles in murine ovaries (42). This shows that beyond cellular populations there are compositional changes in the ECM across compartments, contributions to changes to physical properties or the changes to the physical properties across these compartments and the contribution of these differences to biological

processes of interest such as follicle activation and folliculogenesis have remained unknown and the investigation of these properties is a central theme of this thesis.

The Matrisome

The matrisome, ECM and ECM-associated proteins, is composed of >1000 proteins and includes core matrisome (e.g., collagen subunits, proteoglycans, and glycoproteins), ECM-modifying enzymes, ECM-binding proteins, ECM-associated proteins, and secreted factors (e.g., growth factors that are known to bind to the ECM, as well as receptors and modifying enzymes), as defined by The Matrisome Project (44) forms the ultrastructure of organs.

The matrisome and its constituents make up a complex three-dimensional meshwork of proteins effectively forming the 'skeleton' of an organ. These proteins are secreted by resident cells and although they were previously believed to largely provide structural support to the matrisome, they are now strongly implicated in tissue morphogenesis, development and homeostasis by modulating cell survival, proliferation, differentiation, and stem cell state (45,46). The matrisome itself is also tissue-specific with the composition of the matrisome undergoing extensive remodeling in cases of pathology and specific ECM phenotypes configured to healthy tissues to maintain homeostasis (47-65). Mutations to matrisome genes have been shown to cause musculoskeletal, cardio-vascular, renal, ocular, and skin diseases (306). Dysregulation of matrisome genes resulting in excessive deposition or, in the case of increased expression of genes that remodel or degrade the matrisome, lead to pathologies such as fibrosis or osteoarthritis (306). Studies in cancer have shown that the matrisome plays a functional role in tumor progression and dissemination and that increased deposition, complexity, and composition are indicators used by pathologists have been used to indicate poor prognosis in patients (306).

SEM images of different organ systems show different ultrastructure in decellularized organs with pore size and ECM organization being tissue-specific (41). This same group showed that human mesenchymal stem cells (hMSCs) seeded onto "tissue papers" derived from the decellularized extracellular matrix (dECM) of different organ systems have differing mechanical properties, microstructure, and cellular responses to materials derived from different organ systems (66). Experiments examining gene expression used microarray analyses of human bone marrow mesenchymal stem cells (hBMMSCs) seeded onto dECM bioinks derived from porcine live, heart and skin (307). Whole transcriptome analysis revealed tissue-specific alterations in gene expression patterns for hBMMSCs (307). This is only two examples of work that has now been done across multiple tissues and organ systems all indicating that tissue-specificity of the matrisome is necessary to preserve cell specificity and function (67-69). The matrisome is in a state of dynamic reciprocity with cells by providing biochemical and physical cues that modify cell signaling and behavior as cells transform the matrisome by assembly and disassembly. Recent research has shown that replicating the microenvironment including its spatial distribution, via 3D scaffolds, results in better outcomes by providing tissue-specific signaling cues for cell attachment, differentiation, vascularization, and function across multiple tissues (70).

Experiments on ECM composition in the ovary have been relatively limited with most research leveraging IHC analysis that focuses on the basement membrane (132-135, 189, 308). Heeren, et al 2015 examined the development of the basement membrane during human gametogenesis and folliculogenesis finding that ECM-molecular niche compartmentalizes the female gonads from the time of germ cell colonization until adulthood focusing on the distribution of collagen IV, laminin and fibronectin (308). They found that (cortical) mesenchymal compartment are encapsulated by a basement membrane of collagen IV and laminin, but not fibronectin at week 10 of gestation

while the follicular basement membrane in adults at primary and secondary follicles was composed of collagen IV, laminin and to a lesser extent fibronectin (308). Significant work in bovine ovaries has examined changes to the matrisome across folliculogenesis in a bovine model, focusing specifically on changes to the matrix that develops between granulosa cells (focimatrix, abbreviated from focal intraepithelial matrix) and of the follicular basal lamina in ovulating bovine ovarian follicles (132-135, 189). These studies found stage-specific differences in ECM composition, specifically nidogen-1 and perlecan which increased substantially as follicles enlarged to a size capable of ovulating (132-145, 189). These IHC studies indicate the possibility of follicle-specific matrisome signatures and when taken together with the body of research in other organ systems shows the importance of an organ's specific microenvironment and matrisome composition to normal biological processes of interest an area which until recently had not been explored in great depth in the ovary and will be the focus of **Chapters 2** and **3** of this dissertation.

Biochemical Cues and Physical Cues

Matrisome biochemical cues facilitate the translation of the extracellular environment into inner cellular signaling via cell surface receptors (115-119). Additionally, matrisome physical cues are converted into intracellular signals via mechanotransduction, in which stressors elicit a cellular response such as adhesion, proliferation, and differentiation in a tissue-specific fashion (120-122). Table 1 summarizes the physical properties (as measured by Young's modulus) of multiple tissues and shows how these properties vary quite widely across the human body. External physical signals require mechanosensing units, such as the cytoplasmic complex integrin, extracellular components, and intracellular components (123). In addition, the interstitial cells, including stromal and endothelial cells, are important for the influential microenvironment, especially during the later stages of follicular growth and ovulation (298,299). The following sections focus on these

two significant microenvironment factors, biochemical and physical cues, that could influence the longevity of a bioprosthetic ovary (via the rate of primordial follicle activation).

Biochemical cues include binding sites along fibrous proteins, or matrisome-associated proteins, that bind to transmembrane complexes and translate the extracellular environment into responses within the cell (124-128). Binding to ligands allows the ECM to function as a "reservoir" or "sink" creating concentration gradients of growth factors, or "morphogens," that can determine cell fate based on availability (50). Research has shown that the ECM can specifically create concentration gradients of bone morphogenetic proteins (BMPs), fibroblast growth factors (FGFs), hedgehogs (HHs), and Wnts (Hynes 2009; Rozario and DeSimone 2010). Further, research has shown that this same property ECM can affect hormone availability and responsiveness by sequestering, trafficking, or presenting factors including growth factors, androgens, and estrogens via sequestration of sex hormone-binding globulin in reproductive tissues (82). The ECM also plays a role in ligand maturation, specifically the conversion of pro-TGF-β to mature and biochemically active TGF-β (309). Maturation of TGF-β occurs after MMP-dependent proteolysis releases

Tissue	Physical Properties	ECM Proteins	Function	Ovarian Mapping	References
Intestine	2.6-2.9kPa	Collagens I, III, IV, V, VI, VII; Laminin	Tensile Strength to tissues	Collagen 1 increased in cortex, Collagen 4 uniform throughout	87, 88, 89
		Heparin, Heparan Sulfate, Chondroitin Sulfare, Hyaluronic Acid	Modulation of enzyme activity, ECM organization, and assembly	Hyaluronic Acid increased in cortex compared to medulla	

Bone	25-40kPa (Osteoid Matrix)	Collagen I	Primary structural ECM, overall bone strength, durability, regulation of fibrillogenesis	Collagen 1 increased in cortex, primary structural collagen of the ovary	90-95
	1.3-7.8GPa (cancellous)	DCN	Promotes collagen I fibrillogenesis, promotes bone formation	Detected in proteomics screen, higher in cortex than medulla	
	12-20GPa (cortical)	Biglycan	Promotes collagen I fibrillogenesis, promotes bone formation	Detected in proteomics screen, no significant patterning between compartments	
Brain	0.1-1kPa	Laminins	Basal lamina, expansion, proliferation, and differentiation of NSCs	Multiple laminins mapped, Laminin A/C higher in cortex than medulla, major components of basal lamina	91, 96
	130Pa (white matter)	AGRN	Laminin network stabilization	Increased in cortex, involved in Hippo kinase cascade	
	70Pa (grey matter)	COLIV	Major component of basal lamina at NMJs	COLIV expressed evenly throughout cortex and medulla, major component of basement membranes	
HMEC	N/A	Fibronectin	Cell Adhesion	FN1 increased in medulla	97

Liver	100-200kPa (tensile) 1-3.5MPa (compression)	Collagen, Biglycan, laminin, Vitronectin	Sequestration of cytokines, stress induced remodeling	Collagen 1 high in cortex, laminin increased in cortex, VTN increased in medulla	98, 99
Pancreas	0.14MPa	FGF-1, Heaprin	Cell proliferation, maintenance, insulin production	FGF-1, Heparin detected in ovarian proteomics but no discernible patterning	98, 100
Ovary	N/A	**TGFβ**	**ECM formation and remodeling**	**TGFβ increased in Cortex**	**101, 102, 103**
		Collagen, Elastin, FBN1, Emilin1, GAGs	**ECM is age dependent: ex. Collagen levels increase with age, FBN1 decreases after menopause but is constant prior**	**Collagen 1, EMILIN 1 both identified as higher in the Cortex.**	
		TGFβ, STRAP	**Follicle Development**	**TGFβ increased in Cortex**	
		TGFβ	**Follicle Quiescence**	**TGFβ increased in cortex**	
Heart	10-12MPa	CCN2	Infarction reduction, attenuates ECM remodeling	Not detected in proteomics screen, important downstream effector of Hippo promotes primordial follicle activation	104-107
		Tenascin-C	Reduces inflammation	Detected, no specific patterning between compartments	

Tissue	Physical Property	Matrisome Proteins	Influence on Cellular Behavior	Potential Location	Reference
		Collagens	Structural component, pro-inflammatory in heart during infarction	Collagen 1 significantly higher in cortex, multiple other collagens detected including IV, VI, III	
Lung	1.9kPa	Collagens I, III, V; Laminin A/C; ECM1	Quantification of matrisome in the Lung	Collagen 1, Laminin A/C, and ECM1 increased in cortex	108
Kidney	4.1 Mpa	EMILIN1, FBN1	ECM Anchoring, HUVEC proliferation and migration	EMILIN1, FBN1 increased in cortex over medulla	109, 110, 111
		Collagens, AGRN, Perlecan	ECM increases during Fibrosis, structural proteins	AGRN, Perlecan Collagen 1 increased in cortex; other collagens vary (IV same in both compartments)	
Muscle	8-17kPa	Laminin, Collagen, Fibronectin	ECM and Integrin clustering	Laminin, some collagens, and FN1 increased in the cortex over medulla	112, 113,114
	30-50kPa (skeletal)	COL VI	Functional integrity of Muscles	COL VI detected, but no significant pattern across compartments	

Table 1. Biochemical and Physical Properties of Tissues, the Influence of Cellular Behavior, and Potential Locations of Matrisome Proteins in the Ovary. N/A, not available.

pro- TGF-β making it accessible or through alterations mechanical tension of tissues (309). ECM components enhance the binding affinity between receptors and their ligands. An example of this being the heparan sulfate proteoglycan, which binds to various growth factors and facilitates interactions between ligands and their receptors (310). Likewise, betaglycan (TGF-β type III receptor), an integral membrane proteoglycan, binds to TGF-β and presents it to the core type II receptor (311). In regenerative medicine applications, the inclusion of tissue- and compartment-specific matrisome with the appropriate biochemical cues within an engineered microenvironment can also induce metalloproteinases (MMPs) and tissue inhibitors of metalloproteinases, which regulate the activation and follicle growth and ovulation (130,131). Findings in cat ovaries have identified links between ECM enzymes and MMPs, specifically by stimulating the activity of MMP9 via high doses of retinoic acid, activity leads to increased rates of follicle activation (34). Additionally, significant immunohistochemical (IHC) staining work done in multiple species has found ECM signatures of follicles that are stage specific (132-135). As an example of this Irving-Rodgers, et al showed in bovine ovaries that Perlecan is localized to the basal lamina, specialized sheets of ECM that influence cellular behavior and form a selectively permeable barrier to soluble molecules, of primordial, primary, preantral, antral, and atretic follicles (132-135).

Physical cues are both intracellularly generated and externally applied forces, and, like biochemical cues, they have a broad impact on cell behavior (e.g., growth, differentiation, and function) (129, 137, 138). Physical properties of the matrisome include its rigidity, density, porosity, insolubility and topography (spatial arrangement and orientation) which are all properties essential for supporting tissue structure and integrity, and for its role in migration and cell anchorage. These signals require mechanosensing units, which include cytoplasmic complexes such as integrins, extracellular components such as ECM cell adhesion molecules, and intracellular

components including the cytoskeleton (139). Stiff matrices induce integrin clustering, robust focal adhesions, Rho and MAP kinase activation, leading to increased proliferation and contractility (312). Specifically, the ECM transduces information via cell surface processes, stress of cellular membranes, stretch-sensitive ion channels, surface receptors, changes in biopolymers, extracellular fluid pressure, and tissue-dependent enzymes or proteins at the cell surface (140-145). Mechanosensitive proteins change conformation in response to these physical cues, leading to alterations in binding affinities and other downstream effects (such as phosphorylation) (141). It is important to understand this and then also the dynamic reciprocity relationship that cells (and follicles) have with their environment, which includes highly dynamic ECM remodeling and cell-cell or cell-matrix interactions that alter physical properties of the microenvironment (147-149). While hormonal regulation of folliculogenesis (including endocrine, paracrine, and intraovarian) has been well investigated, the contribution of the microenvironment including physical cues has received less attention. Research in murine ovaries has shown changes in physical cues across the lifespan with older mice having more rigid ovaries compared to those of reproductive age with these changes being reversed when the ovaries are treated with collagenase indicating that the matrisome is providing the difference in rigidity of ovaries at different ages (156, 157). Significant *in vitro* work has examined the effects of rigidity using alginate encapsulation (which removes from biochemical cues) of isolated follicles (150, 151, 152, 153, 154). These experiments encapsulation of primordial follicles from rhesus macaque in 2% alginate, thus replicating a high-rigidity environment, which maintained optimal primordial follicle survival and morphology, whereas a more pliable 0.25–1.25% alginate environment supported increased hormone production in activated or growing follicles (150, 151, 152, 153, 154). In one study, five different processing conditions were tested: 3% alginate, 1.5% alginate, 0.7% alginate, 1.5% oxidized

alginate, and 1.5% irradiated alginate with the 0.7% alginate alongside the oxidized/irradiated alginates having an overall lower storage modulus (as an indicator of stiffness) (313). The researchers found that follicle growth and oocyte quality were optimized in the soft hydrogels (0.7% alginate, 1.5% oxidized alginate, 1.5% irradiated alginate), but antrum formation and estradiol production were optimized when the alginate solids concentration was smallest (0.7% alginate) (313). Taking this a step further, researchers used Interpenetrating Fibrin-Alginate Matrices (FA-IPN), which recapitulates the dynamic mechanical properties observed ruing the natural developmental process for ovarian follicles as the fibrin degrades over time in culture (314-316). Secondary follicles encapsulated in FA-IPN ad a survival rate of 80% and grew from 110μm diameter on day 0 to 320μm on day 12, which is significantly greater than in less permissive environment of 1% and 1.5% alginate, and the rate of meiotically competent oocytes produced was 75-82% an improvement over alginate alone improved upon alginate alone (67%) (135). Together this data indicates stage-specific and physical property specific effects on follicle activation, growth, and also functionality as measured by hormone production. Significant work has been done in murine ovaries, and some in humans as well, to examine changes in rigidity in the ovary especially in cases of pathology. Dysregulated physical forces within the ovary are present in disease states, such as polycystic ovarian syndrome (PCOS) and Turner syndrome, where increased rigidity may contribute to anovulation in PCOS and loss of structural support may contribute to POI in Turner syndrome (159,160). In PCOS research by Woods et al used magnetic resonance elastography to show that the ovaries of patients with PCOS were significantly more rigid than those of healthy individuals (150). Together, these studies show that rigidity can influence follicle quiescence and folliculogenesis. However, the native rigidity gradient has only been inferred and never quantified. Indeed, our lack of knowledge about the ovarian

microenvironment hampers our ability to mimic the main features of this organ, either in an in vitro model or functional transplantable engineered bioprosthetic. We predict that advanced engineering solutions that can induce the production of, or recapitulate, the tissue-specific structural and biochemical support of the matrisome will enable tissue-specific function. By engineering these features into a scaffold, researchers could potentially reduce the rapid primordial follicle activation and subsequent depletion that occurs in current clinical solutions (161). Given differential responses the hypothesis of my work, and experimentally examined in **Chapter 2**, is that the ovarian cortex is stiffer than the medullary compartment and that this property supports primordial follicle quiescence

PI3K/Akt Signaling in the Ovary

One of those most intensely investigated pathways in primordial follicle activation is phosphoinositide 3-kinase (PI3K) and Akt signaling pathway (PI3K/Akt) in the oocyte. This body of work has shown that PI3K-Akt signaling is associated with ovarian function, including the activation of primordial follicles, granulosa cell proliferation, corpus luteum survival, and folliculogenesis (8–10). The PI3K/Akt pathway is a kinase cascade that is activated by RTK. Akt is a serine/threonine kinase that is regulated by both PTEN and PI3K and is involved in primordial follicle activation. Akt translocates to the cell membrane and binds to phosphatidylinositol 3,4,5-triphosphate (PIP3) by its pleckstrin homology domain where it can then be activated via phosphorylation. Phosphoinositide-dependent kinase-1 (PDK1) phosphorylates Akt on its Threonine 308 residue (317,318), while mTOR complex 2 (mTORC2) phosphorylates Akt on its Serine 473 residue (319). Phosphorylation at both Threonine 308 and Serine 473 is required for full Akt activity (319). Once activated, Akt can then phosphorylate its downstream targets. Through phosphorylation the PI3K/Akt pathway regulates multiple cellular processes including

metabolism, cell cycle, apoptosis, proliferation, angiogenesis, survival, and protein synthesis via the phosphorylation of numerous downstream targets including, but not limited to: mTOR, BAD, p21Cip1, p27Kip1, TSC2, MDM2, PRAS40, eNOS, ER, AR, and FOXOs (318). An important and well-studied antagonist of the PI3K/Akt pathway is phosphatase and tensin homolog (PTEN) which dephosphorylates PIP3 to phosphatydylinositol 4,5-biphosphate (PIP2). More recent work has shown that microRNAs (miRNAs) are also important for regulating the PI3K-Akt signaling pathway, specifically miR-494 and miR-20a (319). Using *in silico* target prediction and follow-up luciferase assay to examine functionality showed these miRNAs specifically targeted and regulated the activity of both PTEN and BMPR2 in a bovine model (319).

Downstream targets of the PI3K/Akt pathway in the ovary includes members of the Foxo forkhead transcription factor family which are involved in development, metabolism, gametogenesis, and stem cell functionality (320). The transcription factor family includes four family members in mammalian species, Foxo1, Foxo3, Foxo4, and Foxo6. The family member Foxo3, a transcriptional repressor, has been heavily researched in mammalian models with Foxo3−/− mice being born with a normal complement of follicles that is rapidly depleted via global premature follicle activation resulting in premature ovarian insufficiency within days (320,321). In contrast, overexpression of Foxo3 via constitutive activation in a transgenic mouse model caused infertility via reduced oocyte growth, follicle activation, and anovulation (320). In these transgenic mice constitutive activation of Foxo3 resulted in reduced expression of BMP15, connexin 37, and connexin 43 which are important to gap junction formation and proper oocyte:granulosa cell communication in the ovary (320). Additionally, the continued activation was shown to facilitate the nuclear localization of $p27^{kip1}$ in oocytes, which is a known inhibitor of cyclin-dependent kinase 1 (Cdk1) resulting in inhibited oocyte growth (323). In wild type mice using

immunohistochemistry Foxo3 has been localized specifically to the oocyte of primordial and primary stage follicles before becoming undetectable at later stages of folliculogenesis starting at the secondary stage (324). Further genetics work has been done in mice using conditional Foxo3 ablation in the oocyte, which leads to global follicle activation and depletion similar to the previously mentioned mouse line which confirms oocyte-centric function of transcriptional repressor. Follow-up investigations to examine gonadal expression patterns of Foxo1 and Foxo3 in non-rodent species, including humans and non-human primates, using immunohistochemistry-based methods validated using western blots found that while Foxo1 expression in granulosa cells was conserved in non-rodent species evaluated, Foxo3 expression in oocytes was not (322). However, large genetics studies in humans experiencing premature ovarian insufficiency have found sequence variations at the human Foxo3 locus including six novel single-nucleotide variants and multiple nonsynonymous single-nucleotide variants that were not detected in controls though functional impact of these single nucleotide polymorphisms (SNPs) when induced in a murine model showed no functional impact on Foxo3 activity (322,321). These results indicate that there still may be a role for Foxo3 in human fertility and follicle activation, however functional redundancy of Foxo family members in primordial follicles could explain lack of an effect in these studies. Work leveraging PI3K/Activators (via either PI3K stimulators or PTEN inhibitors) has shown that these pharmacological approaches can induce primordial follicle activation and survival though the downstream mechanism may not specifically be Foxo3-reliant in humans (321,322).

Conditional knockouts in the oocyte of PTEN, the negative regulator of PI3K/Akt pathway activity, have been shown to induce follicle activation and the rapid depletion of the entire primordial follicle pools or ovarian reserve resulting in premature ovarian insufficiency (325).

Further experimentation in the ovary has shown that conditional knockouts of PTEN in the oocyte result in the hyper-activation of PI3K/Akt pathway and hyperphosphorylation of Foxo3. However, hyper-activation of AKT using oocyte specific constitutive activation of PI3K (PI3KCA) does not fully recapitulate the phenotype seen in knockout animals (326). Instead, by PND50, the primordial follicles show a reduction by about 50% compared to wild-type mice (326). The slower rate of global primordial follicle activation in oocyte specific Pi3kca mice compared to PTEN knockouts may be attributed to the increased survival rate of follicles at all stages of development suggesting a secondary role for the PI3K/Akt pathway in follicle growth and survival (326). Using an inhibitor of the PTEN (bpV(pic)) and a PI3K activating peptide (740Y-P) showed that after short-term treatment increased the nuclear exclusion of Foxo3 in the oocytes of primordial follicles in neonatal mouse ovaries as measured by immunohistochemistry (327, 328). Transplantation of these ovaries into ovariectomized mice revealed increased follicular growth and that using *in vitro* fertilization allowed for the generation of viable and fertile offspring (327,328). Further synergistic effects have been shown by combining mammalian target of rapamycin (mTOR) activator together with AKT activators (327). Incubation of ovaries for 2 days, followed by allografting into ovariectomized mice for 5 days, led to marked increases in graft weights and promotion of follicle development and mature oocytes derived from these ovarian grafts were successfully fertilized and resulted in healthy offspring (327).

Attempts have been made to leverage these results in a clinical setting to assist with treating premature ovarian insufficiency or infertility. With cryopreservation, and later auto-transplantation of tissue, being the only method of fertility preservation for a growing population of pediatric cancer survivors. A major obstacle to this type of transplant is the rapid activation of primordial follicles during the transplantation process (329-332). Recent research using

LY294002, a PI3K inhibitor, and rapamycin, an mTOR inhibitor, on 4–8-weeks old or neonatal murine ovaries that were cryopreserved and then cultured on transwells revealed using Western blot and immunofluorescence analyses showed that in vitro incubation with these inhibitors significantly inhibited the activation of the PI3K/PTEN/Akt or mTOR pathways (333). Further, it was shown that Cryopreserved ovaries cultured for 24 h in the presence of inhibitors showed a higher percentage of primordial follicles relative to the total number of follicles and lower proportion of follicles that reached the secondary stage, which together indicate a lower amount of primordial follicle activation (333).
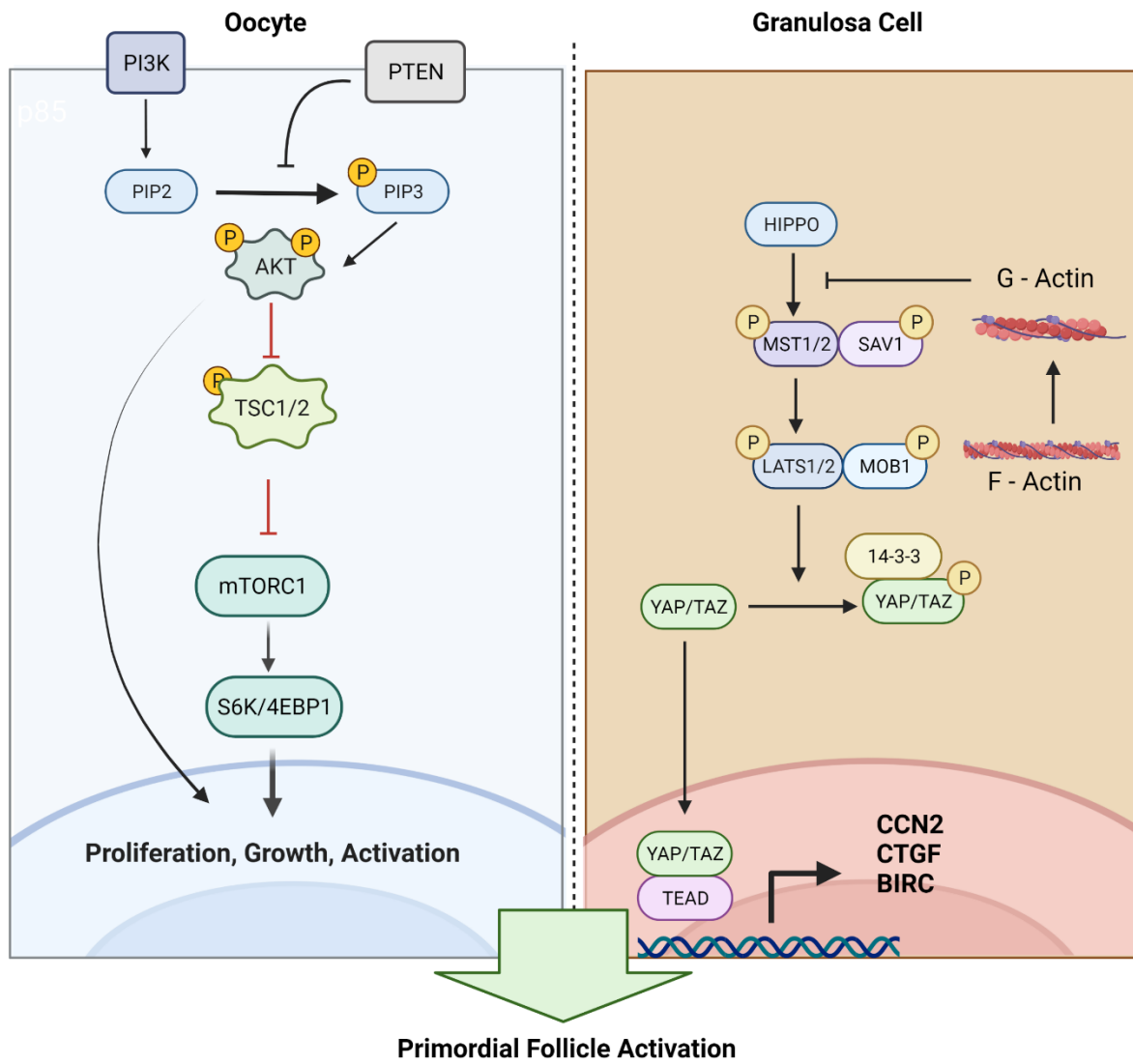
Figure 3. Follicle Activation via PI3K/Akt/mTORC and the Hippo pathway. (left) PI3K/Akt/mTOR pathway expression towards activation in oocytes with crosstalk between PI3K/Akt via regulation of TSC1/2 activity by active phosphorylated AKT. (right) Hippo pathway expression in the Granulosa cell showing G-actin suppression of Hippo pathway kinase cascade, preventing the downstream phosphorylation and degradation of YAP/TAZ allowing for nuclear inclusion and binding to TEAD transcription factors with downstream gene expression resulting in increased proliferation and primordial follicle activation.

Mammalian Target of Rapamycin (mTOR) Signaling in the Ovary

Rapamycin is a macrocyclic lactone found to be produced by the bacterium *Streptomyces hygroscopicus* and was originally utilized as an anti-fungal agent in humans (334, 335). The protein target of rapamycin (TOR) was originally discovered in genetic mutation studies using *Saccharomyces cerevisiae* (336) and subsequently found to be the target of the rapamycin–FKBP12 complex in mammalian cells that is now more commonly known as mTOR (337-339). mTOR is a complex of two different complexes mTOR complex 1 (mTORC1) composed of the sub-units mTOR, Raptor, mLST8/GβL, PRAS40, and DEPTOR and mTOR complex 2 (mTORC2) which consists of the subunits mTOR, Rictor, mLST8/GβL, DEPTOR, mSin1, and protor1/2 (340,341). Both complexes influence different activity with mTORC1 positively regulating cell growth and proliferation while mTORC2 is primarily involved in the phosphorylation of Akt, whose downstream functions as previously mentioned promote cell growth and proliferation (340,341). mTORC is negatively regulated by the tumor suppressor sclerosis complex 1 (TSC1) or 2 (TSC2). In mouse ovaries, oocyte specific deletions of either TSC1 (OoTSC1-/-) or 2 (OoTSC2-/-) leads to the rapid activation of primordial follicles and onset of premature ovarian insufficiency due to depletion of the ovarian reserve in early adulthood (12-13 weeks of age) (342,343). Both of these conditional deletions showed hyperphosphorylation of 6K1 and rpS6 in oocytes, which indicated increased activation of the mTOR pathway (342,343). The increased activation of mTOR in both conditional deletions was rescued by the application of rapamycin (342,343). In these experiments there is no corresponding increase in PI3K/Akt activity indicating that mTORC signaling occurs in parallel with this pathway instead of downstream which is supported by additional research showing that double deletion of TSC1 and PTEN synergistically enhanced the rate at which the ovarian reserve was depleted in a mouse model

(342,343). Combining this research with other work on PI3K/Akt it is clear that both Tsc/mTORC1–S6K1–rpS6 signaling and the PTEN/PI3K–PDK1–S6K1–rpS6 signaling in oocytes regulate the steady activation of ovarian follicles in a coordinated fashion with PTEN, TSC1/2 in oocytes as part of an inhibitory mechanism for both pathways which suggests that deregulation of signaling events may be a cause of defects in primordial follicle activation in humans which result in premature ovarian insufficiency (342,343).

Transforming Growth Factor Beta Superfamily Signaling in the Ovary

TGF-β superfamily proteins are extracellular, secreted growth factors that function via autocrine or paracrine signaling. Research on TGF-β signaling has shown that these proteins direct multiple cellular processes during both embryonic and postnatal development, including driving differentiation, apoptosis, proliferation, and cell specification (344). In mammals there are >40 TGF-β family proteins belonging to one of two major sub-groups; growth differentiation factors and bone morphogenic proteins (GDF/BMP) or activins/TGF-ßs (344). TGF-β ligands are homodimeric or heterodimeric molecules bind to and signal through plasma membrane-spanning serine/threonine kinase receptors which are clustered into type I receptors and type II receptors. (345,346) Following ligand binding to the type I and type II receptors at the cell surface both receptor types dimerize forming a tetrameric signaling complex. The type II receptor is considered to be constitutively active, and it activates the type I receptor via phosphorylation. Furthermore, an additional type 3 receptor class is made up of betaglycan and endoglin that modulate TGF-β activity by functioning as accessory proteins (345-347).

Phosphorylation of ALKs within a serine-rich juxtamembrane domain leads to the activation of receptor Smad proteins (348). Smads are diverse and classified by function. These classifications include receptor-activated (R-) Smads (Smad1, -2, -3, -5 and -8), common-partner (Co-) Smads

(Smad4) or inhibitory (I-) Smads (Smad6 and -7). Smads generally function as intracellular transcription factors that mediate the signaling of the TGF-β superfamily. Once activated Smads are phosphorylated and in turn form protein complexes with the co-Smad protein Smad4 (345). These Smad complexes translocate into the nucleus and promote TGF-β superfamily target gene transcription (345). Depending on the combination of type I and type II receptors, different R-Smads are activated through phosphorylation by the type I receptor upon ligand binding. TGF-β signal transduction is also antagonized by inhibitory Smad proteins (I-Smads). I-Smads are believed to inhibit signaling by either preventing phosphorylation of type I receptors or by sequestering Smad4 (345). Although I-Smads inhibit the signaling of TGF-β superfamily proteins through intracellular means, signaling suppression also occurs extracellularly. Inhibition by extracellular binding proteins, including follistatin, noggin, EMILIN1, and chordin, prevent interaction between TGF-β superfamily ligands and their receptors by decreasing ligand availability or by blocking binding to the receptor (349).

In the Ovary, during folliculogenesis, Smad2 and Smad3 are expressed in a stage specific fashion in rats, this research shows the possibility for differing, or stage-specific, effects of TGF-β superfamily ligands utilizing the same signaling pathways (354). Further work in a murine model examining Smad2/3 has shown that nuclear exclusion of these factors in murine granulosa cells drives follicle activation alongside an increase in Ki67 expression (66). Knockouts of Smads in murine models are generally embryonically lethal (Smads1, 2, 4, 5) however mutations to Smad3, via the disruption of exon 8, showed defective folliculogenesis with significant decreases in rates of follicle activation, increased atresia, and reduced litter sizes likely due to an inability to respond to TGFβ family signaling including factors such as BMP15, GDF9, and TGFβ (350-353). Serine threonine kinase receptor associated protein (STRAP) is another regulator of TGFβ signaling

acting by the TGFBR1 and SMAD7 complex, which prevents phosphorylation of SMAD2 and SMAD3 by blocking access to TGFBR1 (355). Follow-up experiments combined STRAP siRNA and immune-neutralization treatment *in vitro* of neonatal (d4) ovarian fragments, which contain a high-density of primordial follicles, showed a reduction in the number of primordial follicles and an increase in the number of activated follicles when compared to untreated controls (456). Perhaps counter-intuitively, STRAP showed stage-specific differences in function with exogenous STRAP treatment increasing oocyte size of activated follicles in neonatal ovaries with little to no effect on primordial follicle growth though a deeper examination of the literature finds this to be consistent with research in other tissues including the activation of PI3K/Akt signaling (456). The upstream mechanism of action that maintains follicle quiescence or precipitates follicle activation via TGFβ remains unclear however, co-expression of SMADs and regulatory pieces such as STRAP during the early stages imply that the TGFB pathway is important to the process, while the effect of STRAP on growing follicles shows that these signaling pathways are incredibly complex with subtle interactions between proteins across signaling pathways as seen via STRAP (456).

Transforming Growth Factor Beta (TGFβ)

TGF-ßs are homodimeric cytokines of which three isoforms are expressed in mammals (TGF-β1, TGF-β2, and TGF-β3) (357). These cytokines have diverse roles and are known to influence tissue development, cell migration, proliferation, and has been implicated in the molecular regulation of several reproductive processes including folliculogenesis via oocyte maturation, early embryogenesis, embryo implantation, and placental morphogenesis by binding to TGFβ receptors (357). There are significant challenges develop *in vivo* models of TGFβ action in the ovary due to TGFβ2 or TGFβ3 null mice being embryonically or perinatally lethal (344). Studies of TGFβ1 are also limited as mice lacking this gene develop inflammatory lesions eventually resulting in early

postnatal lethality at 3-4 weeks of age (358). However, work in 2006 by Ingman using a TGFβ1 null mouse line found that that the onset of sexual maturity was delayed, ovarian function was disrupted with irregular progression through the estrous cycle, a 40% reduction in oocytes ovulated, and compromised preimplantation embryo development (359). More recent work by Hardy, et al in 2019 used *in vitro* culture methods to examine primordial follicle activation by exposing neonatal ovaries to TGFβ1 (66). Exposure to TGFβ1 ligand promoted a shift to a SMAD-independent pathway in granulosa cells shown via uncoupling of SMAD3 from Ccnd2 and Myc and increased mTOR signaling which drove granulosa cell proliferation and eventual follicle activation (66). The receptor-mediated second messenger system SMAD2/3 downstream of TGFβ appears to be intact in humans based on experiments that have found SMAD2/3 mRNA and protein expressed in the granulosa cells of preovulatory follicles (85, 86,101). Further, TGF-β1 was observed in oocytes of primary follicles and in thecal and granulosa cells of antral follicles (85, 86,101). Expression levels of TGF-β1 increased in the thecal and granulosa cell layers as the follicle matured as indicated by IHC (85, 86,101). However, despite this growing evidence the activating signal (and corresponding maintenance signal) that drives these changes and follicle activation in native ovaries is
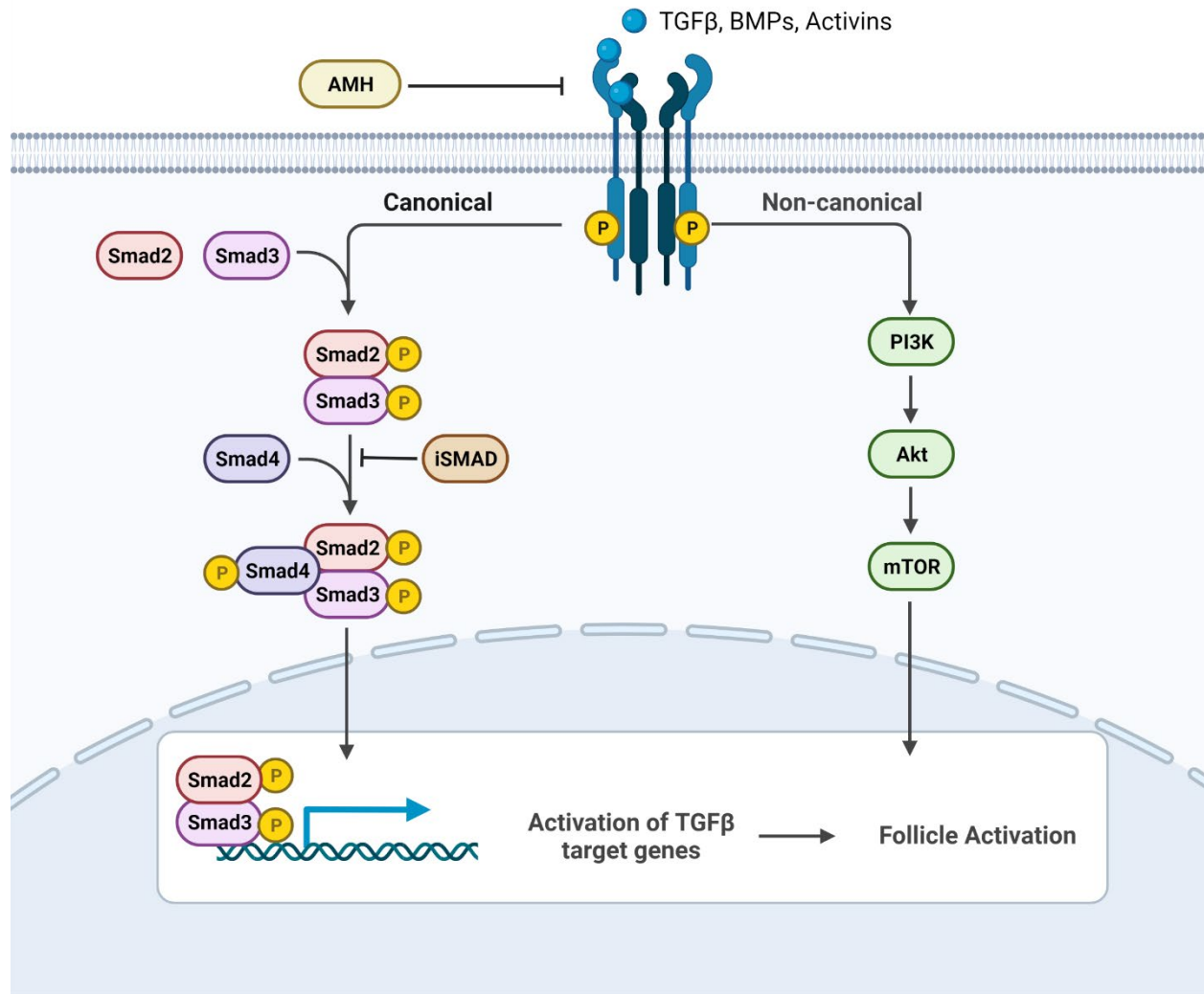
Figure 4. TGFβ signaling towards follicle activation. Canonical signaling of TGFβR via action of soluble TGFβ, activin or BMPS leading to the phosphorylation of SMAD2/3, recruitment of SMAD4 and nuclear inclusion of phosphorylated SMAD2/3 resulting in activation of TGFβ target genes, proliferation, and follicle interaction. Non-canonical signaling is represented on the right showing phosphorylation of PI3K and activation of the PI3K/Akt/mTOR pathway (detailed earlier in the chapter) that leads to follicle activation.

as of yet unknown though TGFβ superfamily members and the crosstalk involved in regulating SMAD signaling is likely downstream of these signals (85, 86,101).

Bone Morphogenic Factors and Growth Differentiation Factor 9

Bone Morphogenic Factors (BMPs) are the largest sub-group of the TGFβ family and have been shown to regulate cell death, differentiation, and proliferation in multiple different tissues (360). Several different BMPs have important functions in the ovary starting at organogenesis and the establishment ovarian reserve (BMP2, -4, -7) in association with the regulatory machinery gremlin 1 (GREM1) (361,362). Specific to primordial follicle activation however significant work using *in vitro* culture methods has been done examining BMP function. BMP4 treatment of 4-day old rat ovaries showed increased follicle activation via increased proportion of primary activated follicles to quiescent primordial follicles (363). Subsequent antibody neutralization experiments of BMP4 showed smaller ovaries and progressive loss of oocytes implicating as being involved not only in activation but also as a follicle survival factor (363). Culturing murine ovaries with exogenous BMP7 resulted in additional follicle growth (363,364).

The two most important oocyte-secreted factors in these two families to follicle growth and activation are likely BMP15 and GDF9, which are TGFβ family members that signal through ALK4/ALK5/ALK6/ALK7/BMPR2 receptor complex and activates the Smad pathway via phosphorylation of SMAD2/3 (365-368). Both GDF9 and BMP15 are shown to be produced starting at the primary stage of ovarian follicles (365-368). In humans, mutations in GDF9 at the transcriptional regulatory region and multiple mutations of BMP15 have been associated with premature ovarian insufficiency and dizygotic twinning (369-371). GDF9 mRNA is expressed exclusively in the oocytes of primary and growing follicles in humans, rats, and mice (372). GDF9 null mice have been found to be infertile due to arrest at the primary follicle stage with follow-up

work showing that GDF9 specifically promotes the transition from the primary to secondary stage due to the inhibited proliferation of granulosa cells (373). Proliferation of granulosa cells being a requirement of transitioning from the primary to secondary stage (373). Further, the follicles of rodent models lacking GDF9 do not contain theca cells, the second type of supporting cell that is required for full production of steroid hormones (374). In support of this treatment of primary rat granulosa cells with exogenous GDF9 show increased granulosa cell proliferation and rescued theca cell numbers (374).

BMP15 is the closest homologue to GDF9 within the TGFβ family and can form either a homo or heterodimer with GDF9 (360). Similar to GDF9 expression of BMP15 is limited to the oocyte and begins at the primary stage (360). However, unlike the severe phenotypes seen in the ovaries of GDF9 null mice BMP15 null mice are sub fertile with histologically similar ovaries to those of their wild-type littermates (375). Multiple experiments have shown that BMP15 and GDF9, using null mice, have shown that these two proteins work synergistically to promote ovarian function (375). Extensive murine breeding experiments specifically have shown that null females (Bmp15−/−) are sub fertile with minimal ovarian defects shown in IHC analysis but demonstrate decreased ovulation and fertilization rates (375). Double homozygote females (Bmp15−/−Gdf9−/−) display oocyte loss, infertility, and the formation of cysts with an overall phenotype similar to those of GDF9 null animals (375). Finally, Bmp15−/−Gdf9+/− female mice have more severe fertility defects than Bmp15−/− females with abnormalities observed in ovarian folliculogenesis, cumulus cell physiology, and fertilization rates (375). The biopotency of the heterodimer has been deciphered using *in vtiro* culture methods mouse granulosa cell and cumulus cell expansion assays with the GDF9:BMP15 heterodimer ~10- to 30-fold more bio-potent than the mouse GDF9 homodimer, and human GDF9:BMP15 heterodimer ~1,000- to 3,000-fold more

bioactive than human BMP15 homodimer (376). GDF9/BMP15 heterodimers have been found to induce Anti-Mullerian Hormone (AMH) expression in multiple studies (377). GDF9/BMP15 has been shown to increase AMH receptor expression in granulosa cells in mice and to regulate AMH expression in human primary cumulus cells (377). Further work examining the role of GDF9/BMP15 in AMH production has shown that this occurs through the PI3K/Akt and Smad2/3 pathways synergistically recruiting the coactivator p300 on the AMH promoter region that promotes acetylation of histone 3 lysine 27 (H3K27ac), facilitating AMH/Amh expression which was inhibited by FSH (377). Taken together these results suggest synergistic effects of GDF9/BMP15 heterodimers, with equally synergistic effects of mutations to these genes, that act through the TGFβ signaling pathway and SMAD2/3 that affects the proper progression of folliculogenesis via granulosa cell proliferation and AMH production with dysregulation of this complex system causing premature ovarian insufficiency in both human and mouse models (377).

Anti-Müllerian Hormone

Anti-Müllerian hormone or müllerian-inhibiting substance controls the regression of müllerian ducts during testes development (378). Clinically AMH is used as a marker of the ovarian reserve as serum levels of AMH decline with age, and AMH levels are undetectable in individuals experiencing premature ovarian insufficiency (379,380). In the ovary, AMH is expressed in granulosa cells of activated follicles beginning at the primary follicle stage within humans and mice in a GDF9/BMP15 dependent fashion as detailed in the previous section (377). Two different AMH receptors are expressed by ovarian follicles in a stage and follicular compartment-specific fashion with AMH type 2 receptor being expressed in granulosa cells of pre-antral follicles and AMH type 1 receptor being expressed by oocytes and granulosa cells of developing follicles (381). In murine models the ablation of the AMH gene increases activation of primordial follicles

resulting in the rapid depletion of the ovarian reserve and premature ovarian insufficiency (382, 383). These animals remain fertile until their reserve is depleted by 13-months of age though sharp declines in the reserve, as measured by number of primordial follicles, are seen within 4 months (382). However, Depletion of the AMH type 2 receptor in a murine model results in a similar phenotype to ablation of the AMH gene with increased follicle activation and resulting onset of premature ovarian insufficiency (384). Multiple *ex-vivo* studies have shown that AMH inhibiting primordial follicle activation with neonatal mouse ovaries cultured in AMH containing media developing 40% fewer growing follicles than controls and human ovarian cortical strips cultured with AMH at 100ng/mL showed similar results with decreased growth of primordial follicles (383,385). Some controversy however does exist here with extended exposure to AMH over 4 weeks in culture promoting primordial follicle activation *in vitro* with 54% of primordial follicles cultured in media containing AMH advancing to the primary stage compared to 41% in control medium without AMH (383). Though of note in these experiments is that follicle recruitment increased in all medias irrespective of composition when compared to the uncultured control (383). The inhibitory effects of AMH are further supported in its target genes which have been primarily investigated in rats (386). Most of these target genes are members of the TGFβ including extracellular growth and regulatory factors (386). The inhibitory effects of AMH are reversed by treatment with the BMP inhibitors GREM1 and GREM2 using a whole-ovary culture system (386). GREM1 inhibited AMH activity that prevented the primordial to primary transition by binding to BMP4 (386). GREM2 also reversed the effects of AMH and promoted primordial follicle activation and was found to bind both BMP4 and to AMH using co-immunoprecipitation experiments (386). mRNA for both of these proteins was found to be localized to the granulosa cells of activated follicles, which was supported by IHC analysis that found both proteins localized

to granulosa cells in later stage follicles with multiple layers of granulosa cells (386). GREM2 expression was also localized to primordial, and early-stage activated follicles suggesting it plays a role in activation by reversing the inhibitory effects of AMH though the upstream signal promoting its expression remains elusive (386). Despite the controversy detailed earlier, when the results of this research are combined with previous data from GDF9/BMP15 research it would indicate that activated growing follicles play a regulatory role in primordial follicle activation by secreting AMH which could serve as a maintenance signal preventing increased activation by physical stressors caused by large growing follicles (follicle activation in response to physical stressors will be discussed in the overview of HIPPO signaling and in **Chapter 4**).

Inhibin and Activin

Inhibins and activins are granulosa cell secreted peptide hormones that are made up of structurally related peptides which are disulfide-linked to form heterodimers of α and β subunits (387). There are two isomers of Inhibin, Inhibin A is comprised of α and βA subunits and Inhibin B is composed of α and βB subunits (387). Activins are dimers of the β subunits: activin A (βAβA), activin B (βBβB), and activin AB (βAβB) (387). All subunits are expressed in the granulosa cells of growing follicles (388). Activin activity is mediated by binding to one the two isoforms of its type-II receptor (ACTRIIA or ACTRIIB) followed by the downstream activation of SMAD2/3/4 (390). Inhibin regulates activin activity by competitively binding to the type-II receptor (390). Regulation of activin also occurs through competition for subunit assembly, its binding to follistatin (FST) which is produced by the ovary, and through inhibin activity in the pituitary suppressing follicle-stimulating hormone (FSH) production (391-394).

In vitro studies performed in rats have shown that activin stimulates granulosa cell proliferation and promotes the growth of preantral follicles in both mice and rats (395). The effects of activin

are age-dependent with it stimulating the growth of preantral follicles isolated from immature mice and not from adult mice (395). Indeed, in preantral follicles isolated from adult mice, Activin A was found to block the effects of FSH which was reversed by treatment with exogenous FST (395). In contrast, FSH alone showed no effect in pre-antral follicles isolated from immature mice while Activin A alone or in combination with FSH showed increased follicle diameter (395). In the ovaries of mice that overexpress FST, which acts to suppress Activin activity, follicles arrest at the primary follicle stage (395). FST also antagonizes TGFβ ligands including BMP7 and other growth factors (395). Regardless of the age-specific effects complete loss of Activin A and B in mouse granulosa cells causes infertility, with implications that there's some dose responsiveness with Activin A playing a dominant role in fertility based on single allele conditional inactivation studies in mice (396). Loss of either β subunit in granulosa cells showed decreased expression of factors that are associated with granulosa cell survival and proliferation such as Kitl, Taf4b, and c-Myc (396). Activin treatment is found to induce expression of Esr1 and Esr2 in a SMAD2/3-dependent manner in proliferating granulosa cells indicating crosstalk between activin and known nuclear receptor signaling that induces granulosa cell proliferation (188).

Hippo Signaling in the Ovary

The Hippo signaling pathway is extremely well conserved across all metazoan animals and is essential for controlling organ size (397,398). The Hippo pathway is composed of a kinase cascade that consists of several negative growth regulators arranged in a serine kinase cascade that ultimately phosphorylates and deactivates downstream transcriptional coactivators, yes-activated protein (YAP) and the transcriptional coactivator with PDZ-binding motif (TAZ) via nuclear exclusion and promoting degradation of these effectors (399). The Hippo signaling kinases also includes mammalian sterile 20-like (MST) 1/2, Salvador homolog 1 (SAV1), and large tumor

suppressor (LATS) 1/2. When Hippo signaling is disrupted the now non-phosphorylated YAP/TAZ enters the nucleus where it activates transcriptional enhanced associate domain (TEAD) transcriptional factors leading to an increase in the expression of downstream cystein-rich 61, connective tissue growth factor, and nephroblastoma overexpressed (CCN) growth factors and baculoviral inhibitors of apoptosis repeat containing (BIRC) apoptosis inhibitors which in turn stimulate cell growth, survival, and proliferation (3). Disruption of the Hippo pathway can come from external mechanical forces such as changes to the cellular microenvironment or extracellular matrix, or changes to the polymerization of actin from globular actin (g-actin) to filamentous or (f-actin) (399).

In both murine and human ovaries, key Hippo signaling genes (YAP, TAZ, MST1/2, SAV1, and LATS1/2) are expressed in a stage-specific fashion in ovarian follicles (103). YAP1 null animal models are embryonically lethal, so most research has leveraged small molecule inhibitors to decipher the function of Hippo signaling genes in the ovary (400). Microarray experiments have shown that components of the Hippo pathway Mammalian STE20-like protein kinase 1 (MST1) and large tumor suppressor kinase 2 (LATS2) are expressed in bovine granulosa and theca cells (399). IHC analysis in this study further revealed that YAP1 and TAZ were localized to the nucleus of activated follicles in stage and compartment-specific fashions (399). Treatment with verteporfin and siRNA targeting
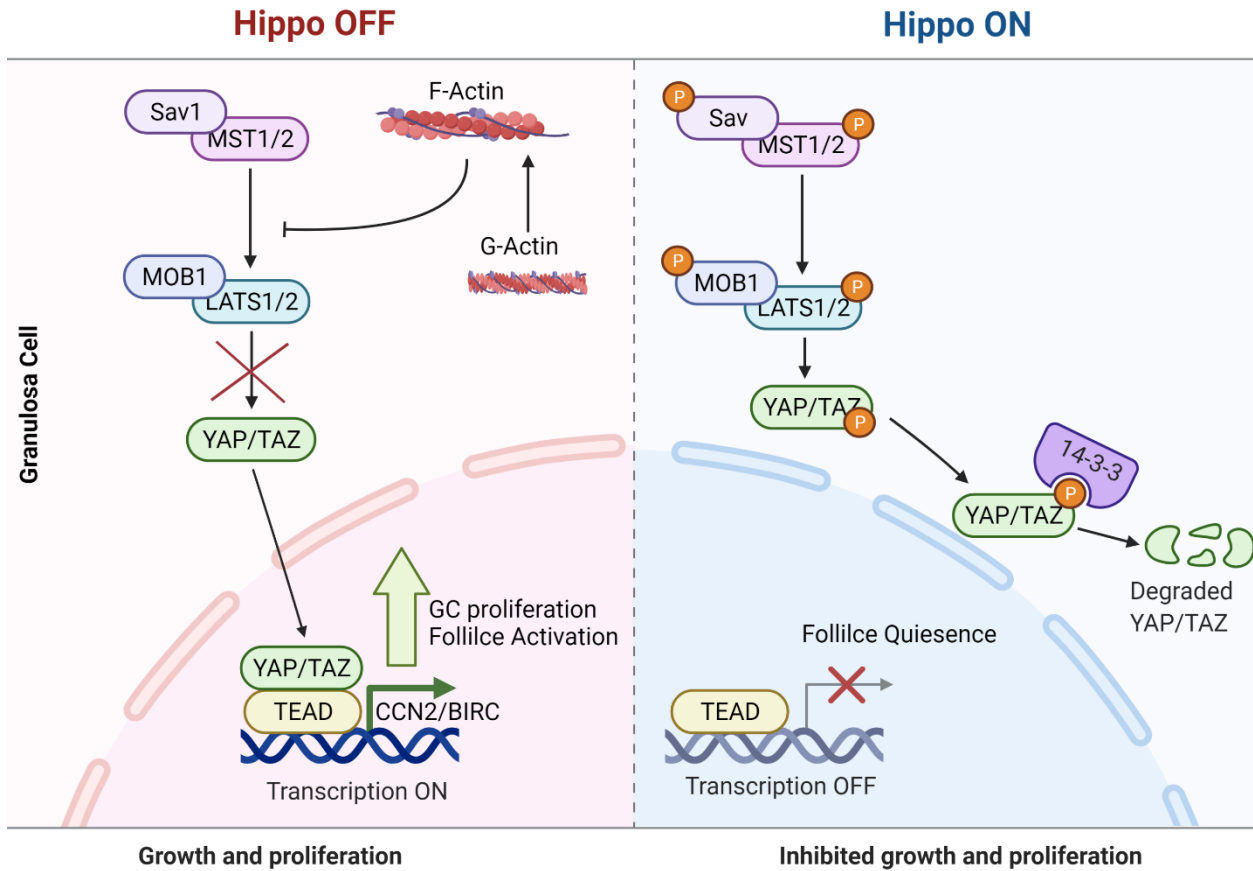
Figure 5. Hippo signaling and primordial follicle activation. (Left) Hippo is turned off due to polymerization of G-Actin to F-Actin leading to YAP/TAZ entering the nucleus and co-activating TEAD transcription factors promoting downstream gene expression that results in granulosa cell proliferation and primordial follicle activation (Right) Homeostatic conditions in which Hippo signaling pathway is turned on, leading to the phosphorylation of YAP/TAZ and nuclear exclusion. Phosphorylation of YAP/TAZ also leads to degradation of the protein by 14-3-3.

YAP1 or TAZ revealed a critical role for these transcriptional co-activators in granulosa cell proliferation, significantly suppressing basal and TGFα-stimulated DNA synthesis and granulosa cell proliferation (399). Furthermore, knockdown of YAP1 in granulosa cells inhibited FSH-induced estradiol biosynthesis (399). These data indicate that Hippo pathway transcription co-activators YAP1/TAZ play an important role in granulosa cell proliferation and estradiol synthesis, two processes critical for maintaining the normal progression of folliculogenesis (399).

Initial interest in Hippo and its role in primordial follicle activation comes from ovarian fragmentation studies (159, 160, 181). Using a murine model, ovaries from juvenile mice (day 10) were fragmented followed by allotransplantation under the kidney capsule of adult hosts (159). Histological analysis and follicle counting of grafts for these ovaries showed an overall loss of total follicles following fragmentation and grafting (159). However, these ovaries also showed significant increases in the number of late secondary and antral/preovulatory follicles (159). Real-time RT-PCR and immunoblotting analyses showed alterations to the actin polymerization and decreases in phosphorylated YAP protein (pYAP) relative to unphosphorylated YAP indicating a disruption of the Hippo signaling pathway in these ovaries (159). Intact ovaries from this same series of experiments showed that YAP was localized predominantly to the cytoplasm of granulosa cells at the primary and secondary stages with this pattern changing 4 hours after fragmentation (150). Increased rates of activation in fragmented ovaries were abrogated using a combination of veterporfin (an inhibitor of YAP) and treatment with antibodies for CCN2 (a downstream effector of YAP) (159). Fragmentation studies were also done examining synergistic relationships between the Hippo signaling pathway and PI3K/Akt, a well-studied signaling pathway involved in follicle activation detailed earlier in this chapter (160). Using PI3K/Akt stimulating drugs, a PTEN inhibitor and PI3K Agonist, promoted secondary growth (160). When stimulators were combined

with fragmentation increased follicle growth and activation were found to be additive with significant increase in the number of activated follicles compared to controls and PI3K/Akt stimulators or fragmentation alone (160).

The crosstalk between PI3K/Akt and the Hippo signaling pathway has been expanded to include interactions with mTOR signaling in multiple studies (401). One study focused on characterizing the crosstalk between all three pathways in immature murine ovaries (d3) cultured for 4 or 48 hours after sectioning or chemotherapy exposure (4-hydroperoxycyclophosphamide (4HC, 3 and 20 μM) (402). Subsequent exposure to the mTORC1 inhibitor everolimus (EVE) by itself or in co-culture with 4HC was assessed at the morphology, gene transcription, and protein levels (402). The study found that isolation alone was enough to trigger a significant increase in primordial follicle activation and cellular growth, which was also seen in sectioned ovaries (402). PI3K gene expression levels remained stable during the culture, but phosphorylated protein levels of AKT and RPS6 were decreased compared to fresh ovaries, despite massive follicular activation though the study notes that lack of increased expression was likely caused by the absence of growth factors in culture media (402). Significant increase of YAP was observed in 4HC-exposed ovaries alongside increases in Ccn2 expression when compared controls which was prevented by EVE co-treatment (402). Together these data suggest significant cross talk especially given the context that EVE, which interacts only with mTORC1 a downstream component of PI3K/Akt activity, shows reductions in the downstream gene expression seen from dysregulation of the Hippo signaling pathway. Further it indicates that chemotherapy drugs, specifically 4HC, increase follicle activation via Hippo signaling pathway dysregulation and increased nuclear localization of YAP which is of significant clinical relevance (402).

Further clinical interest in the Hippo pathway has grown over time, specifically in cases of polycystic ovarian syndrome (PCOS), infertility, and premature ovarian insufficiency (403). Specific to patients with POI a small-scale study was done by Suzuki et al 2015 on 37 patients, 54% of whom had residual follicles based on histological analysis (404). Patients underwent a laparoscopic ovariectomy (404). After removal ovarian cortices were dissected into strips for vitrification then thawed later for oocyte retrieval and in vitro fertilization (IVF) (404). After warming, two to three strips were fragmented into smaller cubes before culturing with Akt stimulators, a combination of PTEN inhibitor and PI3K stimulator, for 2 days (404). Following cutting ovarian strips into cubes (Hippos signaling disruption) and Akt stimulation using IVA drugs, multiple antral follicles were detected in 45% of POI patients containing residual follicles with twenty-four oocytes being retrieved from six patients and two successful pregnancies resulting from embryo transfer (404). However, other studies using fragmentation alone have not successfully activated follicles in human cortex strips despite detection of Hippo components including YAP, CCN 2, -3, and -5 (404). Researchers were unable to verify changes to actin polymerization and dysregulation of the Hippo pathway remained inconclusive with the possibility that these changes are transient, requiring multiple time points to capture the point of activation (404). Efforts in patients with PCOS have shown higher expression of Hippo signaling pathway components in cumulus cells of patients with PCOS compared to controls (404). Li et al. 2012 concluded that a key effector in the Hippo signaling pathway, YAP1, is differentially expressed in PCOS patients compared to controls using RT-PCR and SNP analysis for genome wide association significance (404). Other studies have shown aberrant expression of components of the Hippo signaling pathway including LATS1, LATS2, and MOB1B which were localized to germ and somatic cells of primordial to antral follicles with deletion of LATS1 in resulting in ovarian germ

cell apoptosis and the formation of follicular cysts (404). Multiple studies by the Kawamura group focusing on patients with POI and PCOS have shown a synergistic relationship between Akt/mTOR pathway and Hippo by using Akt stimulators in combination with inhibition of Hippo and leveraging physical disruption of ovaries via ovarian fragmentation and wedge resection, which appears to increase the number of mature follicles in patients by adjusting follicular growth and ovulation, thereby leading to successful fertilization and pregnancy (159, 160). Taken together it appears that there is an additive relationship between PI3K/Akt and the Hippo signaling pathway and that this is a potential modality of treatment for patients experiencing infertility due to POI or PCOS. However, much remains unknown and there have been significant challenges recapitulating results. The upstream mechanism of Hippo signaling in the ovary is unknow though current data from PCOS patients indicates that the structure of the microenvironment (including both physical and biochemical cues, which will be discussed later) influence signaling that may drive follicle quiescence.

Ideal Properties of a Bioprosthetic Ovary

It is increasingly clear that the biochemical and physical characteristics of the ovarian microenvironment are important to drive function within the ovary. It should be possible to apply this growing understanding to the engineering of organ matrisome products that can be applied to a variety of medical needs, including tissue modeling and tissue restoration and regeneration.

The ideal engineered microenvironment should exhibit biomimicry and mechanical properties to the ovary. Meaning it would have similar compositional and microstructural characteristics to the natural target tissue and provide relevant physical and biochemical cues (such as those listed in Table 1) to the ovary. Beyond being present, however, these components must also be arranged to emulate the characteristics of the distinct compartments of the *in vivo* matrisome. For the ovary,

this requires that emulation of both the cortical and medullary regions, which are defined by micro-layered ECM 'sheets' and nanoscale ECM 'webs', respectively (15). In addition, because the natural matrisome is non-static, the engineered matrisome should exhibit dynamic reciprocity through being able to change and remodel in response to the surrounding biological microenvironment. Finally, the engineered matrisome must be manufacturable – capable of being produced safely, consistently, and at rates and costs that do not inhibit their adoption.

Current Tools and Engineered Biomaterials

Alginate Encapsulation

A follicle is a spherical aggregate of cells with an oocyte at the center surrounded by supporting cells, granulosa, and theca cells. These supporting cells, which surround the oocyte in three dimensions produce hormones and exchange necessary signals with the oocyte for the proper progression of folliculogenesis (190,191). Traditional two-dimensional (2-D) culture systems disrupt the interactions between the oocyte and its supporting cells which hinders the progression of folliculogenesis and reduces the survival rate of *in vitro* cultured follicles (192, 193). This is likely due to disruption of gap junctions which are essential to maintaining bidirectional communication between an oocyte and its supporting cells. These gap junctions allow for the delivery of nutrients, growth factors and hormones required for follicle and oocyte growth, indeed research has indicated that oocytes lack specific amino acids and are unable to perform either glycolysis or cholesterol biosynthesis without factors from supporting cells (196). Granulosa cells also require communication from the oocyte to drive proliferation and certain metabolic process (194, 195). Hydrogel encapsulation supports the maintenance of the three-dimensional (3D) architecture seen in the ovary and maintains the communication between the supporting cells and the oocyte (267).

Alginate is a naturally derived polymer that is produced by brown algae and is a common material used in *in vitro* follicle culture. Alginate is a copolymer of two types of uronic acid: α-L-guluronic acid (G) and β-D-mannuronic acid (M), that is cross-linked in the presence of calcium. The resulting gel shows a wide range of pore sizes (5-220mm) which can allow for the diffusion of large molecules through the alginate gel (197). Alginate culture of isolated follicles *in vitro* has shown to support the communication between follicular compartments, promoted oocyte growth, and granulosa cell proliferation using follicles isolated from mice (197). Significant work further supported the assumption that the physical and chemical properties of alginate encapsulation support follicle survival and growth (197-203).

Alginate has been used in work to show how the physical environment regulates follicle function and growth (151-154). This is because alginate is a hydrogel whose physical properties can be tailored by altering concentration (higher alginate concentration equals higher rigidity) and through the choice of cross-linking agent for studying cell growth and differentiation both *in vitro* and *in vivo* (204-207). Recent work by Freeman and Kelly on tuning alginate stiffness showed that by using $CaSO_4$ in place of the more common $CaCl_2$ you can increase the rigidity of the resulting biomaterial though this choice comes with balancing the cross-linking time required due to insolubility of some cross-linking agents (204). Further, Alginate itself does not interact with integrins of mammalian cells, which allows for the controlled introduction of outside factors (such as matrisome components, growth factors, etc.) or for the study of physical property changes in isolation from external biochemical signals. The tunability of alginate and ability to mimic ovarian compartment specific rigidities is the topic of **Chapter 3** of this dissertation.

Decellularized Extracellular Matrix

As previously mentioned, the matrisome, made up of ECM and ECM-associated proteins, makes up the skeleton of an organ, so it would appear to be an ideal tool for studying tissue-specific biochemical cues and how they drive biological processes of interest. To do this we use decellularization to enrich for matrisome proteins. Decellularization is a common tool in regenerative medicine and tissue engineering and involves the use of a physical, chemical, or enzymatic process to remove cells and cellular components while preserving the biochemical and structural components of the matrisome (208-210). Multiple decellularization methods have been developed and tested in multiple species including mice, pig, cow, and humans. Methods include the use of sodium dodecyl sulfate (SDS), sodium deoxycholate, sodium lauryl ester sulfate (SLES), triton X100, and sodium chloride (211-215). Additionally, combination methods have been tested such as SDS and sodium deoxycholate (216). These methods have demonstrated minimal residual DNA and retained ECM composition though how well the composition is retained does vary across these methods and this retention is tissue specific (216). Decellularized ECMs have been heavily used in in regenerative medicine and tissue engineering research in reproductive tissues, and in the ovary specifically (41, 215-217). Engineering applications have used dECM-based scaffolds seeded with cells restore tissue function with a bovine dECM scaffold seeded with murine primary ovarian cells initiating puberty in ovariectomized mice and similarly a murine primary ovarian cell seeded into a human-derived dECM scaffold showing hormone production restoration in ovariectomized mice (41). Additional strategies for the application of dECM have been the recent focus of work including the derivation of 'tissue papers' made of dECM from various bovine organ systems, specifically the heart, kidney, liver, muscle, uterus, and ovary (66). Lyophilized dECM was milled and subsequently suspended in a biocompatible polymer matrix composed of poly(lactic-co-glycolic acid) (PLGA) resulting in a final material that was 65 vol% dECM (66).

Microstructures, topology, and physical properties of the 'tissue paper' varied by the organ they were derived from (66). The final materials showed desirable physical properties that were clinically relevant (being able to be cut, folded, and sutured) (66). hMSCs were seeded onto these papers and cultured for 28 days and were assessed using SEM and IHC-based methods which showed tissue paper-specific adherence, proliferation, and infiltration (66). More recently we have seen ovarian dECM hydrogels used in encapsulation and 3D printing applications. In these applications we see decellularized tissue lyophilized and digested using an acidic pepsin solution prior to use in engineering applications for murine and porcine testicular organoids (218, 219). In both studies we see rheological and mass spectrometry analyses of testicular tissue derived hydrogels that show significant differences in terms of ECM stiffness and composition when compared to a collagen control (218, 219). Porcine-derived testicular organoids were cultured over 45 days and secreted stem cell factor and testosterone demonstrating functionality of Sertoli cells and Leydig cells, respectively. In both testicular organoids germ cell numbers decreased and Sertoli cell numbers increased (219). Leydig cell numbers decreased significantly in the collagen hydrogel testicular organoid suggesting a better preservation and better potential to restore reproductive function in the dECM testicular organoid (219). These results support the idea that dECM is tissue-specific and drives differing cellular responses as seen with hMSCs and testicular organoids (66, 218, 219). The use and characterization of ovarian compartment-specific dECM hydrogels will be the focus of **Chapter 3**.

3D Printing

Three-dimensional printing (3DP) is a now common tissue engineering and regenerative medicine technique that has broad application with a wide variety of materials, techniques, and scaffold types. The most common of these is extrusion-based 3DP or fusion-deposition modeling (FDM)

in which a motion control platform or dispensing head is utilized to extrude material. In general, with this style of printing a solution of biomaterial (bio-ink), cell suspension, or hydrogel is loaded into a syringe or pressure-based system and deposited in a layer-by-layer fashion to build a 3D object. 3DP has been utilized to print many of the materials commonly used in reproductive tissue engineering including alginate, collagen, fibrin, gelatin, hyaluronic acid, PEG, and a variety of bioinks (including cells suspended in hydrogels, dECM, etc.). In the ovarian context 3DP has been used to fabricate a bioprosthetic ovary in which a gelatin scaffold with 60° advancing angle struts spaced 600μm was printed (15). This resulted in scaffolds with struts ~250μm and a pore size (edge of one strut to the other) of ~350μm, which was shown to maintain the three-dimensional structure of ovarian follicles (15). This scaffold was seeded with murine follicles and transplanted and restored fertility and endocrine function to ovariectomized mice (15). Additionally, these scaffolds became highly vascularized, resulted in live births, supported natural mating and maternal lactation, which all together indicate a physiologically relevant restoration of fertility and endocrine function for these animals (15). However, room for improvement exists for the next generation of bioprosthetic ovaries to support a heterogeneous population of cycling follicles, including maintenance of a quiescent pool of primordial follicles, and promoting the healthy progression through folliculogenesis of activated growing follicles though we anticipate translation from mice to humans will be more complex. Towards this end we can examine ink composition/rigidity tailored towards replicating native ovarian physical and biochemical cues which will require leveraging new 3DP techniques.

Freeform Reversible Embedding of Suspended Hydrogels (FRESH) printing is a printing technique that allows printing of soft materials that are otherwise unprintable using traditional 3DP techniques in air due to poor print fidelity of these materials. Previous work involved

compromising the biologically relevant properties of a material to enhance their printability (220-223). Instead, using the FRESH printing method bioinks are extruded into a sacrificial yield-stress support bath, meaning that the material acts as a solid until a sufficient shear or yield stress is applied, that holds the bioink in place until it is cured or cross-linked. In FRESH printing the yield stress is caused by the syringe needle passing through the material. Printing into this support bath de-couples bioink cure time or cross-linking mechanisms from print fidelity with the support bath limiting the effects of gravity on the print. The support material is made up of hydrogel microparticles and a surrounding aqueous phase, which are stable at room temperature but can be melted at 37° C and washed away. This method has been used to print a wide array of materials including dECM alongside more traditional materials such as alginate, collagen, fibrinogen, and hyaluronic acid (224). It has also been used to print complex structures including replicating a human femur from a CT scan and whole organs including an embryonic chick heart, though these were proof of concepts and not tested for functionality (224). Using this process, researchers printed fibers embedded in 3D printed hydrogel components to achieve significant structural reinforcement (e.g., tensile modulus improved from 56.78 ± 8.76 to 382.55 ± 25.29 kPa and tensile strength improved from 9.44 ± 2.28 to 45.05 ± 5.53 kPa) of their prints using a wide range of material types, sizes, and in both 2D and 3D embedding patterns displaying the incredible flexibility and tunability of materials printed using the FRESH method (405). FRESH printing has been used to print vascular achieve mechanically stable small-scale hydrogel construct incorporating vascular network with a structure area and length that were three times higher compared to other bioinks using a combined 1.0% fibrin-0.5% hyaluronic acid bioink, which was previously impossible with traditional extrusion methods (405). In addition to improved construct fidelity, increased biomimicry that FRESH printing methods allows, this technique is known to

have a cell viability of 99.7% in cell laden inks thanks to low cellular toxicity of cross-linking and tunable ink viscosity (405). Leveraging this technique, we can print otherwise unprintable materials including ovarian dECM which is the focus of **Chapter 3** of this dissertation in which we characterize and implement compartment specific dECM hydrogel inks.

Model Animal Choice

Mammalian ovaries are incredibly diverse in both their structure and development across species from interstitial tissue organization, degree of compartmentalization, and organogenesis. A significant amount of research previously has been done in mice examining follicle activation, folliculogenesis, aging, and *in vitro* follicle culture. However, we have chosen to focus on the use of, initially, porcine, and later bovine models for our examinations of physical and biochemical cues in the mammalian ovary. Ovarian regionalization or compartmentalization differs significantly across species and these compartments are more similar in size and composition in the ovaries of pigs and cattle in comparison to the ovaries of rodents including both mouse and rat ovaries in comparison to human ovaries (225). Large animal models, particularly bovine and porcine models (though other large animal models have also seen use including ovine and equine) have been used to gain foundational understanding of ovarian function in humans (225). Both porcine and bovine models see use because their ovaries contain defined regions including, medulla, cortex, and tunica in proportions similar to a human ovary (226). Further, humans are mono-ovulatory animals and both pigs and mice are poly-ovulatory, which informed our later transition to a bovine model which was undertaken primarily to focus on an animal model that was mono-ovulatory in place of poly-ovulatory (226).

Goals of This Thesis

There are multiple objectives in this Dissertation. The first objective is to provide an introduction to ovarian biology, mammalian folliculogenesis with a focus on follicle activation, the matrisome, and the importance of physical and biochemical cues to biological processes in the ovary using existing literature. Additionally, this section will cover the ideal properties of a bioprosthetic ovary and current tools that are used in *in vitro* follicle culture alongside a discussion of why porcine and bovine models are ideal for the work detailed within. These are outlined in current chapter, **Chapter 1.** The next two chapters will seek to address the overall hypothesis of this dissertation: "Physical and biochemical properties of the ovary differ between compartments and that these properties affect the maintenance of the ovarian reserve and follicle activation." **Chapter 2** will address the research aim "Interrogating the composition of the matrisome across ovarian compartments and follicle stages" with the hypothesis of the section being that "The ovarian cortex and medulla have distinct matrisome compositions, which contributes to the process of folliculogenesis". This chapter is adapted from a paper published in *Scientific Reports* (Henning, et al 'Proteomic analyses of decellularized porcine ovaries identified new matrisome proteins and spatial differences across and within ovarian compartments' *Scientific Reports. 2019*). **Chapter 3** will cover the mapping of ovarian rigidity across compartments, an examination of matrisome protein distribution in a bovine model, and the development of new *in vitro* tools to dissect the matrix-follicle interactions using two candidate proteins: EMILIN1 and AGRN. The overall aim of this section is twofold. The first aim being "Investigating the physical properties of the bovine ovary and contributions to follicle activation" with the hypothesis that "The ovarian cortex is stiffer than the medullary compartment and that this property is primarily derived from the Extracellular Matrix." The second aim focuses on the candidate proteins EMILIN1 and AGRN with the aim of "Developing *in vitro* tools for the selective depletion of candidate proteins and those that duplicate

the native physical properties of the native tissue" This work is adapted from an article currently submitted to the preprint archive BIORXiV and currently in preparation for submission. **Chapter 4** summarizes the results presented in this dissertation, details future directions that can be taken to examine the mechanistic relationship between matrisome proteins and ovarian follicles alongside next-generation proteome and physical cue mapping.

Overall, the results of these studies demonstrate that the physical and biochemical properties of the ovary are significantly different across compartments and depths. For biochemical cues, there were 42 matrisome proteins that were significantly differentially expressed across ovarian depths with 11 novel proteins that had not been previously discovered in the ovary (**Chapter 2**). For physical cues, there was a statistically significant difference in the rigidity of the cortex (8.87±0.80 kPa) versus the medulla compartments (1.04±0.14 kPa) of bovine ovaries (**Chapter 3**). Using dECM derived from the cortex and the medulla in cast gels or 3D printed scaffolds we were able to examine whether or not the physical properties of the compartments was derived from their ECM composition finding a similar relationship between cortex and medulla for both cast and 3D printed materials (**Chapter 3**). For engineering platforms, we developed and implemented a magnetic assisted protein filtration (MAPF) method which we used to selectively deplete two candidate proteins from a cortex derived dECM homogenate prior to use in engineered applications without showing significant changes to off-target proteins (represented by COL1) and additionally measured no changes in rigidity of the depleted materials compared to whole dECM materials (**Chapter 3**). Human derived mesenchymal stem cells (hMSCs) plated on these depleted materials showed no acute toxicity and showed changes to gene expression that was rescued upon restoration of EMILIN1 (**Chapter 3**).

These studies describe the first spatial maps of the ovarian matrisome and the physical properties across ovarian compartments and depths. By examining these and developing novel engineering tools to further investigate the role of specific proteins on folliculogenesis this feeds our underlying knowledge towards creating an effective next generation bioprosthetic ovary.

Chapter 2

Defining the Porcine Ovarian Matrisome

Introduction

The ovary is divided into two visibly distinct compartments: the denser cortex, containing the pool of primordial follicles, or ovarian reserve, and the more permissive medulla containing the majority of activated and growing follicles (41, 42). After activation, follicles respond to soluble signals as well as physical stresses, created by mechanical forces and osmotic shifts, to grow, mature and ovulate (reviewed in 232). It is hypothesized that the two compartments have varying rigidities and that during folliculogenesis the activated follicles migrate into the less rigid medullary compartment of the ovary. It is believed that passage down this rigidity gradient alters cellular responses of the follicle to hormones, which changes gene expression of the cells making up the follicle (69, 159). This is supported by analyzing health, growth and gene expression of isolated murine and primate follicles cultured in different biomaterials (151, 153, 154, 233, 234). However, the relationship between the native extracellular environment or niche and ovarian follicle in the form of signal transduction cues to maintain quiescence or trigger activation continues to remain unclear.

Previous work has shown that a bioprosthetic ovary made with a 3D printed gelatin scaffold restores hormone production and fertility in ovariectomized mice (15). To improve upon this work and move toward translation for human use, a clear understanding of the native environment and how scaffolding components can influence folliculogenesis is required. An appropriately functioning organ will require specific extracellular cues and understanding those cues will inform bioengineering for tissue regeneration. The matrisome provides the ultrastructure that supports the tissue-specific microenvironment in vivo (235). There are several examples of three-dimensional ECM materials providing the ideal transplantable scaffold 20,21 (41, 236-239). This is because

such a scaffold provides the necessary signaling cues that control tissue-specific cell attachment, differentiation, vascularization, and functionality (119, 240).

Previous studies examined the ovarian matrisome of human cortical tissue or whole ovaries (163, 241). However, none have examined the differences between the two main compartments or considered the three-dimensional composition of the ovarian matrisome. The goal of this study was to spatially map the matrisome composition of the ovary in order to determine the ovarian cortical and medullary matrisome signatures using a proteomic-based approach on decellularized tissue. We chose to use porcine ovaries, as they have similar compartmentalization and folliculogenesis waves to human ovaries and can be processed in the same way (242-245). This data and future functional assays will inform an improved bioprosthetic ovary with a better biomimetic scaffold.

Materials and Methods

Porcine ovary processing for protein analysis

Porcine ovaries were purchased from Tissue Source, LLC. Pigs were peri-pubertal (4–6 months old) when sacrificed and ovaries retrieved. Ovaries were shipped overnight in PBS. Porcine ovaries were processed in two ways: (1) *uniform slices:* Upon arrival, ovaries were bisected sagittally through the hilum or axially into two equal halves (Fig. 6). Bisected pieces were further processed using a Stadie-Riggs slicer, which produces 0.5 mm slices (Fig. 6a). Slices were imaged using a pathology scope (Virtus Imaging, PX-XT-PC) and weighed. Sliced tissue was either flash frozen in liquid nitrogen for RNA extraction or proceeded through decellularization steps. (2) *removal of cortex prior to slicing:* Porcine ovaries were bisected sagitally as above. The first two slices (1 mm) of
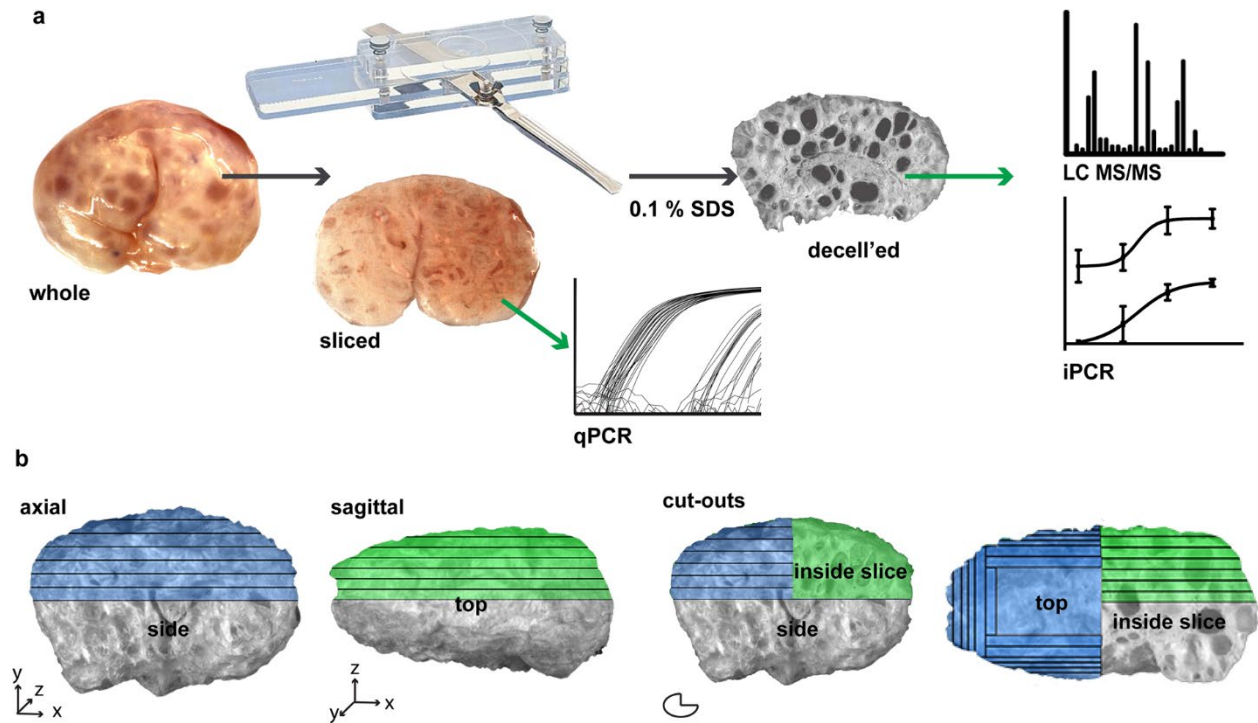
Figure 6. Schematic of (**a**) processing the porcine ovary with a tissue slicer, prior to qPCR analysis, decellularization then proteomics analysis and iPCR validation. (**b**) Ovaries were sliced axially and sagittally. SDS, sodium dodecyl sulfate; decell'ed, decellularized; LC

the ovary were taken and decellularized together as the cortical region. The remaining tissue was pinned and trimmed using a razor blade 1 mm in from the ovarian surface, leaving only medullary tissue. The medulla was then processed into 0.5 mm slices. Trimmed pieces (cortex) were taken whole for further processing as well. All slices were decellularized.

MS/MS, liquid chromatography tandem mass spectrometry; iPCR, immuno PCR.

Porcine ovary decellularization

Decellularization was carried out using 0.1% sodium dodecyl sulfate (SDS, Sigma, 75746) in phosphate buffered saline (PBS, Thermo, 10010023). Slices were placed on a nutator at 4 °C and SDS solution was changed every 24 hours for 48–72 hours prior to protein extraction. Several slices were set aside for DNA extraction (Zymo, D4075) and quantification. Extracted DNA was quantified using a spectrophotometer (MidSci NanoPhotometer, NP60). All slices contained less DNA than the recommended standard of 50 ng/mg of tissue (209) and contained an average of 20.75 ng/mg.

Sample preparation for liquid chromatography tandem mass spectrometry (LC-MS/MS) analysis

Two technical replicates of four porcine ovaries from four separate animals (two ovaries per direction) were used to generate seven slices each in the proteomics analysis. 50 µg of protein was precipitated with eight volumes of cold acetone (Fisher, A18–4) and one volume of trichloroacetic acid (Sigma, T9159-250G) overnight at −20 °C. After washing the pellet with ice-cold acetone, resulting protein pellet was resuspended in 50 µL 8 M urea (Invitrogen, 15505-035) in 400 mM ammonium bicarbonate (Fisher, A643-500), pH 7.8, reduced with 4 mM dithiothreitol (Sigma, 10197777001) at 50 °C for 30 min., and cysteines were alkylated with 18 mM iodoacetamide

(Sigma, I1149) in the dark for 30 min. The solution was then diluted to <2 M urea and trypsin (Promega, V5280) was added at final trypsin:protein ratio of 1:50 prior to overnight incubation at 37 °C with shaking. The resulting peptides were desalted using solid phase extraction on a Pierce C18 Spin column (Thermo, 89873) and eluted in 80 mL of 80% acetonitrile (ACN) (Thermo, 51101) in 0.1% formic acid (FA) (Fisher, LS118). After lyophilization, peptides were reconstituted with 5% ACN in 0.1% FA.

LC-MS/MS data acquisition and processing

Peptides were analyzed by LC-MS/MS using a Dionex UltiMate 3000 Rapid Separation nanoLC and a Q Exactive™ HF Hybrid Quadrupole-Orbitrap™ Mass Spectrometer (Thermo Fisher Scientific). Approximately 1 μg of peptide samples was loaded onto the trap column, which was 150 μm × 3 cm in-house packed with 3 μm C18 beads. The analytical column was a 75 μm × 10.5 cm PicoChip column packed with 3 μm C18 beads (New Objective, Inc.). The flow rate was kept at 300 nL/min. Solvent A was 0.1% FA in water and Solvent B was 0.1% FA in ACN. The peptide was separated on a 120-min analytical gradient from 5% ACN/0.1% FA to 40% ACN/0.1% FA. The mass spectrometer was operated in data-dependent mode. The source voltage was 2.10 kV and the capillary temperature was 320 °C. MS1 scans were acquired from 300–2000 m/z at 60,000 resolving power and automatic gain control (AGC) set to 3×106. The top 15 most abundant precursor ions in each MS1 scan were selected for fragmentation. Precursors were selected with an isolation width of 2 Da and fragmented by higher-energy collisional dissociation (HCD) at 30% normalized collision energy in the HCD cell. Previously selected ions were dynamically excluded from re-selection for 20 seconds. The MS2 AGC was set to 1×10^5. All samples were run in duplicate.

Proteomics validation via immuno-PCR (iPCR)

Protein was extracted from porcine ovary slices that were decellularized (as described above). Tissue was placed in a protein extraction buffer (1% SDS, 50 mM Ammonium Bicarbonate, 50 mM NaCl, Halt Protease Inhibitors (100 µL per 10 mL of buffer). Tissue was placed in reinforced 2 mL tubes (Omni International, 19–648) with 2.8 mm polycarbonate beads (Omni International, 19–646). Tissue was homogenized with an Omni BeadRuptor12 in a cold room (Omni International, 19-050 A) using the following settings: six cycles at speed 6.0, 45 s homogenization, 75 s delay between cycles. Homogenate subsequently sonicated on ice 3 times at 75% amplification for one minute. Samples were then centrifuged at 10k rpm for 15 minutes. A 1 mL aliquot was taken from the samples and sample was treated with an SDS-Out kit (Thermo Scientific, 20308). Protein concentration was measured using a BCA method (Fisher Scientific, PI23227). Samples were normalized to a concentration of 1,000 ng/µL using protein lysate buffer from the Taqman Open Kit (Thermo Fisher, 4453745).

Antibodies were biotinylated using EZ-Link Sulfo-NHS-LC-Biotin, No-Weight format kit (ThermoFisher,21327). Antibody information is listed in Appendix A Excess biotin was removed using two cycles of filtration utilizing Zeba Micro Spin Desalting columns, 40k (Fisher Scientific, PI87765). Probes were then tested for suitability using method described under Thermo Fisher's Taqman Protein Assays Probe Development Protocol (Thermo Fisher, 4448549). To compare protein quantity between depths a standard method described in Thermo Fisher's Taqman Protein Assays Sample Prep and Assay (Thermo Fisher,4453745) was used. A four-point dilution series was used with 2000 ng of total protein then serially diluted 1:10. A qPCR machine (Applied Biosystems, QuantStudio 3) was used for running the assay. Because some samples had

undetectable levels of protein, dose curve data are presented as change in CT over no template controls. Two-way ANOVA and multiple t-test based analyses were used.

Gene expression analysis using real-time semi-quantitative PCR (qPCR)

Tissue was flash frozen in liquid nitrogen and stored at −80 °C prior to homogenization. Tissue underwent Proteinase-K digestion (3–4 hours, 37 C, Zymo, D3001-2-5) prior to homogenization using Beadruptor12 in a cold room (6 cycles at Speed 6.0, 45 s shake, 75 S delay between cycles). RNA extraction was done using Zymo mini-prep kit (Zymo, R1054). RNA preps were cleaned and concentrated using RNA-Clean up kit (Denville Scientific, Z5214). Total RNA (0.5 µg) was reverse transcribed into cDNA using Superscript IV Vilo kit (Life Technologies, 11756050). qPCR was carried out using a QS3 using standard SYBR reagent templates from manufacturer. Primer information is listed in Appendix A

Immunohistochemistry (IHC) analysis of matrisome protein candidates

Bisected porcine ovaries were fixed in Modified Davidson's Fixative (MDF) at 4 °C and processed using an automated tissue processor (Leica) and embedded in paraffin. Deparaffinization was carried out using a soap-based method, as described previously (246). Antigen retrieval was performed using citrate buffer (10 mM sodium citrate, 0.05% Tween 20, pH 6.0) in a pressure cooker for 35 minutes. Tissue was blocked using 2% donkey serum (Sigma-Aldrich, D9663), 1% BSA (Fisher Scientific, BP671), 0.1% cold fish skin gelatin (Fisher Scientific, NC9369923), 0.1% TritonX-100 (Sigma-Aldrich, P1379), 0.05% Sodium Azide (Fisher Scientific, AAJ62036K2), in PBS (Fisher Scientific, AAK62036K2). Tissue sections were incubated with primary antibody in block solution (2% Donkey Serum, 1% BSA, 0.1% Cold Fish Skin Gelatin, 0.1% Triton X-100, 0.05% Tween 20, 0.05% Sodium Azide, in 1X PBS; overnight, 1:200). Antibody information is

listed in Suppl. Table 1. Staining visualized using 488 secondary antibody (1 hour incubation, 1:100, Novus Biological, NBP1-75292). Nuclear staining performed using propidium iodide (30 minutes, 1:1000, Sigma-Aldrich, P4864-10ML) or hoescht (30 minutes, 1:200, Sigma, B2261). Sudan Black incubation (15 minutes, 0.1%, Alfa Aesar, J62268-09) was used to reduce background. Stained sections were mounted using clear-mount with PIPES buffer (Electron Microscope, F6057-20ML). Stained sections were imaged (Keyence, BZ-X700), and analyzed using BZ-X Analyzer (Keyence). These analyses were performed across six experiments with at least two technical replicates each for three biological replicates (three ovaries from three different animals). At least two sections for each experiment were not incubated with the primary antibody and acted as our "no primary controls". These sections were used to set the exposure settings for that fluorescent channel to reduce the background fluorescence and reveal secondary (fluorophore) binding to primary antibodies. Additional controls were used to confirm the specificity of each antibody to our protein of interest within the ovarian tissue section. Primary antibodies were incubated with 10 times more peptide (based on antibody molarity) and incubated at room temperature for 1 hour to block specific binding (Appendix A. Table 2). The IHC protocol above was followed with these blocked antibodies (Appendix A. Fig. 1).

Proteomic data processing and statistical analysis

A total of 64 LC-MS/MS raw files were analyzed. Protein Tandem MS data was queried for protein identification and label-free quantification against the SwissProt *Sus scrofa* database using MaxQuant (247, 248). The following modifications were set as search parameters: peptide mass tolerance at 6 ppm, trypsin digestion cleavage after K or R (except when followed by P), two allowed missed cleavage site, carbamidomethylated cysteine (static modification), and oxidized methionine, protein N-term acetylation (variable modification). Search results were validated with

peptide and protein false discovery rate (FDR) both at 0.01. Proteomic stringency was increased by requiring: (1) all proteins to have more than one identified peptide, (2) proteins must have peptide reads in two planes to allow for intersections, (3) and peptides must have a read in each biological replicate to be considered for analysis. Proteins that passed these three rules were used for further analysis using a custom SAS script (see Supplemental Files). Peptide intensities were log transformed to control for multiplicative errors associated with FT-ICR MS. These intensities were then standardized to allow unbiased comparisons between peptides of the same protein. Least squares (LS) means were used to estimate differences in protein composition across depths, and differential expression in proteins. All annotation of data was performed utilizing Panther (http://www.pantherdb.org/, version 14.1, 2018) and MatrisomeDB (http://matrisomeproject.mit.edu/, version 2.0, 2016) databases, conversion of unknown IDs were performed using DAVID (https://david.ncifcrf.gov/, version 6.8, 2016). Statistical analyses for qPCR and iPCR data were performed using GraphPad Prism (version 8.1.2) software. qPCR results were subjected to unpaired, two-tailed t tests with $\alpha = 0.05$ and iPCR data was subjected to a two-way ordinary ANOVA with $\alpha = 0.05$ and multiple t tests where the statistical significance was determined by the Holm-Sidak method with $\alpha = 0.05$; each group (cortex, medulla, etc.) was analyzed individually without assuming consistent standard deviations. All bar graphs display means with standard errors. Ranges of significance are described in each figure legend and P values for comparisons that are not significant are listed in the text.

Literature search of matrisome proteins

Literature searches were performed using the National Institutes of Health (NIH) PubMed database (ncbi.nlm.nih.gov/pubmed) with the following search terms "((protein name) OR protein ID) AND ovary" and "((protein name) OR protein ID) AND ovarian". Articles were scanned to determine if

and how the protein was identified in the ovary and articles that investigated only non-mammalian species were omitted from further analysis. The remaining articles were reviewed to identify the function of the protein Appendix A. Table 4. For those proteins that had no results that met the above criteria, the GeneCards human gene database (genecards.org) was searched for aliases to our protein names and IDs and additional searches were performed where necessary. Proteins without identified articles that include characterization or potential function of that protein within the mammalian ovary have "none" and "unknown" in the corresponding fields. Proteomic analysis data on ovarian tissue or cells that were provided as figures or supplemental spreadsheets were searched using protein names and protein IDs.

Results

Ovarian processing

We sought to identify and spatially map the matrisome of porcine ovaries. Bisected porcine ovaries were processed sagittally and axially into uniform 0.5 mm slices (to 3.5 mm depth) to create intersecting planes that together created complete coverage of 1/8th of the organ (Fig. 6a,b). The cortical region that contains the primordial follicle pool is within the first 0.5 mm slice (Appendix A. Fig. 2). Samples were decellularized prior to LC-MS/MS and iPCR analyses and native samples were used for comparative mRNA expression (Fig. 3a). A total of 6,711 peptides were detected with an $FDR < 0.01$, these peptides were identified as belonging to 615 proteins. Following data filtration with our three stringency rules, the remaining 440 proteins were analyzed using our SAS-based bioinformatics pipeline (see Suppl. SAS script). 134 proteins were significantly differentially expressed across depths with LS-means.

Classification of identified proteins

Of the 440 proteins identified, 82 are core matrisome (collagens, proteoglycans, ECM glycoproteins) and ECM-associated (ECM regulators, secreted factors, and ECM-affiliated proteins) proteins (Fig. 7a). Secreted factors, including a calcium binding protein (S100A11) and the growth factor pleiotrophin (PTN), were identified in our analysis; however, they failed to pass the stringency filters. Of the 82 matrisome proteins 42 were shown to be significantly differentially expressed across depths. The core matrisome included 55 and 32 proteins for our total and significantly differentially expressed proteins respectively. Our data includes 11 collagens, 7 of which were differentially expressed; 36 ECM glycoproteins, 20 of which were differentially expressed, and 8 proteoglycans, 5 of which were differentially expressed. The matrisome-associated proteins included 16 ECM regulators and 11 ECM-associated proteins of which 6 ECM regulators and 4 ECM-affiliated proteins were significantly differentially expressed.

Gene ontology analysis subdivided the proteins into 11 biological process (Fig. 7b), 7 cellular component (Fig. 7c), 24 protein class (Fig. 7d) and 8 molecular function (Fig. 7e) categories. The proteins represented localization, response to stimulus and reproduction processes (Fig. 7b). Specifically, zona pellucida proteins were identified, which are specialized ECM glycoproteins that surround the oocyte. Proteins within both the intracellular and extracellular compartments were identified including nucleic acid binding proteins, organelle, extracellular matrix, extracellular region, and cell junction proteins (Fig. 7c,d). Most proteins that were identified as significantly differentially expressed were within the nucleic acid binding protein class (17.2%), followed by extracellular matrix proteins (3.4%), cytoskeletal proteins (9.3%), cell junction (0.3%), cell adhesion (4.0%),
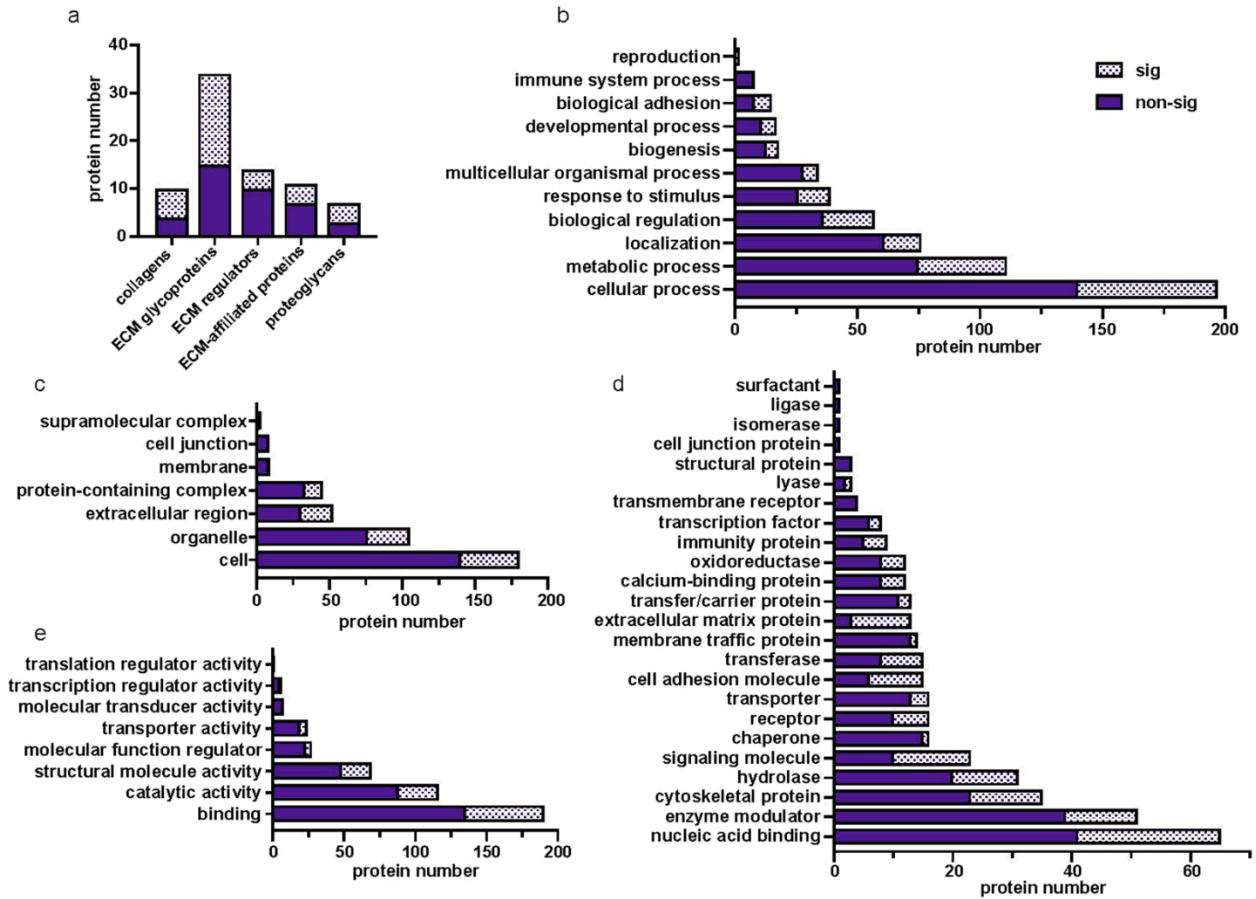
Figure 7. Number of proteins identified within (a) matrisome (b) biological process, (c) cellular component, (d) protein class, and (e) molecular function categories. sig, significantly differentially expressed.

and structural proteins (0.8%, Fig. 7d). 80% of all gene ontology categories contained at least one protein that was significantly differentially expressed across depths (Fig. 7b–e).

Validation of select proteins

A selection of core ECM proteins were further evaluated and validated. We chose collagens I (COL1A2) and IV (COL4A2), Agrin (AGRN), Extracellular Matrix Protein 1 (ECM1), Elastin Microfibril Interfacer 1 (EMILIN1), Fibronectin (FN1), Transforming Growth Factor Beta 1 (TGFB1), Vitronectin (VTN), and Zona Pellucida Glycoprotein 3 (ZP3). LS means data from both sagittal and axial slices were combined to determine standard deviations from LS means for each protein across depths (0.5 mm – 3.5 mm, Appendix A. Fig. 3). COL1 and EMILIN1 expression was consistently lower in 1.0–3.5 mm slices when compared to 0.5 mm expression. COL4A2 was consistent across depths. AGRN, FN1, TGFB and ZP3 had a peak in expression around 1.5 mm, while VTN had a peak at 2.0 mm. ECM1 had undetectable levels in the 0.5 mm slices and remained relatively consistent at 1.0–3.0 mm.

The results of these selected proteins were validated by comparing the most superficial (0.5 mm, cortex) to the deepest slices (3.5 mm, containing deep medulla) using qPCR and iPCR and relating these to peptide reads from the proteomic analysis at the same depths (Fig. 8). While all proteins chosen for this analysis were significantly differentially expressed across depths (0.5 mm–3.5 mm), except for COL4A2, a comparison of the 0.5 mm to 3.5 mm samples did not always produce significant differences. AGRN
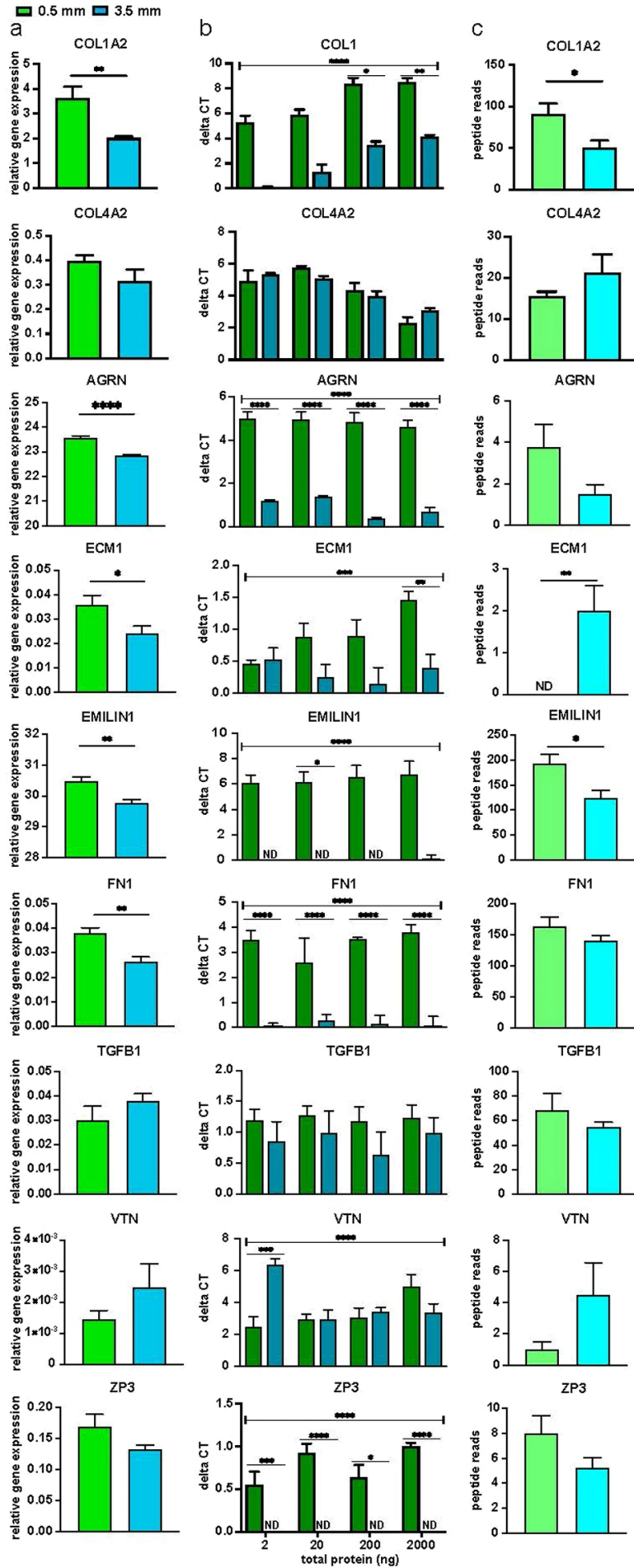
Figure 8. Comparison of protein or gene expression between most superficial and deepest slice. A selection of matrisome proteins were evaluated within 0.5 mm and 3.5 mm slices using (**a**) qPCR (n = 4–6 per slice), (**b**) iPCR (n = 4), and (**c**) peptide reads (n = 8 per slice, 4 ovaries with 2 technical replicates each). Bars represented as mean, SEM; *P < 0.05; **P < 0.005; ***P < 0.0005; ****P < 0.0001; ND, not detected.

(p = 0.083), and ZP3 (p = 0.110) were trending towards greater peptide reads in 0.5 mm samples compared to 3.5 mm, while COL1A2 and EMILIN1 were significantly more highly expressed in the 0.5 mm samples (Fig. 8c). ECM1 (p = 0.005) and VTN (p = 0.140) were more highly expressed in 3.5 mm samples, and COL4A2 (p = 0.228), FN1 (p = 0.216) and TGFB1 (p = 0.368) were not significantly differentially expressed by our analysis (Fig. 68). Transcriptional and iPCR analyses that matched the statistical significance of the peptide reads were considered similar to the proteomics data. From the pool of selected proteins, 6/9 proteins, COL1A2, COL4A2, EMILIN1, AGRN, VTN, and ZP3, had similar gene expression (Fig. 6a) and iPCR profiles (Fig. 8b) to the proteomics results (Fig. 8c). One protein, FN1 was expressed significantly more in the 0.5 mm slices by qPCR and iPCR, but this difference did not reach significance when comparing the peptide reads from these slices. Additionally, 2/9 proteins, TGFB1 and ECM1, did not match with expected trends based on our peptide reads. ECM1 had significantly higher protein abundance and higher gene expression at 0.5 mm and 3.5 mm counter to the expected trend based on the peptide reads.
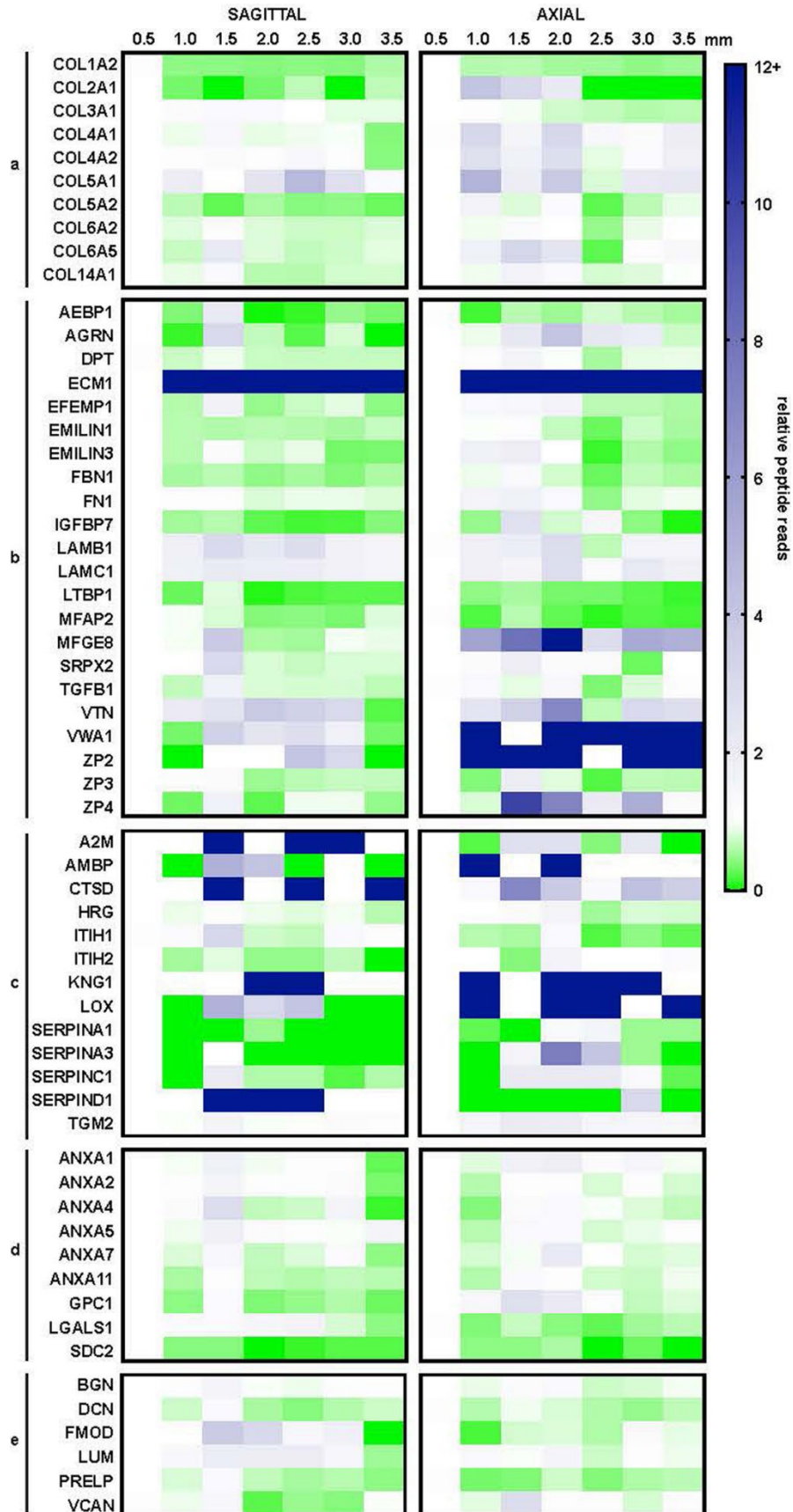
Figure 9. Relative protein reads of matrisome proteins. Proteins within matrisome categories, (a) collagens, (b) ECM glycoproteins, (c) ECM regulators, (d) ECM-affiliated proteins, (e) proteoglycans are represented as relative reads to the average reads at 0.5 mm.

Spatial composition of ovarian matrisome

Proteins were grouped into their matrisome protein categories and examined across depths in the two anatomical directions (Fig. 9). In our data, there was greater expression of ECM-affiliated proteins (Fig. 9d) and proteoglycans (Fig. 9e) in the cortex (0.5 mm) than the majority-medulla slices (1.0 mm–3.5 mm). Some proteins, such as COL1A2, EMILIN1 and SDC2 had consistently less protein reads across 1.0–3.5 mm depths in comparison to 0.5 mm (cortex slice) in both sagittal and axial processing methods. Other proteins, such as COL5A1, ECM1 and LAMC1 had consistently more protein reads in the majority medulla (1.0–3.5 mm) samples than the cortex (0.5 mm). Still other proteins were more heterogeneous or did not produce consistent trends in expression across ovarian depths or between sagittal and axial processing.

Localization of Protein candidates

We identified the protein distribution of nine proteins across ovarian compartments and within ovarian cells with IHC. Qualitative examination of these proteins as an overview across compartments (Fig. 10a) and within small (Fig. 10b) and growing follicles (Fig. 10c), revealed that COL1, AGRN, FN1, TGFB and VTN are abundantly expressed in the ovarian surface epithelium (OSE). Most proteins were localized to at least some stromal cells; ZP3 did not. ECM1 and FN1 appeared more abundant in medullary over cortical
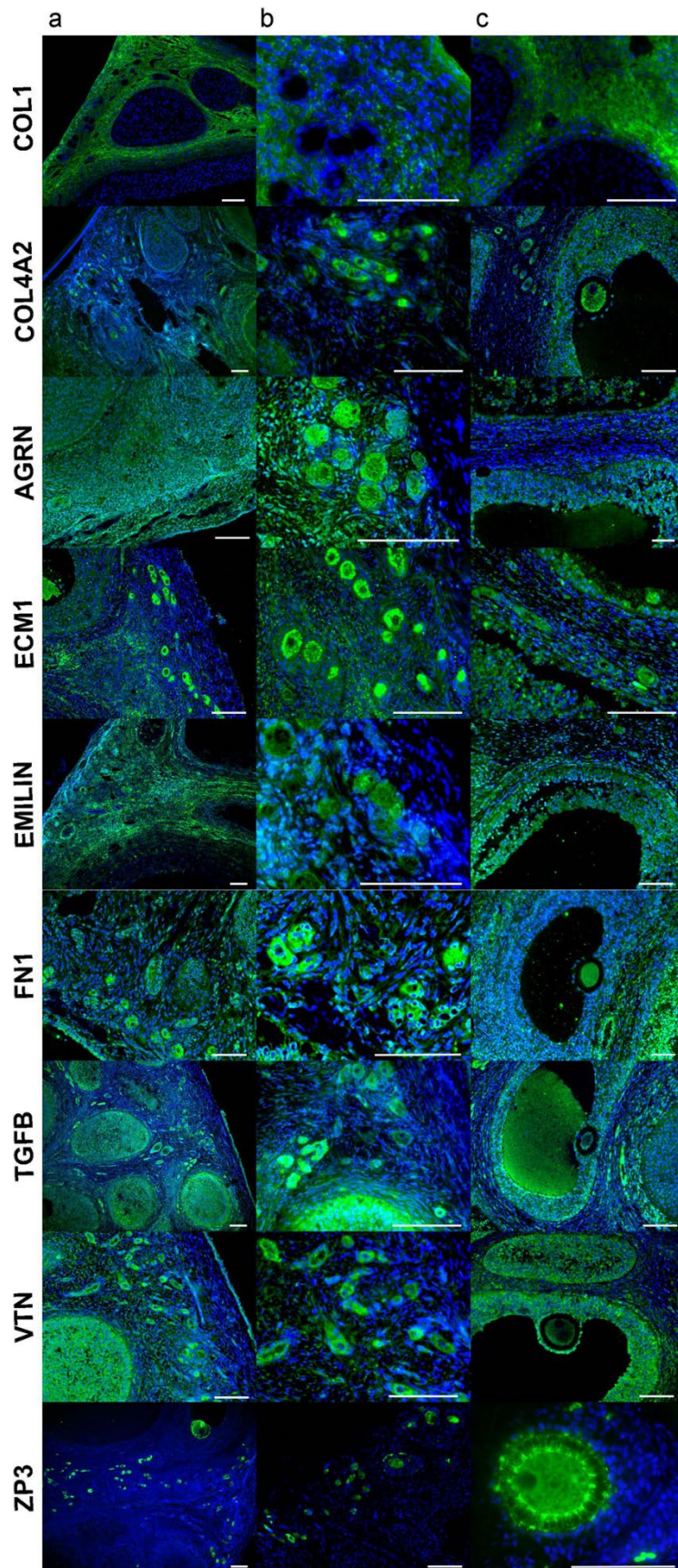
Figure 10. IHC analysis of selected proteins in (a) an overview across compartments, (b) small follicles, and (c) growing follicles. Scale bar, 100 μm.

stromal cells. COL4A2 was localized to granulosa cells of small and growing follicles and antral follicle oocytes. EMILIN1, FN1, TGFB and VTN were also localized to granulosa cells of small and growing follicles. AGRN was expressed in all cell types including oocytes and granulosa cells, while ECM1 expression was localized to the outer perimeter of oocytes. FN1 was localized to the outer perimeter of small oocytes. ZP3 was expressed in the oocyte and was more highly localized to the transzonal projections in large growing follicles.

Protein expression across compartments

We used an additional processing technique, method 2, to examine protein expression differences across the defined ovarian compartments. We removed the first 1 mm of tissue using a Stadie-Riggs slicer, and then trimmed 1 mm of tissue from the edge of the remaining tissue. From the remaining tissue, we obtained two slices in the sagittal orientation, which we refer to as intermediate (medulla 1) and deep medulla (medulla 2, Fig. 11a). This produces a lower resolution (1 mm and fewer slices) in comparison to processing method 1 but removes the cortical region from the medullary slices (represented as 1.0 mm–3.5 mm in method 1).

We chose four proteins to investigate, COL1, AGRN, EMILIN1, and VTN (Fig. 11b) by iPCR. All proteins had similar expression patterns to the previous methods with COL1,
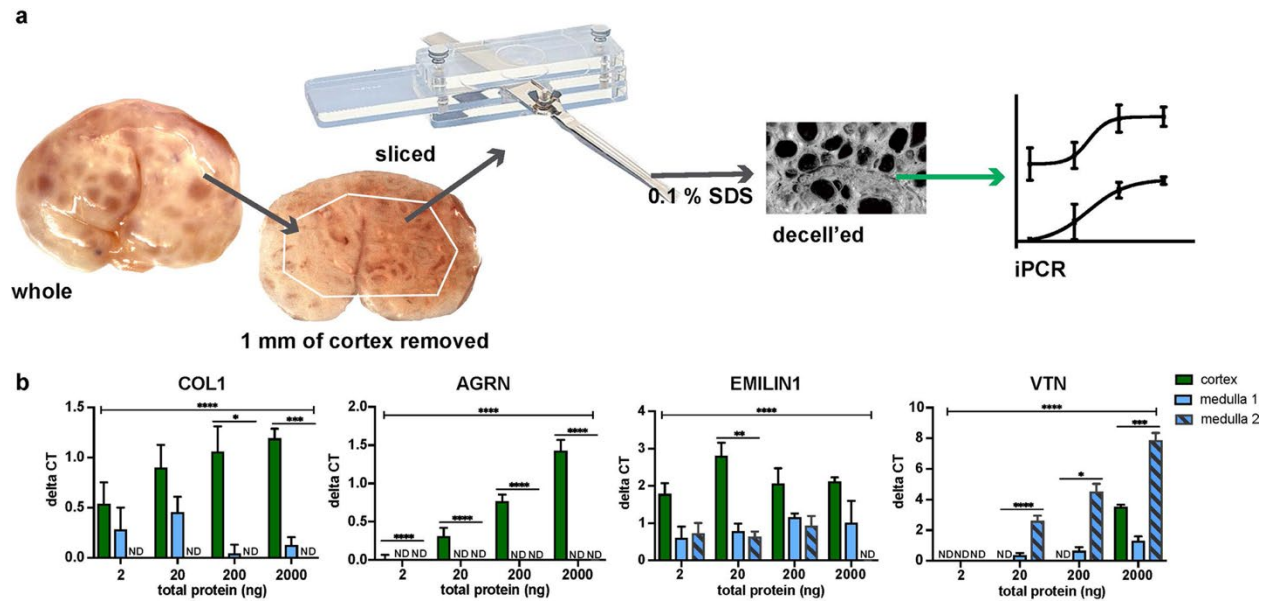
Figure 11. Schematic of (**a**) processing the porcine ovary by removing ~ 1 mm from the ovarian surface followed by a tissue slicer, prior to decellularization then iPCR analysis. (**b**) COL1, AGRN, EMILIN1 and VTN protein expression in cortex region and slices of medullary tissue (n = 4 per slice). Bars represented as mean, SEM; *P < 0.05; **P < 0.005; ***P < 0.0005; ****P < 0.0001. iPCR, immuno PCR; ND, not detected.

AGRN and EMILIN1 having higher abundance in the cortex compared to the medulla and VTN had higher abundance at the medullary slices compared to the cortex. This indicates that the small amount of cortex present in medullary slices used in our proteomic analysis does not greatly alter the protein composition signature of the compartment.

Visualization of COL1A2 and EMILIN1 expression across intersecting planes

To visually represent the relative expression of COL1A2 and EMILIN1 spatially across the ovarian area analyzed, we normalized the peptide reads for each protein to its universal mean (Fig. 12a,c). This was then represented visually as axial slices superimposed over each sagittal slice from 0.5–3.5 mm (Fig. 12b,d). Because the samples analyzed only represent half of the ovary in each direction, the axial slices covered half of each sagittal slice. There were patterns of increased expression in the cortical regions of both protein maps represented by the 0.5 mm sagittal column and 0.5 mm axial row. This was more confined to the 0.5 mm depth in both directions in COL1A2 in comparison to EMILIN1, which had an increase in expression to the 1.5 mm depth in the sagittal direction.

Figure 12. Heatmaps of (a,b) COL1A2 and (c,d) EMILIN1 expression at sagittal and axial intersections (a,c) relative to universal mean of peptide reads. (b,d) Schematic representation of expression at axial depth slices (top to bottom) visualized on each sagittal slice (left to right).
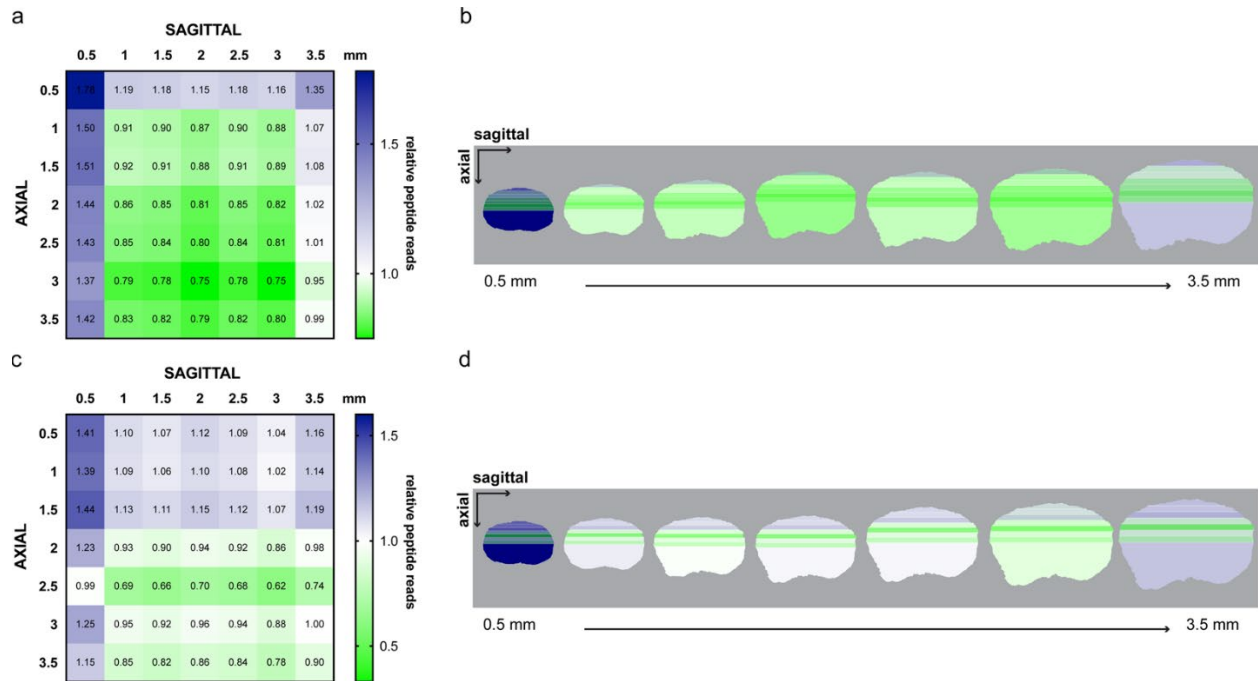
Discussion

This work describes a pipeline for mapping matrisome proteins across an ovary and could be utilized in other organs to identify spatial or compartmental differences in matrisome protein content. With this analysis, the quantity of proteins can be represented at a resolution of 0.5 mm × 0.5 mm × ovary width with full coverage of 1/8th of the ovary. The processing techniques utilized previously described decellularization methods that had removed significant cellular contents while maintaining the integrity of the scaffold as detected by scanning electron microscopy (41). This method enriches matrisome proteins and reveals their relative spatial quantities (249). While the decellularization and stringent criteria used for our analyses are meant to reveal robust matrisome proteins within the ovary, these techniques may omit important proteins. Additionally, modifications that would reveal the activity status of a protein are also not revealed in bottom-up proteomics analyses. However, these data have provided novel insights into matrisome quantity and compartmentalization and experiments that reveal the roles of matrisome proteins in controlling folliculogenesis were selected from this analysis and are ongoing.

While pigs are poly-ovulatory mammals, and humans are mono-ovulatory, there were several reasons for choosing porcine ovaries for this study. Unfortunately, there are no perfect models for human ovaries; some monkeys have premeiotic germ cells after birth and monkey ovaries are smaller than human ovaries and would not result in the same resolution that we achieve with our 0.5 mm slicer of a larger ovary (250-252). The follicular waves are more similar in porcine ovaries to humans than other mono-ovulatory species like cows or sheep, which have short follicular, versus luteal phases and more intra-ovulatory waves than humans (250). These may be important distinctions as we interrogate the effects of these matrisome proteins on folliculogenesis. There may be universal and intra-compartmental differences in matrisome quantity and composition as

the ovary grows in size and develops from prepubertal ovaries that contain primordial follicles exclusively to post pubertal ovulating ovaries. The ovaries that were analyzed were from peripubertal animals, where they are not reproductively mature and are not cycling, but there were follicles present at each stage within the tissue (Appendix A. Fig. 2). The primordial follicle compartment was also within the first slice of 0.5 mm and was important for this analysis. Finally, there is significant precedent for using porcine materials in human regenerative medicine (182, 253-255), which is an important consideration for our planned downstream applications of utilizing this information to create informed biomaterial inks for an engineered ovarian transplant.

Ovary processing method 1, where the organ is sliced in a uniform manner, resulted in the 1.0–3.5 mm slices containing some cortical tissue (at 0–0.5 mm from the edge). Because the differences in the cortical versus the medullary compartment may be essential in identifying proteins that influence quiescence versus activation and growth of ovarian follicles, we chose to test an additional processing method. This method would produce a map at a lower resolution but removes the cortical tissue from the analysis of medullary slices. We found that COL1, AGRN, EMILIN1 and VTN protein expression was consistent with the comparison of the 0.5 mm to 3.5 mm slices from the previous method, indicating that the cortical tissue did not significantly contribute to the analysis of the mostly-medulla slices. Additionally, some differences were detected between the intermediate (medulla 1) and deep medulla (medulla 2), indicating that the heterogeneous expression of proteins within the medulla, demonstrated by the sagittal and axial heatmaps, is preserved during this processing method, and is not solely attributed to the addition of cortical tissue in these slices.

There have been previous reports examining the ovarian proteome with one focusing on the ovarian matrisome (163, 241). However, this study focused solely on the human ovarian cortex

and did not examine the composition of the medulla. Our study and the previous study performed on cortical tissue from human ovaries, both found a similar number of matrisome proteins (82 versus 85, respectively) and they were dispersed among the same matrisome sub-categories (163). The previous study found four secreted factors, including S100 proteins; however, these proteins were not detected or were removed here for failure to meet the stringent analytical criteria. This exclusion may be due to the reduction in peptide reads due to the decellularization treatment of our ovarian slices prior to proteomic analysis. The proteomic analysis described here identified matrisome proteins that were previously not identified in mammalian ovaries or have only been identified in transcript screens including collagen subunits (COL5A1, COL5A2, COL6A5), ECM glycoproteins (AEBP1, AGRN, DPT, EMILIN3), ECM-affiliated proteins (ANXA7, GPC1, SDC2) and a proteoglycan (BGN) (Appendix A. Table 4). Additionally, this study aimed to identify differences in matrisome protein abundance between ovarian compartments and was able to spatially map these across depths of the ovary.

The spatial analysis performed here revealed proteins that may control folliculogenesis. The largest number of matrisome proteins that were identified and were significantly differentially expressed across depths were glycoproteins, a class of matrisome proteins that can facilitate the translation of the extracellular environment into signal transduction cues (119). Our dataset revealed two glycoproteins, AGRN and EMILIN1, which have not been functionally described in the normal ovary but have been shown to be involved in important pathways that translate extracellular or mechanical signals into cellular responses via Hippo and PI3K-AKT associated pathways in other organs (177, 256). Both of these proteins were significantly differentially expressed across depths and compartments in the ovary. However, EMILIN1 expression decreased deeper into the ovary, while AGRN (FN1 and TGFB) had peaks in protein reads at 1.5 mm depths (Appendix A. Fig.

3c,g). This peak may correspond to an area with more growing follicles, as each of the proteins were localized to follicles by IHC and this pattern matches with that of ZP3 (257) (Appendix A. Fig. 3i). Localization of the protein to follicular cells versus stromal cells will be important to identifying structural support proteins that may be used for creating biomaterial scaffolds for isolated follicles. FN1 expression appears greater in the cortical slices, by qPCR and iPCR of 0.5 versus 3.5 mm slices (though not significantly different by peptide reads for these slices). However, FN1 may be more useful as a structural protein for creating the medulla, as it is localized by IHC to stroma around growing follicles (41, 258).

In addition to biochemical signals and structural support, matrisome proteins also provide physical cues. Compression of primordial follicles is required for them to remain quiescent in murine ovaries (158). Digestion of the ovary with collagenase IV and trypsin released the primordial follicles from the ECM-associated stress as indicated by loosening of actin stress fibers and a progression in granulosa cell morphology from squamous to cuboidal. Growing these enzyme-treated ovaries in a pressure chamber reversed this phenotype and the primordial follicles were maintained in the cortex of the ovary (158). Future studies linking how the matrisome composition directly relates to the physical forces on the follicles and the resulting follicle behavior will reveal essential protein composition, ratios, and localization in relation to quiescent versus growing follicles. The technique described here looks to provides a unique toolset to identify matrisome proteins that are differentially expressed depending on compartment and spatial location. This pipeline will play a key role in identifying essential proteins that influence folliculogenesis to better inform biomedical engineering approaches to tissue regeneration.

Chapter 3

The matrisome contributes to the increased rigidity of the bovine ovarian cortex and provides a source of new bioengineering tools to investigate ovarian biology

Introduction

The ovary is compartmentalized into two regions, the cortex, and the medulla. The outermost of these is the cortex containing the quiescent primordial follicles which make up the ovarian reserve while the innermost compartment, the medulla, contains most growing follicles. The ovarian extracellular matrix (ECM) can affect hormone availability and responsiveness by sequestering, trafficking, or presenting factors including androgens and estrogens via sequestration of sex hormone binding globulin (83, 130). Significant work has shown a role for the mechanical control of follicle activation and folliculogenesis using *in situ* primordial follicles or isolated growing follicles. These experiments revealed that primary follicles, found within the cortical region of the ovary, grow better when encapsulated in higher percentages of alginate while larger follicles, generally found in the medullary region, grow better in lower percentages (45, 151, 153, 154, 233, 266). In fact, culturing a secondary follicle in a high percentage alginate results in transcriptional changes and increased androstenedione production (150). Additionally, exogenous physical pressure has been shown to maintain quiescence in primordial follicles that are released from their immediate environment, while disruption of the surrounding tissue induces increased primordial follicle activation via dysregulation of the HIPPO pathway (150, 158-160, 182). The composition and distribution of matrisome proteins were recently mapped across the porcine ovary. Forty-two matrisome proteins were significantly differentially expressed across the cortical and medullary compartments, revealing some proteins that may play critical roles in regulating primordial follicle activation and growth (43). Here we sought to further understand the physical properties of a mammalian ovary that contains distinct ovarian compartments and identify how the matrisome may contribute to the properties within these compartments. Furthermore, we created matrisome-

based biomaterials and developed additional tools for *in vitro* investigations to explore the contribution of matrisome proteins, EMILIN1 and AGRN, found to be differentially distributed across ovarian compartments. This data and future functional assays will inform an improved bioprosthetic ovary.

Two candidate proteins: AGRN and EMILIN1

The matrisome provides biochemical alongside structural support. Matrisome proteins can create concentration gradients of growth factors and hormones and provide biochemical cues that are interpreted by cell surface receptors (115-121). To find potential signaling cues we used unbiased proteomics screens to map the ovarian matrisome (**See Chapter 2**). By comparing both expression patterns, found using LS-means analysis with the expression of known proteins that were associated with the ovarian cortex (COL1) or follicle activation (ZP3), and immunofluorescence data to localize proteins around primordial or primary follicles we were able to identify candidate proteins for modulating primordial follicle activation. Two candidates were identified that fit these criteria: Elastin microfibrillar interface protein 1 (EMILIN1), a matrisome glycoprotein, and Agrin (AGRN), a matrisome proteoglycan (43).

Elastin microfibril interface-located protein 1 (EMILIN1), is a glycoprotein which associates with elastic fibers at the interface between elastin and microfibrils and may play a role in the development of elastic tissues including large blood vessels, dermis, heart, and lung. Beyond providing elastogenesis and mechanical properties, these
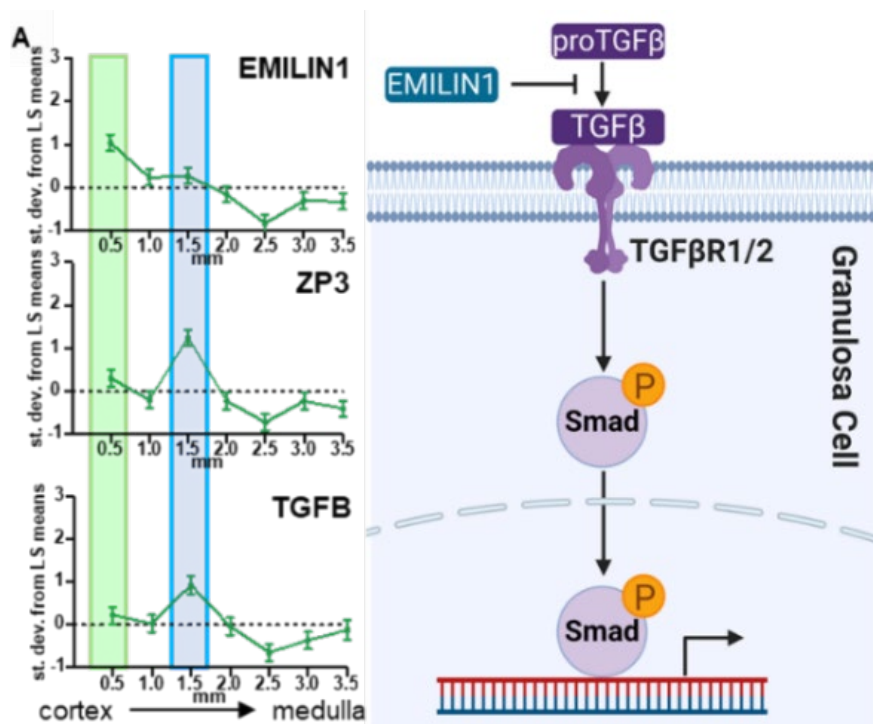
Figure 13. EMILIN1 may inhibit follicle activation by disrupting TGFB signaling. (A) LS-Means showing high concentration of EMILIN1 located with primordial follicles (green) decreasing towards depth with activated/growing follicles (blue) coinciding with an increase in TGFB and ZP3. (B) EMILIN1 inhibits proTGFB processing, inhibiting TGFB signaling through SMADs. This inhibition provides dose-dependent SMAD signaling that drives follicle activation/quiescence.

molecules are linked to a myriad of molecular signaling pathways (162). Previous proteomics data in humans and pigs have identified EMILIN1 in the ovary (43, 163). Using matrisome maps based on our proteomics work in pigs we found that EMILIN1 is most highly expressed in the cortex (**Figure 13**) (43). The level of EMILIN1 decreases through to the deep medulla, but ZP3 (a marker of activated follicles) is more abundant at 1.5mm which is the depth at which activated/growing follicles reside. A study by Ouni, et al done in human ovaries showed that EMILIN1 was localized to primordial follicles in both pre- and post-pubertal samples with higher EMILIN1 being found around primordial follicles as compared to either primary or secondary staged follicles (164). EMILIN1 has been shown to interact with TGFβ-mediate signaling, primarily in cardiac and other organ systems (165-167). The TGFβ pathway itself is ubiquitously expressed and the super family of TGFβ associated proteins includes multiple growth factors (168). in the ovarian context multiple studies have implicated TGFβ-mediated signaling as being involved in other ovarian processes including early ovarian development, homeostasis, and follicle development (168). Specifically, to primordial follicle activation TGFβ signaling, and factors have been shown to act via PI3K and BMP-associated pathways though the exact mechanism of follicle activation continues to be elusive even with significant active research and evidence pointing at an element that interacts with the PI3K/AKT/mTOR axis of pathways (169-171). However, a more recent study examining the activation of primordial follicles and induction of primordial granulosa cells from squamous to cuboidal proposed a TGFβ-mediated signal maintaining nuclear localization of SMAD2/3 maintaining follicle quiescence in murine ovaries (101). In this study they found that an unknown maintenance signal maintains SMAD2/3 signaling in the granulose cell, which inhibits granulosa cell proliferation. An unknown activation signal would then drive nuclear export of SMAD2/3 leading to increased granulosa cell proliferation and cuboidilization resulting in the activation of

primordial follicles (101). This was further supported in work where SMAD3 was found directly regulate cell cycle genes that maintain arrest of granulosa cells around primordial follicles. SMAD3 was found to drive the expression of the downstream genes *Myc* and CCND2. In this paper they proposed a TGFβR mediated model of follicle activation where increases in TGFβR drive repression of SMAD3 via SMAD7 activity and activation of mTOR signaling machinery that results in promoting growth and proliferation of granulosa cells (172). EMILIN1 has been shown to negatively regulate TGFβ by blocking conversion of pro-TGFβ to TGFβ (**Figure 13**) inhibiting TGFβ signaling and resulting in altered SMAD2/3 localization in a dose, and stage-dependent manner (173-176). However, despite these promising results the maintenance signal being proposed that would maintain this system remains elusive and evidence points towards EMILIN1 being an important component of this system. This hypothesis is also supported in proteomics which indicates TGFB is less abundant in the cortex and more abundant at 1.5mm in tandem with reduced EMILIN1 expression. Because of this we predict that EMILIN1 is an extracellular mediator that interacts with TGFβ to maintain primordial follicle quiescence.

Agrin (AGRN) is a large extracellular heparan sulfate proteoglycan, which is known to interact with α -Dystroglycan (Dag1) which connects ECM components such as AGRN to the cytoskeleton and drives cellular responses via the dystrophin–glycoprotein complex (DGC) (81). Multiple researchers have found that AGRN interacts with YAP/TAZ, key effectors of the HIPPO pathway, activity in other tissues, with blocking antibodies showing reduced YAP/TAZ nuclear localization and decreased proliferation as a result (177). In the ovary, according to proteomics performed in a porcine model AGRN is present in the cortex but is more abundant at 1.5mm coinciding with increases in the population of activated follicles (**Figure 14**). It has also been shown that increased

nuclear localization of YAP occurs in granulosa cells coincides with increases in follicle activation (178-182).

The Hippo signaling pathway is an important intracellular signaling known primarily for its role in conserving optimal organ size and modulating cell proliferation (182-184). The HIPPO signaling system itself is built around a complex kinase cascade that is mechanoresponsive with mediators of the pathway phosphorylating and inactivating the yes-associated protein (YAP) and transcriptional coactivator with PDZ-binding motif (TAZ) by nuclear export (182, 185). Additional coactivators have been described in a murine model with both Rho GTPase and Rho-associated protein kinase (ROCK) having been shown to regulate YAP/TAZ. These two proteins respond to changes in the external environment, such as changes in contractility or rigidity with research showing that the Hippo signaling pathway is regulated mainly by a network of upstream components involved in regulating cell adhesion, shape, and polarity (186, 187). When HIPPO signaling is disrupted you see a decrease in YAP phosphorylation followed by increases in nuclear levels of YAP. In conjunction with increased nuclear localization of YAP/TAZ we see interactions with Transcription factors containing the TEA/ATTS DNA binding domain (TEAD)) transcriptional factors, nuclear YAP thus induces several CCN growth factors and baculoviral inhibitors of apoptosis repeat containing (BIRC) apoptosis inhibitors. These proteins, in turn, stimulate cell growth, survival, and proliferation (182). The HIPPO pathway is also modified via changes in actin polymerization. Actin is a
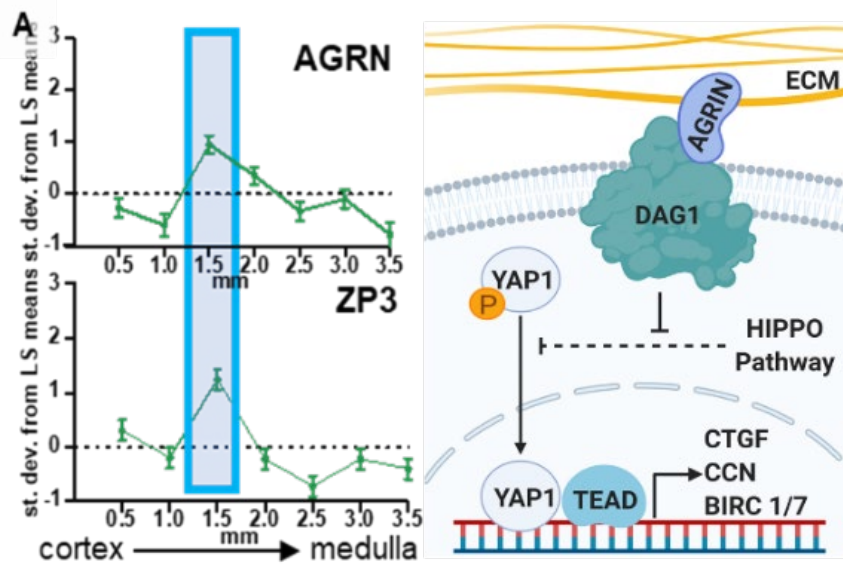
Figure 14. AGRN drives primordial follicle activation. (A) LS-Means distribution of AGRN and ZP3 showing highest concentration at depth associated with activated/growing follicles. (B) AGRN signaling via DAG1 inhibits the phosphorylation of YAP by the HIPPO pathway, leading to nuclear import of YAP expression of genes.

multifunctional protein that forms microfilaments modulating multiple important cellular processes. Rapid changes in the polymerization of globular actin (G-actin) to the filamentous form (F-actin) help to mediate cell adhesion and shape. Polymerization changes and F-actin formation has been shown to disrupt Hippo signaling leading to nuclear YAP accumulation (186, 187). When looking specifically at HIPPO in the ovaries research in both murine and human ovaries has shown that key genetic components of the HIPPO pathway are expressed in a follicle stage-dependent fashion (YAP, TAZ, MST1/2, SAV1, and LATS1/2) (180, 182). Additional studies have shown that the fragmentation of ovaries induces transient increases in the polymerization of G-act to F-actin, decreasing phosphorylated YAP levels, increases in nuclear localization, and the upregulation of downstream CCN growth factors and BIRC proteins alongside increased rates of primordial follicle activation (180, 182).

When examining folliculogenesis and HIPPO pathway signaling specifically research shows that the treatment of murine ovaries with Jasplakinolide, an actin polymerization-promoting cyclic peptide, or sphingosine-1-phosphate, a follicular fluid constituent known to promote actin polymerization, increased the ratio of F-actin to G-actin, this resulted in increased nuclear localization of YAP and expression of downstream CCN growth factor leading to follicle growth (186,187). The same research group also demonstrated the important role of YAP in ovarian fragmentation-induced follicle growth by using verteporfin (180), a small molecule inhibitor that reduces interactions between YAP and TEAD transcriptional factors (188). In human ovaries, the amount of CCN growth factors were also increased in ovarian cortex pieces that were processed into small cubes after being thawed (180), which indicates an essential role of CCN growth factors in ovarian follicle growth alongside the mechanoresponsive nature of the HIPPO pathway. Looking specifically at the candidate protein AGRN, which binds to DAG1 to mediate HIPPO

signaling via increased Yap localization to the nucleus in hepatocarcinoma cells (189-192). Therefore, we predicted that AGRN is a mediator of the HIPPO pathway signaling in the ovary which drives granulosa cell proliferation and follicle activation.

We hypothesize that biochemical cues from matrisome proteins, EMILIN1 and AGRN, regulate primordial follicle activation and disruption of these pathways will result in increased activation or quiescence, respectively.

Materials and Methods

Obtaining and Processing Bovine Ovaries

Bovine ovaries were purchased from Applied Reproductive Technology, LLC (ART, Wisconsin). Cows were post pubertal, but exact age ranges for the cattle at time of sacrifice and ovary retrieval was not available. After retrieval, ART washes the ovaries with 2% chlorohexidine gluconate diluted with distilled water followed by a series of washes with distilled water. Ovaries were then shipped chilled overnight in phosphate buffered saline (PBS) with penicillin, streptomycin and gentamicin. Bovine ovaries without clear hemorrhagic cysts or other abnormal distortions were used for our experiments. For production of hydrogels, any large corpus lutea were removed prior to decellularization.

Bovine ovaries were placed in L-15 containing 1x antibiotic-antimycotic (Caisson, ABL02-100ML) solution prior to processing. Initial processing of tissue involved removing excess mesovarium and bisecting through the hilum. Tissue was further processed using a custom-made tissue slicer that produces slices that are 1 mm thick (Northwestern Simulation Lab). Tissue was sliced on the cut side after bisecting to allow atomic force microscopy (AFM) sampling from both

cortex (first 0.5 mm) and medullary regions (>0.5 mm). Tissue slices were then placed in DMEM containing 1x antibiotic-antimycotic overnight at 4°C.

Atomic Force Microscopy for Mapping Ovarian Rigidity

AFM was carried out using a Bruker Hysitron BioSoft Indenter with a 100 µM radius probe. Bruker Bioscan (v1.0.0.1) software was used for data acquisition and Origin 2018 software was used for data analysis and force curve fitting to a Hertzian model as recommended by core facility. Prior to AFM testing, 1 mm thick slices of ovarian tissue were rinsed with PBS (Thermo, 10010023), then adhered to 35 mm petri dishes using PELCO Pro CA44 Instant Tissue Adhesive (Pelco, 10033). Samples were then submerged in PBS to prevent drying. The AFM probe was calibrated in PBS to remove background noise from the liquid interface. This probe was manually brought to the surface of the bovine ovary slice. Once the surface was reached, the probe was manually retracted from the surface prior to data acquisition. Data acquisition was performed using a three-step protocol (approach, hold, retraction) with the following settings: approach/retraction rate of 5.00 µM/s with a target value of 150 µm, and a 5 second hold.

Decellularization

Decellularization was carried out using 0.1 % sodium dodecyl sulfate (SDS, Sigma, 75746) in PBS (Thermo, 10010023) as used previously (43). Slices of tissue and isolated medulla were placed on a nutator at 4 °C and SDS solution was changed every 24 hours for 48 - 72 hours for slices or 2 - 3 weeks for larger medulla pieces prior to use in ink manufacturing.

Ovarian Hydrogel Manufacturing

Decellularized ovarian tissues were lyophilized using a Freezone 6 Plus System. After lyophilization, tissue was milled until it fit through a 60-mesh screen. Residual SDS and lipids, which would interfere with gelation, were subsequently removed using three 100% ethanol washes and the washed milled tissue was subsequently lyophilized again using the Freezone 6 Plus System. Pepsin digestion is then performed on the tissue, 20 mL of a 1 mg/ml pepsin (Sigma P7012) digest solution in 0.1 M HCl. The pH of the solution was verified to be ~1-2 (the ideal range for pepsin activity) and then 25 mg/mL of tissue was added and placed on a magnetic stir plate for 72 - 96 hours at room temperature. After digestion, the solution was neutralized using NaOH. The gel was then placed at 37°C for 1 hour prior to use to promote gelation in either 3D printing or as a cast gel.

3D Printing

The 3D printed scaffold design was used previously by Laronda, et al (9). The design is a 15 mm x 15 mm square that includes a solid bottom, with each subsequent layer printed at a 60⁰ advancing angle and struts were spaced 1 mm apart. Five layers were printed using this design for use with AFM-based analysis. FRESH printing was performed as described previously.[36] Cortex and medulla-derived dECM inks were mixed 1:1 with 35 mg/mL COL1 Lifeink 200 (Advanced Biomatrix, 5278) to assist with printability (COL1 control data included in appendices). Hydrogel was loaded into low temperature cartridges for use with an Envisiontec 3D-Bioblotter manufacturing model. After mixing and loading into cartridges they were incubated in the print head to obtain a uniform temperature of 8 ⁰C, then printed using 32-gauge needles (Nordson, 7018462).

Atomic Force Microscopy for Engineered Materials

AFM was carried out on engineered materials using a Piuma Nanoindenter with accompanying software (V3.2.0). Prior to AFM runs, printed scaffolds were rinsed with PBS then adhered to 35 mm petri dishes using PELCO Pro CA44 Instant Tissue Adhesive (Pelco, 10033). Subsequently, samples were submerged in PBS to prevent scaffolds from drying out. For cast gels, a small volume of gel was added to a transwell insert (Millipore, PICM01250). Cast gels were then spun in a centrifuge for 5 minutes at 2,000 g to remove bubbles. After centrifugation a small volume of PBS was added to the top of the gels to assist with AFM measurements. Analyses for all materials was carried out using a probe manufactured by Optics 11 with the following properties: a rigidity of 0.033 N/m rigidity, and a tip radius of 29 µM. The AFM probe was calibrated in PBS to remove background noise from the liquid interface and was calibrated against a plastic dish as per Piuma calibration requirements. Piuma software was used to find the surface of materials and then to acquire data. Data acquisition was carried out using a three-step protocol (approach, hold, retraction) with the following settings: An approach/retraction rate of 5.00 µM/s with a target value of 150 µm, and a hold time of 5 seconds.

Quantitative iPCR

Protein was extracted from bovine ovary slices that were decellularized (as described above). Tissue was placed in a protein extraction buffer made of 1% SDS, 50 mM ammonium bicarbonate, 50 mM NaCl, and 10 µL/mL Halt Protease Inhibitors (Cell Signaling Technology, 5872S). Tissue was placed in reinforced 2 mL tubes (Omni International, 19–648) with 2.8 mm polycarbonate beads (Omni International, 19–646). Tissue was homogenized with an Omni BeadRuptor12 at 4 °C (Omni International, 19-050 A) using the following settings: 6 cycles at speed 6.0, 45 second

homogenization and a 75 second delay between cycles. Homogenates were subsequently sonicated on ice 3 times at 75% amplification for 1 minute. Samples were then centrifuged at 10,000 rpm for 15 minutes. A 1 mL aliquot was taken from the samples and samples were treated with an SDS-Out kit (Thermo Scientific, 20308). Protein concentration was measured using a BCA assay (Fisher Scientific, PI23227). Samples were normalized to a concentration of 1,000 ng/µL using protein lysate buffer from the Taqman Open Kit (Thermo Fisher, 4453745).

Antibodies were biotinylated using EZ-Link Sulfo-NHS-LC-Biotin, No-Weight format kit (ThermoFisher, 21327). Antibody information is listed in Appendix Table 1. Excess biotin was removed using two cycles of filtration with Zeba Micro Spin Desalting columns, 40k (Fisher Scientific, PI87765). Probes were then tested for suitability using the method described in the Taqman Protein Assays Probe Development Protocol (Thermo Fisher, 4448549). To compare protein quantity between the medulla and cortex a standard method described in the Taqman Protein Assays Sample Prep and Assay (Thermo Fisher, 4453745) was used. A four-point dilution series was created with 2000 ng of total protein then serially diluted 1:10. A qPCR machine (Applied Biosystems, QuantStudio 3) was used for running the assay. To quantify the amount of protein of interest present a standard curve was created with proteins of known concentrations in a dilution series (see Appendix Table 1). Because some samples had undetectable levels of protein, dose curve data are presented as change in CT over no template controls (see Appendix Figure 1). Two-way ANOVA and multiple t-test analyses were used to determine significance, GraphPad PRISM version 9 was used to interpolate concentrations based on the standard curves.

Targeted Depletion of Matrisome Proteins

Targeted depletion of gels was carried out using antibodies for the protein of interest and a seven-step magnetic assisted depletion process. Antibodies used for targeted depletion were prepared using goat anti-rabbit magnetic beads (NEB, S1432S) following the manufacturer's protocol. Tagged antibody was added to decellularized extracellular matrix (dECM) homogenate following manufacturers recommended concentration in a 1.5 mL Eppendorf tube. After incubation with the antibody a strong magnet was applied and the dECM was transferred to the next tube for further depletion. This process was repeated 7 times to maximize reduction.

Human Mesenchymal Stem Cell (hMSC) Culture

hMSC was carried out using StemPro BM Mesenchymal Stem Cells (Thermo, A15652). Cells were seeded at a density of 5,000-6,000 per cm^2 on 6-well plates coated with CTS CELLstar substrate (Thermo, A1014201) for expansion prior to culture on engineered materials per manufacturer's instructions. Cells were cultured using Cts StemPro MSC SFM (Thermo, A1033201) and were fed every 3 days. Once cells had reached 50-60% confluency cells were collected using Trypsin 0.25% in HBSS (Caisson, TRL01-100ML) following manufacturer's instructions prior to plating in 48 well plates that had been coated with engineered materials. The 48 well plates were coated using a thin layer of one of three different materials: LifeINK200 a high concentration (35mg/mL) COL1 material (Adv. Biomatrix, 5278-5ML), cortex derived dECM (25 mg/mL), EMILIN-1 depleted cortex derived ECM. The substrate was sterilized using UV radiation for 1 hour prior to plating with hMSCs. The hMSCs were seeded at 15,000 cells per well and cultured using CTS StemPro MSC. Additional wells were done containing cells on EMILIN-1 depleted Cortex dECM and COL1 were given media supplemented with Recombinant Human EMILIN1 Protein (Abnova, H00011117P01) at a concentration of 0.01ug/mL. Cells were cultured

for 7 days on these substrates and fed every 3 days, cells were collected for either RNA Analysis using RNA Lysis buffer or were taken for Live/Dead staining on days 1, 2 and 7.

Live/Dead staining and Analysis

Live/Dead staining was carried out using an Ethidium homodimer and calcein method established in the lab. A staining buffer was made with a concentration 1% BSA (Sigma, A941850G), 1X sodium bicarbonate (Sigma, S8761-100ML), and 1XHBSS (Fisher, MT21023CM). This was refrigerated until ice cold then the following was added per 1 ml of staining buffer used 5µl of 1 mg/ml Hoechst (Sigma B2261), 0.5µl of 2 mM EthD-1 (Sigma E1903), and 1.25µl calcein AM (Sigma C1359). Cells being stained had 200µl of staining buffer added and were placed on an orbital shaker in 4 °C for 20 min. Tissues were then rinsed twice using ice cold HBSS and washed on orbital shaker in 4 °C for 10 minutes per wash. Cells were imaged while in cold HBSS (Keyence, BZ-X700), and analyzed using BZ-X Analyzer (Keyence). Imaging was carried out across 16 wells per experiment. Live/Dead analysis for these images was carried out in Fiji using the following method: 1) images had channels split and converted to 8bit for analysis, 2) images were segmented by first establishing a threshold to eliminate background and then processed using the watershed function in Fiji, 3) positive signal was counted using Analyze Particles function in Fiji giving a raw count of positive signal in that channel. Hoechst, Calcein, and Ethidium stains were then compared to get proliferation and live/dead data over time in culture. Statistical analysis of live/dead and proliferation was carried out in Prism.

Gene expression analysis using real-time semi-quantitative PCR (qPCR)

hMSCs were batch collected using 150 μl of RNA Lysis buffer that was used to collect from all wells seeded for that day's collection. Collected cells were subsequently flash frozen in liquid nitrogen and stored at −80 °C prior to RNA Extraction. RNA extraction was done using Zymo micro-prep kit (Zymo, D7005). RNA preps were cleaned and concentrated using RNA-Clean up kit (Denville Scientific, Z5214). Total RNA (0.5 μg) was reverse transcribed into cDNA using Superscript IV VILO kit (Life Technologies, 11756050). qPCR was carried out using a QS3 using standard SYBR reagent templates from manufacturer using 25ng of cDNA material per well. Primer information is listed in Appendix A. Table 2.

Results

AFM measurements revealed a rigidity gradient in the bovine ovary that can be recapitulated in engineered materials.

There is a rigidity gradient across in bovine ovarian compartments.

The rigidity of the bovine ovary was measured using AFM nanoindentation. Young's moduli of bovine ovary slices were measured at points spaced in 1.0 mm increments from the ovarian surface epithelium inward, where 0.5 mm from the ovarian surface epithelium edge at the mesosalpinx plane was considered the cortical region and 1.5 – 3.5 mm points inward along the central pole were considered the medullary region (**Figure 15A).** A tissue thickness of 1 mm was chosen to eliminate possible contributions from the 35 mm dish to rigidity measurements being taken by the AFM. Further, a probe size of 100 μm was used to better detect the overall rigidity of a region, and to avoid the over-representation of small ovarian structures in rigidity measurements. Two technical replicates were taken per ovary slice, with 4 - 5 biological replicates taken for each

distance. There was a statistically significant difference between the rigidity of the cortex and the

medulla (**Figure 15A**). The rigidity of the ovary was significantly reduced from the cortex (8.87

kPa) to 3.5 mm (1.05 kPa). The rigidity values ranged in the ovary from 0.71 to 11.59 kPa. Overall,

the cortex was 8.5 times more rigid than the deep medulla (3.5 mm) and the deep medulla was

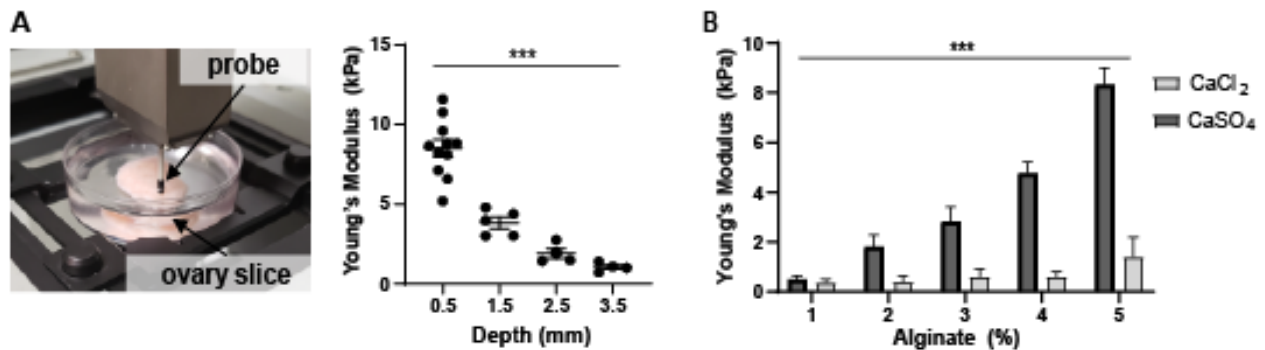approximately two-fold (average 2.05) less rigid per 1 mm step as measured by AFM.

Figure 15. (A) AFM was used to measure the rigidity of bovine ovary tissue (left) at 0.5

mm to 3.5 mm from ovarian surface epithelium inward (right). p-value = <0.0001 (B) AFM

was also used to measure the rigidity of cast alginate gels cross-linked with either CaCl2

or CaSO4.

CaCl$_2$ crosslinked alginate does not recapitulate bovine cortex rigidity.

Several seminal studies on follicular growth, maturation, and transcriptional changes were performed with different percentages of alginate with most papers focusing on alginate gels between 0.5%-3% with 0.5-1.5% alginate being used as permissive environments for culturing growing follicles and 2-3% being used to represent rigid environments for culturing primary follicles (45, 151, 153, 154, 233, 266, 267). However, previous investigations of the rigidity of this material at different percentages were performed using different techniques, specifically rheometry (267). Therefore, we sought to define the rigidity of alginate using AFM in order to compare it to the native environment described above. We first examined the rigidities of alginate gels using varying percentages of alginate cross-linked with either CaCl$_2$, the most common cross-linking substrate used in follicle culture (**Figure 15B**) (45, 151, 153, 154, 233, 266, 267). CaSO$_4$ was chosen as a second cross-linker as previous research has shown that alginate gels cross-linked with CaSO$_4$ achieved higher rigidities than those cross-linked with CaCl$_2$ yet was still able to support murine follicle survival in culture (268). The rigidity of alginate crosslinked with CaCl$_2$ ranged from 0.39 ± 0.13 kPa to 1.42 ± 0.77 kPa, which was significantly less than alginate crosslinked with CaSO$_4$ which ranged from 0.50 ± 0.15 kPa to 8.33 ± 0.67kPa. Measurements for CaCl$_2$ crosslinked gels failed to reach higher rigidities found in bovine ovaries even at the maximum alginate percentage tested (5%, 1.42 kPa). However, CaSO$_4$ crosslinked gels showed similar rigidities to bovine ovaries at 5% (8.33 kPa) and 2% (1.80 kPa) being equivalent to rigidities at the cortex (8.87 kPa) and the deep medulla (1.05 kPa) respectively. In comparison 5% CaCl$_2$ crosslinked gels, the maximum percentage tested, only showed similar rigidity to the deep medulla.

Engineered materials using decellularized bovine ovaries recapitulate compartmental rigidity differences.

In order to examine compartment-specific contributions to rigidity from the matrisome, we performed AFM analysis on both cast hydrogels and 3D printed scaffolds created from decellularized bovine ovary material. Slices from the cortex and medulla were decellularized and lyophilized. The enriched matrisome material was then milled, washed, re-lyophilized and digested with pepsin to create compartment specific hydrogels (**Figure 16A)**. First, the rigidity of cast gels was analyzed using AFM (**Figure 16B)**. Cortex gels had a rigidity of 3.11 kPa ± 0.41, which was significantly higher than gels derived from the medulla material, which were 0.02 kPa ± 0.001. The gel made from the cortex maintains the higher rigidity over the medulla and is 155.5 times more rigid. The cortical matrisome
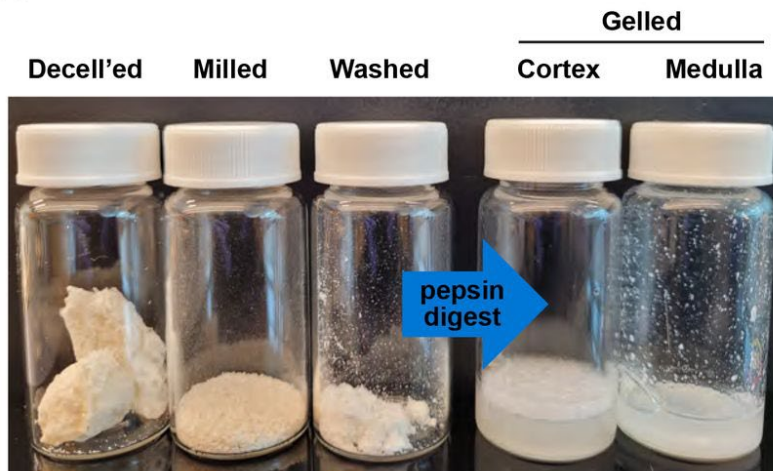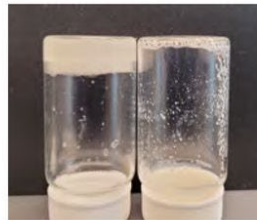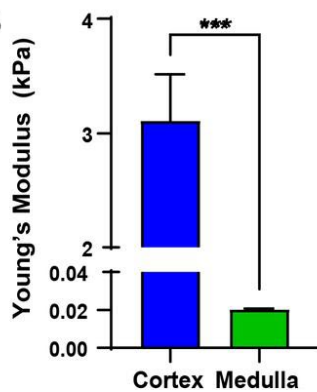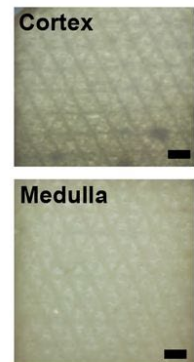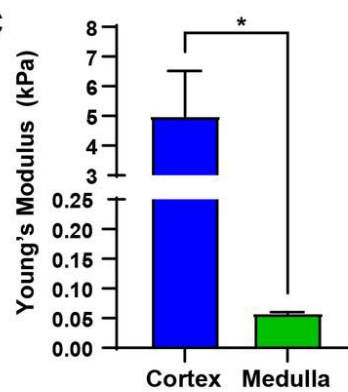
Figure 16. Mechanical analysis of Engineered Materials Using AFM (A) Ovary slices from cortex or medulla (shown) were decellularized (decell'ed) and lyophilized; then milled, washed and re-lyophilized before being digested using pepsin to make gels. (B) The rigidity of cast gels from cortex or medulla material was measured with AFM. The cortex made stronger gel than the medulla (right). $p = 0.0003$ (C) The rigidity of scaffolds printed from cortex and medulla hydrogels mixed with collagen in 1:1 volume was measured using AFM. $p = 0.017$, scale $= 200$ µm.

gel is 2.85 times less rigid than the native cortical region (0.5 mm depth); whereas the medulla matrisome gel is 112 times less rigid than the native medullary compartment (1.5 – 3.5 mm). Then, to determine if these hydrogels maintained their rigidity differences within printed scaffolds, we 3D printed scaffolds in a similar architectural design as previously demonstrated to support murine ovarian follicle growth and maturation.[11] To increase printability, the hydrogels derived from cortex and medulla were mixed 1:1 with collagen 1 (COL1) ink then printed using FRESH methods prior to examining rigidity through AFM (**Figure 16C**) (268). FRESH printed scaffolds containing cortical matrisome were significantly more rigid than those printed with medullary matrisome materials with average rigidities of 4.99 kPa ± 1.52 and 0.06 kPa ± 0.002, respectively. This pattern of cortical materials measuring significantly higher rigidities than medulla materials was maintained even in printed scaffolds. The cortex scaffolds were 83 times more rigid than those derived from the medulla. AFM analysis of scaffolds using only COL1 ink had an average rigidity of 0.17 kPa ± 0.05, which was significantly less than the cortex-derived scaffolds and trending toward statistically significantly higher than medulla-derived scaffolds (p = 0.078, **Appendix Figure 2**).

Quantitative iPCR revealed differential distribution of matrisome proteins across ovarian compartments in bovine ovaries.

To examine the distribution of matrisome proteins across ovarian compartments we performed iPCR on slices of bovine ovaries that were decellularized to enrich for matrisome proteins. Consistent with the above methods, we considered the first 0.5 mm slice cortex, while the rest of the ovary was considered medulla. Candidate proteins for
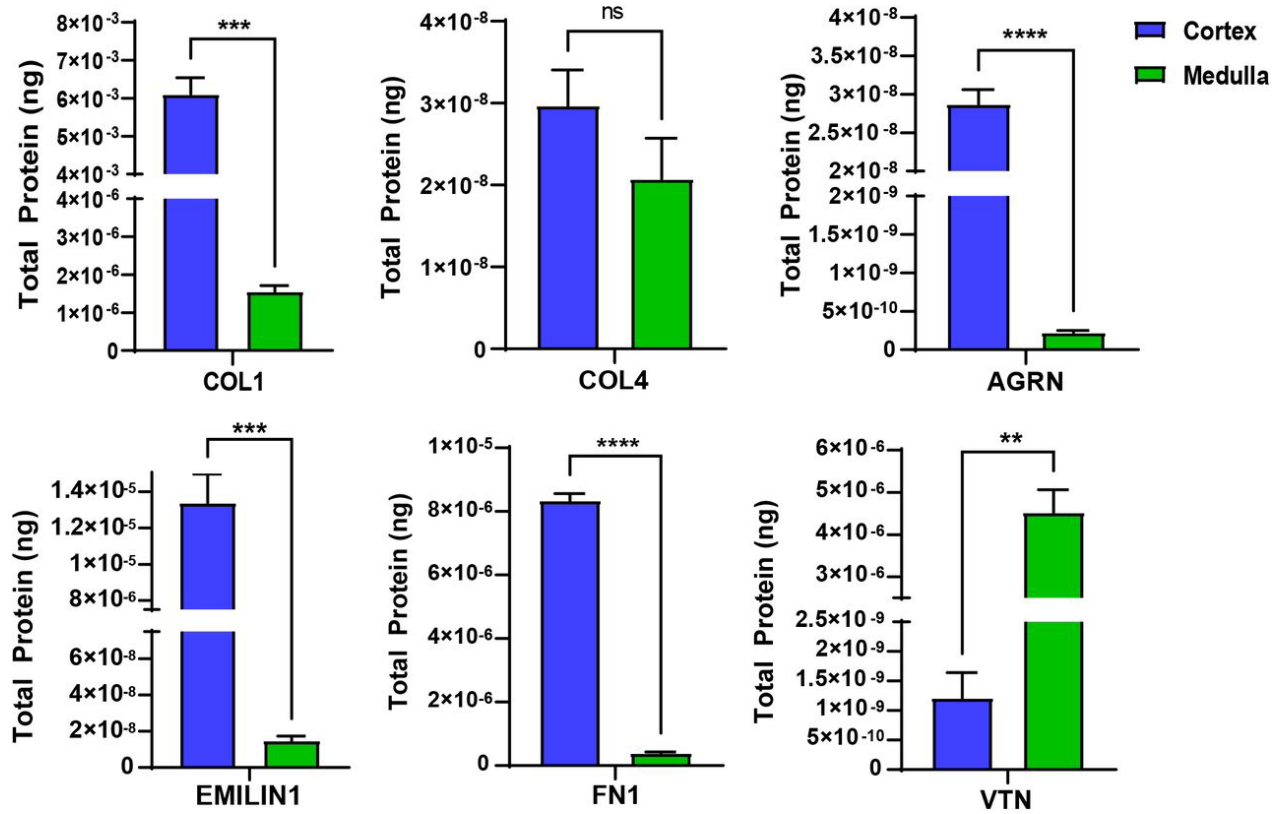
Figure 17. Quantitative iPCR analysis of matrisome proteins in bovine ovaries. Total COL1, COL4, AGRN, EMILIN1, FN1 and VTN protein within decellularized bovine ovary cortex (0.5mm depth) and medulla (3.5mm depth). Bars represent mean with standard error. ns, not significant, ** = 0.001, *** < 0.001, **** < 0.0001

this analysis were chosen based on previous experiments in porcine ovaries (153). We chose the following candidates: COL1 and collagen IV (COL4), agrin (AGRN), elastin microfibril interfacer 1 (EMILIN1), fibronectin (FN1), and vitronectin (VTN). To quantify these proteins a standard curve was created with purified protein (see **Appendix Table 1**). There were significant differences in the distribution of candidate proteins across ovarian compartments that matched the previously published mass spectrometry and iPCR analyses from the porcine ovarian matrisome map (**Figure 17**). COL1, AGRN, EMILIN1, and FN1 are significantly more abundant in the cortex matrisome than the medulla. Whereas VTN is significantly more abundant in the medulla and the amount of COL4 is not different among the two compartments. This was the first time iPCR has been used to quantify matrisome proteins in tissues. Two proteins of interest, EMILIN1, a matrisome glycoprotein, and AGRN, a matrisome proteoglycan, have been shown to act upstream of proliferation and mechanotransduction pathways in other tissues (101, 172, 174, 178-180, 189-192, 269, 270).

Targeted depletion of matrisome proteins from engineered materials

Magnet assisted protein filtration specifically depletes proteins of interest in tissue matrisome samples.

In order to explore the effects or matrisome proteins on follicle activation and folliculogenesis we developed a novel toolkit to study these mechanistic relationships by selectively depleting proteins of interest using magnet assisted protein filtration (MAPF) from ovarian tissue derived matrisome samples. For the purposes of this study, we
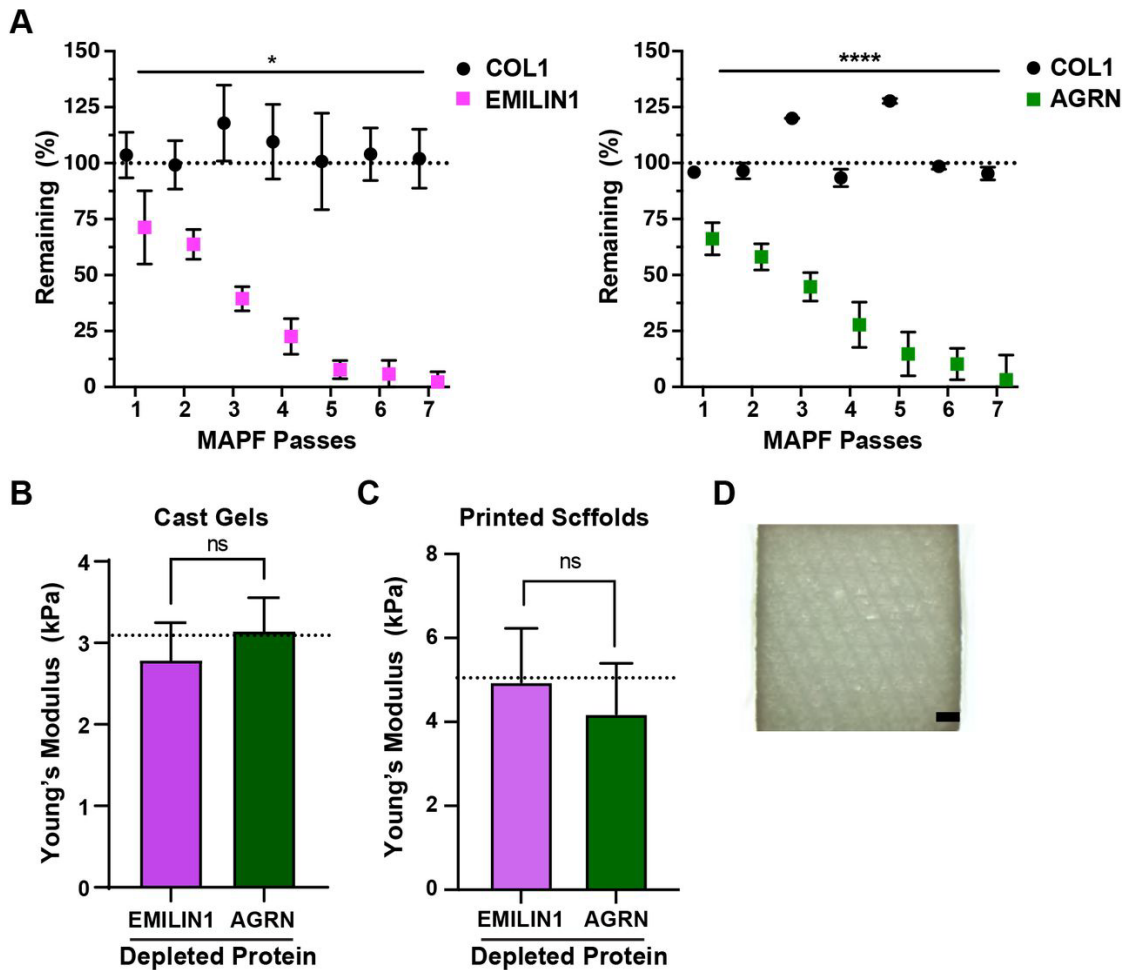
Figure 18. Targeted depletion of proteins of interest and mechanical analysis of resulting hydrogels. (A) iPCR analysis of relative content of COL1 and EMILIN1 or AGRN following targeted depletion of EMILIN1 or AGRN by passing cortical matrisome samples through magnetic activated protein filtration (MAPF). Dotted line = 100 % (B) Rigidity of cast or (C) printed gels with EMILIN1 or AGRN depleted from cortical matrisome materials by seven MAPF passes. Dotted lines = rigidity of control cortex gels (B) or cortex printed scaffolds (C). (D) Light microscopy image of scaffold printed with cortex matrisome (top) and depleted cortex matrisome (bottom). Bars, squares, or dots represent mean with standard error. ns, not significant, * = 0.01, **** < 0.0001, scale = 200 μm.

selectively depleted and removed EMILIN1 and AGRN. Cortex matrisome materials were used because of the significant abundance of these proteins in this compartment and

iPCR was used to measure the remaining proteins of interest against the percentage of an abundant off-target protein, COL1. We determined that a seven-step filtration process significantly reduced the amount of both EMILIN1 and AGRN from cortical matrisome materials to satisfy future knockdown experiments (**Figure 18A, 18B**). Indeed, the seven-step filtration method reduced EMILIN1 by 97.714% ± 7.89 and AGRN by 96.80% ± 19.11 while not affecting the amount COL1 (102% ± 22.76 for EMILIN1 targeted filtration, and 95.36% ± 4.89 for AGRN) that was present in the same samples.

Physical properties of selectively depleted materials are unaffected.

In order to assess the physical properties of matrisome materials that underwent the MAPF process we tested the rigidity of cast gels and printed scaffolds. There were no significant differences in the rigidity as measured by AFM of depleted gels (**Figure 18C**) or scaffolds (**Figure 18D**) in comparison to the base hydrogels from cortical matrisome materials. This indicates that the MAPF process and the individual removal of these matrisome proteins does not affect the rigidity of engineered materials, which is a positive indicator for its use as an *in vitro* platform to explore the influence of matrisome proteins on folliculogenesis.

human Mesenchymal Stem Cells (hMSCs) cultured on depleted substrates show altered gene expression
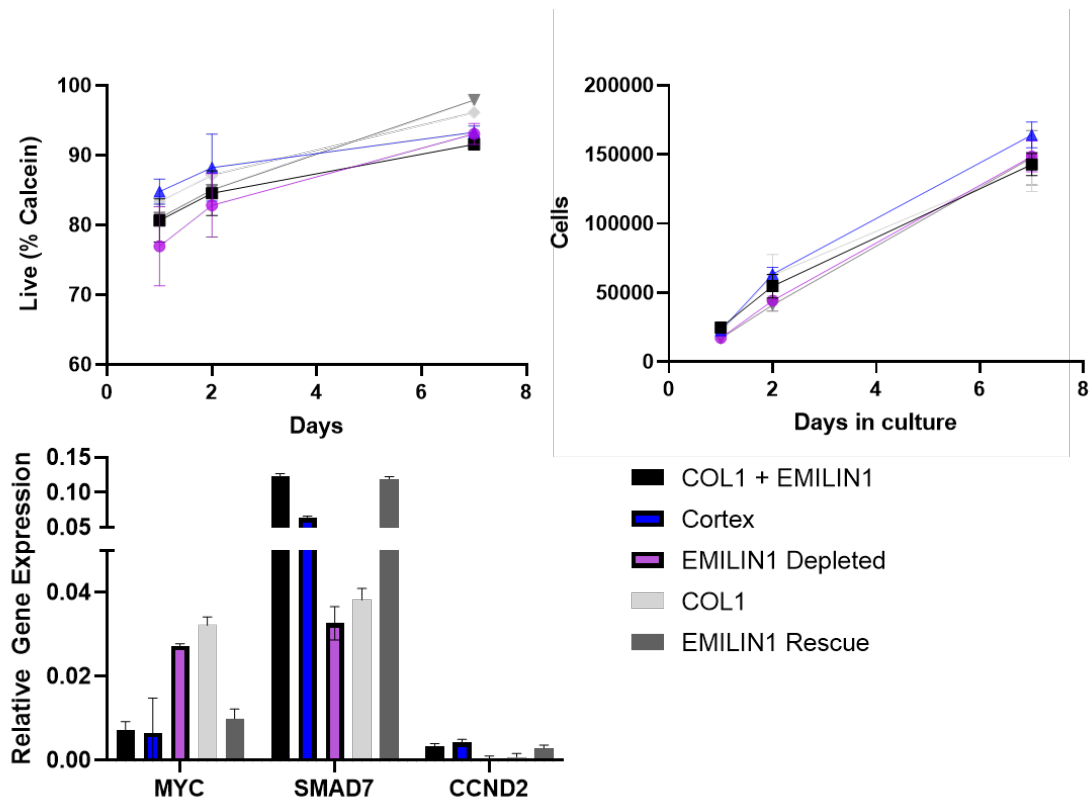
Figure 19. Culture of hMSCs on depleted engineered materials and rescue experiments. (top left) tracking of hMSC survival across culture on engineered materials and cortex dECM (top right) cell count across culture for hMSCs (bottom left) gene expression of candidate genes downstream of TGFβ that have EMILIN1 implicated as a potential regulator.

To assess our engineered materials for cell toxicity and to determine if depleted materials drove differential gene expression of candidates downstream of TGFβ that have EMILIN1 implicated as a potential regulator we cultured hMSCs on our depleted materials for 7 days. Alongside this we performed rescue experiments in which EMILIN1 was provided in the media to our depleted materials to determine if gene expression returned to normal upon supplementation. Across seven days in culture, we see no significant difference in cell survival or cell number for any of the engineered materials or rescue experiments **(Figure 19).** However, we do see significant differences in gene expression between EMILIN1 depleted materials (COL1 and EMILIN1 depleted dECM) and our cortex control. Further, we see a restoration of gene expression for MYC, SMAD7, and CCND2 where EMILIN1 supplemented cultures show no significant difference between whole cortex for MYC or CCND2, but we do see a significant difference for SMAD7 which may indicate that the concentration of EMILIN1 likely overshot levels found normally in our cortex derived dECM (**Figure 19**).

Discussion

In this study we examined the rigidity of bovine ovaries, assessed ovarian compartment specific matrisome hydrogels, and expanded our toolkit to examine the mechanistic connection between the matrisome and folliculogenesis. We found that the bovine ovary contains a rigidity gradient with a cortex that is significantly more rigid than that of the medulla, that this difference in rigidity is maintained in engineered materials (cast gels and printed scaffolds) derived from these compartments, and that we can use MAPF-based methods to deplete proteins of interest. We used the same AFM technique to measure the rigidity of encapsulation materials commonly used for *in vitro* folliculogenesis experiments to compare these measurements with native and decellularized bovine ovary materials. Additionally, we confirmed that the bovine ovary contains the same profile

for COL1, COL4, AGRN, EMILIN1, FN1 and VTN as previously demonstrated in porcine ovaries. For the first time, we quantified the amount of protein in each sample using iPCR. This technique may be useful in building an engineered environment that matches the protein abundance of native tissue. Finally, the new hydrogel materials, cortical and medullary hydrogels, and hydrogels with depleted proteins of interest expand our toolkit to facilitate future investigations, including into molecular mechanisms that begin with external matrisome proteins.

Using AFM, we showed that the bovine ovary has a rigidity that ranges from 0.71 to 11.59 kPa. To place this within context of other organ systems, the rigidity of the ovary contains rigidities seen within many other soft tissue organs (muscle, lung, liver, and kidney, and brain) (271-276). Our findings demonstrated that a rigidity gradient exists between ovarian compartments, not just in native tissue but also within hydrogels formed from matrisome proteins isolated from different compartments. These findings support the hypothesis that primordial follicles, located within the cortex, reside within a more rigid environment than activated or growing follicles within the medulla (41, 69). The significant rigidity differences between compartments also support the growing body of research that implicates multiple mechanotransduction pathways as playing a role in natural and induced folliculogenesis (181, 272-276). Kawamura, et al in particular showed increases in follicle activation after cutting the ovary with a subsequent disruption of Hippo signaling stimulating follicle growth (181).

The data here, however, conflicts with two recent studies, one examining ultrasound shear wave velocities in bovine ovaries and another which examined the micromechanical properties of the murine ovary (155, 277). Both studies indicated that the medullary region was more rigid than the cortex with the study by Hopkins, et al concluding that the major driver of rigidity changes in the murine ovary is most closely associated with mature follicles. However, these differences in

bovine versus murine ovary rigidity measurements using the same nanoindentation methods could indicate that significant species differences exist in the physical properties and organization of the ovary. These differences may be a result of differences in structure between bovine (similar to the human ovary) and murine ovaries that can be specifically identified during organogenesis where less regionalization develops in the murine ovary compared to the human ovary (225). The research by Gargus, et al examined whole bovine ovaries through shear wave velocity (155). We chose to use nanoindentation methods over other methods that measure viscoelastic properties because nanoindentation can work on the micron scale. However, alterations in shear wave velocity could indicate other changes across compartments associated with differences in ECM architecture and composition, density, size, and shape of follicles and other structures (41, 278). One limitation of the study here is that we processed the ovary into 1 mm slices and disrupted existing structures within the ovary that would have surface tension *in vivo*.

In order to expand our toolbox to include biomaterials that could be used to better understand the role of the microenvironment on folliculogenesis, we examined gels and inks made from decellularized cortical and medullary slices from bovine ovaries. Using a consistent method to define rigidity of these materials and to examine the contribution of matrisome proteins to the rigidity of ovary was key. Our data complemented recent work by Amargant, et al, that demonstrated, using AFM, that the increase in rigidity of aged murine ovaries could be contributed to the increased COL1 content indicative of fibrosis (157). The data presented here may offer some explanation as to why primordial follicles from multiple species (primate, mouse, and human) survive and grow better in a higher percent alginate than in the more permissive alginate that is preferred by growing follicles (45, 151, 153, 154, 200, 233, 266). To compare the rigidity of these commonly used materials with the native tissue and newly created biomaterials, we performed

AFM on alginate gels. Notably, we found that the highest rigidity gels used in previous experiments (3% alginate cross-linked with CaCl2) wouldn't recapitulate the rigidities seen in the cortex of native bovine ovaries (267). However, culturing a growing secondary follicle in a high percentage alginate results in transcriptional changes and increased the ratio of androstenedione to estradiol produced which can may be representative of a diseased state (150, 200, 279, 280). While our goal is to create a scaffold or hydrogel microenvironment that mimics the physical and biochemical cues of the native ovary, we cannot overlook the contribution of the interstitial and neighboring follicles to the rigidity in the native ovary. Indeed, the matrisome gels were less rigid than native tissues (1.78 times less for 3D printed scaffolds, 2.85 for cast gels). These differences between native bovine ovary rigidity and the rigidity of biomaterials may also be attributed to the organization of matrisome proteins and fibers. These are properties that may be lost during the decellularization, and homogenization methods required to produce matrisome hydrogels. Support of this comes from current efforts for scaffold design examining fiber morphology, ECM network architecture, and topography in addition to viscoelastic properties such as those defined by AFM analysis (281-284).

Finally, we developed a novel toolkit for examining the contribution of matrisome proteins to follicle activation and folliculogenesis by using MAPF to deplete proteins of interest from engineered materials without disrupting the physical properties of resulting scaffolds or cast gels. The reduction seen using MAPF is comparable to other methods for selective depletion of proteins that are currently in use (285-287). These EMILIN1 and AGRN depleted hydrogels are additional tools that will assist in isolating the role of biochemical cues from physical cues. One possible conclusion that could be drawn from these results is that neither AGRN nor EMILIN1 are directly associated with the physical properties of the ovary. Intriguingly, previous work done in EMILIN1

-/- mice has indicated that these mice show increased rigidity of the aorta in both nano and macro scale experiments (288). The lack of change in the engineered materials utilized here may indicate that EMILIN1 is primarily a driver of a cellular response leading to increased fibrosis, secretion of ECM components, etc. instead of organizing the ECM. Further work will need to be done to explore if the reduction is physiologically relevant to pathways of interest or if the remaining protein is capable of reaching a critical threshold needed for signaling in biological systems. We see in our culture an increase in CCND2 and SMAD7 with a decrease in gene expression of MYC in our whole cortex dECM cultured hMSCs compared to those plated on depleted materials that is restored upon supplementation with EMILIN1 protein. This is consistent with data in multiple model systems including cancer cell lines where TGFβ is shown to promote gene expression of MYC while CCND2 and SMAD7 are shown to be increased when TGFβ expression is low or being blocked (289-293).

Conclusion

We have for the first time examined, quantified, and mapped the rigidity of the bovine ovaries across the anatomical compartments using AFM. Our data reveals that the bovine ovary has a range of rigidity of 1.4 – 8.86 kPa. This data supports the previous observation that the cortex is more rigid than the medulla with a statistically significant decline in rigidity from the outer edge of the ovary toward the center. Then we found that compartmental rigidity of hydrogels and 3D printed scaffolds made from the cortical or medullary compartments of decellularized ovaries retain the physical properties of their originating compartment with cortex derived materials being more rigid than medulla derived materials. Additionally, for the first time, we quantified the content of matrisome proteins in a biological material using iPCR. This revealed that COL1,

COL4, AGRN, EMILIN1, FN1 and VTN matched the pattern previously identified in an unbiased matrisome analysis across compartments of the porcine ovary[35]. Finally, we developed a toolkit for examining the contribution of matrisome proteins to follicle activation and folliculogenesis by selectively depleting the candidate proteins EMILIN1 and AGRN using MAPF. We demonstrated that selective depletion of EMILIN1 and AGRN did not alter the rigidity of gels or printed scaffolds in comparison to native hydrogels and inks. This may not be true for all proteins, and it is likely that some selective depletion of fibrous proteins would affect the rigidity of the resultant biomaterial products. We predict that this foundational work will support future work that will inform the development of bioinks for 3D printed scaffolds by allowing for the incorporation of important physical and biochemical cues that yield the desired follicular behavior. This research enables future implementation of an effective scaffold for a bioprosthetic ovary transplant.

Chapter 4

Summary and Future Directions

Introduction

As outlined in **Chapter 1,** great strides have been made in understanding follicle activation and folliculogenesis. Recent interest in the matrisome (extracellular matrix and matrix associated proteins) and both physical and biochemical cues as major contributors to follicle dynamics has been driven by the fields of tissue engineering and regenerative medicine towards developing the next generation of bioprosthetic ovary. This fertility restoration approach will provide both endocrine and reproductive options to individuals who experience premature ovarian insufficiency (POI), or early menopause that occurs as a result of numerous genetic, autoimmune, iatrogenic, or idiopathic causes. In particular, this will benefit pediatric patients who have few fertility preservation options outside of ovarian tissue cryopreservation (OTC) and especially those individuals whose disease may preclude the auto-transplantation of ovarian cortex tissue due to the risk of re-introducing cancer cells into an individual. The experimentation described here sought to examine the physical and biochemical cues from the matrisome in the ovary and how those cues are differentially expressed across depths. Towards this end we spatially mapped the distribution of the porcine ovary matrisome across ovarian compartments, established a toolkit for selectively depleting matrisome proteins, and for the first time mapped the rigidity gradient in the bovine ovary while also validating matrisome maps established in a porcine model.

Summary and Discussion of Critical Findings

Matrisome proteins are differentially expressed across ovarian compartments in a porcine model and proteins of interest are matched in a bovine model

In **Chapter 2** we showed the first-time maps of the porcine ovarian matrisome ovaries across both the cortical compartment, where quiescent follicles reside, and the medullary compartment, where the larger activated follicles grow and mature. We were able to successfully map 1/8th of the porcine ovary and the distribution of matrisome components in three-dimensions. To do this we

sliced the ovaries, uniformly into 0.5mm slices across two intersecting anatomical planes, enriched for matrisome proteins and performed bottom-up shotgun proteomic analyses. A total of 6,711 peptides were detected with an FDR < 0.01, these peptides were identified as belonging to 615 proteins. Following data filtration with our three stringency rules, the remaining 440 proteins were analyzed using a novel LS-Means SAS-based bioinformatics pipeline. Using our LS-Means based analytics approach we found 134 proteins were significantly differentially expressed across depth. Of these we identified 42 matrisome proteins that were significantly differentially expressed across depths, and 11 matrisome proteins that have not been previously identified in ovarian proteomics experiments. These proteins belonged to all matrisome categories (as identified by matrisomeDB) except secreted factors. However, the secreted factors were identified in the overall dataset but didn't pass our data stringency requirements for our bioinformatics pipeline. We validated these data for nine candidate proteins (COL1A2, COL4A2, AGRN, ECM1, EMILIN1, FN1, TGFB1, VTN, ZP3) and confirmed compartmental differences with a second processing method in which we removed the cortex. These data demonstrate that the matrisome varies significantly across ovarian compartments. Additionally, from this data we identified proteins that are potentially involved in follicle dynamics that were used in subsequent analysis in **Chapter 3**: EMILIN1 and AGRN. Using our LS-Means based analysis we were able to use markers of activation (ZP3) and correlated that to changes in patterns of expression of other significantly differentially expressed proteins. Additionally, in bovine ovaries as detailed in **Chapter 3** we examined the distribution of the following matrisome proteins that had been identified in porcine ovaries: COL1, FN1, EMILIN1, VTN, and AGRN. COL1, FN1, EMILIN1 and AGRN were more abundant in the bovine ovarian cortex than the medulla. Whereas VTN was more abundant in the medulla. All of

these patterns matched with our porcine matrisome proteomics data indicating some amount of cross-species similarity in the distribution of matrisome components across ovarian compartments.

Using spatial mapping of the matrisome to find potential mediators of follicle activation and folliculogenesis

Research over the last decade has implicated multiple signaling networks as having a functional role in controlling follicle activation including (but not limited to) Transforming growth factor β (TGF β) family members, PI3K-Akt, KITL/KIT signaling, Leukemia inhibitory factor (>LIF), Notch signaling, mTORC, p27-CDK, Nobox, and Sohlh1 (16-21). More recently research has also added on new pathways including PKB/Akt, HIPPO, and Notch which regulate this highly intricate process (71,72,73). Cellular, paracrine, endocrine, factors regulate these pathways and a great deal of work has been done discovering the roles of factors with more recent work being done on factors such as: Ube2i, Phoenixin/GPR73, C1QTNF, and α-SNAP (71, 74-80). However, many unknowns still exist including what the upstream regulatory mechanisms of follicle activation are. Research has shown that the ovarian extracellular matrix (ECM) can affect hormone availability and responsiveness by sequestering, trafficking, or presenting factors including androgens and estrogens via sequestration of sex hormone binding globulin (82, 83). Further, it has been shown that there are tissue-specific functions to the matrisome that drive biological functions of interest. This would indicate that synergistically with other factors, the matrisome which as detailed previously provides biochemical and physical support to tissues could act as a regulator of follicle activation. Matrisome biochemical cues facilitate the translation of the extracellular environment into signal transduction cues (115-119).

The proteomics work in **Chapter 2** examined the distribution of these factors and found significant differences in the composition of the extracellular matrix across compartments by leveraging known markers of follicle activation, specifically ZP3, we have been able to find proteins potentially involved in follicle activation and quiescence: AGRN and EMILIN1 that we believe are involved in maintaining follicle quiescence and folliculogenesis, respectively. Indeed, one of the major utilities and significance of the proteomics experiment is that it allows us to have an unbiased platform for matrisome protein candidate discovery.

Using LS-Means based analysis from our proteomics work we know that EMILIN1 decreases through to the deep medulla and ZP3 (a marker of activated follicles) is more abundant at 1.5mm which is the depth at which activated/growing follicles reside, which also coincides with a decalin in TGFβ. Proteomics work performed by Ouni, et al 2018 also detected EMILIN1 in the cortex of human ovaries but as they focused only on cortex pieces were not able to examine the differences across compartments. However, a later study in the same group done in human ovaries examined the distribution of mechanical matrisome components of the human ovary from prepuberty to menopause (164). Using IHC the group found lower amounts of EMILIN-1 detected in the perifollicular ECM of prepubertal ovarian tissue and significantly higher around primordial follicles (164). In both prepubertal and reproductive-age patients they observed a significant decline in EMILIN-1 levels following follicle activation in reproductive-age ovaries (164). EMILIN1 has been shown to serve as a negative regulator of TGFβ-mediated signaling, primarily in cardiac, marfan syndrome, and other organ systems in tandem with Fibrillin-1 (165-167). The TGFβ pathway itself is ubiquitously expressed and the super family of TGFβ associated proteins includes multiple growth factors as detailed in **Chapter 1** (168). In the ovary, multiple studies have implicated TGFβ-mediated signaling as being involved in other ovarian processes including

early ovarian development, homeostasis, and follicle development (168). Specifically, to primordial follicle activation TGFβ signaling, and factors have been shown to act via PI3K and BMP-associated pathways (169-171). Additionally, EMILIN-1 has been shown to be a negative regulator of cell proliferation. A more recent study examining the activation of primordial follicles via the induction of primordial granulosa cells from squamous to cuboidal proposed a TGFβ-mediated signal modulating the nuclear localization of SMAD2/3 towards maintaining follicle quiescence in murine ovaries (101). The changes to granulosa cell morphology and granulosa cell proliferation were shown to precede oocyte growth and nuclear translocation of FOXO3a, a transcription factor important in follicle activation that is specific to murine models (101). By immunolabelling of the TGFβ signaling mediators and transcription factors SMAD2/3 the authors of the study revealed a striking expression pattern specific to granulosa cells of small follicles, that SMAD2/3 were expressed in the nuclei of primordial granulosa cells but were excluded in activated/growing follicles instead having higher expression of Ki67, a well-known marker of cell proliferation (101). These findings suggest that the first phenotypic changes during follicle activation are observed in GCs, and that TGFβ signaling is fundamental for regulating GC arrest and the onset of proliferation which would indicate that a mediator of TGFβ could be a major contributor to follicle activation or quiescence depending on if it suppressed or promoted TGFβ signaling. The researchers propose an unknown activating signal would drive nuclear export of SMAD2/3 leading to increased granulosa cell proliferation and cuboidilization resulting in the activation of primordial follicles (101). This was further supported in work where SMAD3 was found directly regulate cell cycle genes that maintain arrest of granulosa cells around primordial follicles (172). This study exposed ovaries isolated from neonatal mice for 2 hours to 10ng/mL of TGFβ1 *in* vitro, which led to immediate dissociation of SMAD3 from the Ccnd2 and Myc

promoters (172). This coincided with elevated Myc and phospho-S6, an indicator of mTOR signaling, followed by a small increase in mean primordial granulosa cell number after 48 hours (172). The findings from this study showed a concentration-dependent role for TGFβ signaling in the maintenance and activation of primordial follicles in murine ovaries, through both SMAD-dependent and independent signaling pathways and they proposed a multi-step mechanism of follicle activation that initially involves a basal level of SMAD3 expression to prime granulosa cells for activation (172). Increased TGFβ1 ligand exposure then promotes a shift to a SMAD-independent pathway driving granulosa cell proliferation and primordial follicle activation (172). To contextualize this EMILIN1 has been shown to negatively regulate TGFβ by blocking conversion of pro-TGFβ to biologically active mature TGFβ (173-176). Blocking this conversion acts to inhibit TGFβ signaling and results in altered SMAD2/3 localization in a dose, and stage-dependent manner (173-176). Maturation of TGF-β occurs after MMP-dependent proteolysis releases pro- TGF-β making it accessible or through alterations mechanical tension of tissues which also indicates that as follicles activate and remodel their microenvironment, they release more TGF-β stimulating folliculogenesis (309). Indeed, it is also good to note that there is significant crosstalk between TGFβ superfamily members and multiple other pathways including PI3K/Akt/mTOR and that this context will also be important to establish. Despite these promising results from spatial mapping and SMAD-mediate signaling the identity of the maintenance signal being proposed that would maintain this system remains elusive, however the evidence points towards EMILIN1 being an important component of this system showing the utility of matrisome mapping towards unbiased discovery of potential mediators of follicle activation and folliculogenesis. Ongoing work moving forward selectively mediated materials should allow the

dissection of the role of EMILIN1, and other candidate proteins, in primordial follicle activation (See Future directions).

There is a rigidity gradient across ovarian compartments in a bovine model and this is recapitulated in engineered materials derived from these compartments

In **Chapter 3** we sought to understand the contribution of the ovarian microenvironment to its physical and biochemical properties to potentially inform the design of next generation bioprosthetic ovary scaffolds that would support isolated follicles. Using atomic force microscopy (AFM), in this chapter we show that the bovine ovary has a range of rigidity of 1.4 – 8.86 kPa. This data supports the previous observation that the cortex is more rigid than the medulla with a statistically significant decline in rigidity from the outer edge of the ovary (0.5mm) toward the center (3.5mm). Further, the data shows that the ovarian cortex is cortex tissue is 7.6 x more rigid (kPa) than medulla tissue. In order to determine if this difference in rigidity was maintained in isolated matrisome proteins from bovine ovarian compartments, we cast, and 3D printed hydrogels created from decellularized extracellular matrix derived from either bovine ovarian cortex or medulla slices. This material was then cast as a gel or 3D printed using a previously established bioprosthetic ovary scaffold of 60 degree advancing angle design using the FRESH printing method (**Described in Chapters 1 and 3**). The cast gels and 3D printed bioprosthetic ovary scaffolds from the cortex were both significantly more rigid than those derived from the medulla. Specifically, in cast gels the cortex derived ECM gel is 155 x more rigid (kPa) than medulla derived. This data together shows that there is a rigidity gradient in the bovine ovary with cortex being more rigid with rigidity declining and that the matrisome is a major contributor to this rigidity gradient as is seen with the rigidity of engineered materials maintaining this difference. This provides a new toolkit and reference point for future *in vitro* culture experiments to use the rigidities found in the bovine ovary when looking at follicle dynamics.

Investigating the rigidity gradient of the ovary, primordial follicle activation, and controversy within the field

Physical cues are both intracellularly generated and externally applied forces, and, like biochemical cues, they have a broad impact on cell behavior (e.g., growth, differentiation, and function) (129, 137, 138). These signals require mechanosensing units, which include cytoplasmic complexes such as integrins, extracellular components such as ECM cell adhesion molecules, and intracellular components including the cytoskeleton (139). Specifically, the ECM transduces information via cell surface processes, stress of cellular membranes, stretch-sensitive ion channels, surface receptors, changes in biopolymers, extracellular fluid pressure, and tissue-dependent enzymes or proteins at the cell surface (140-145). Significant *in vitro* work has examined the effects of rigidity on isolated follicles based on observational data about a rigidity gradient existing from a more rigid cortex to a more pliable medulla (150, 151,152,153,154). Most *in vitro* work has leveraged alginate encapsulation of primordial and later stage follicles to examine the contribution of rigidity to follicle activation and folliculogenesis (150, 151, 152,153,154). *In vitro* culture of primordial follicles from rhesus macaque in 2% alginate, thus replicating a high-rigidity environment, maintained optimal primordial follicle survival and morphology, whereas a more pliable 0.25–1.25% alginate environment supported increased hormone production in activated or growing follicles (150, 151, 152, 153, 154). Beyond alginate encapsulation work by Nagamatsu et al 2019 leveraged a light enzymatic treatment (CTK: collagenase type IV, trypsin, and knockout serum replacement) on murine ovaries which resulted in export of FOXO3 to the cytoplasm of small oocytes (<20 μm in diameter). The percentage of oocytes with cytoplasmic FOXO3, an indicator of follicle activation, was significantly higher in CTK-treated ovaries than in OBS treated controls as well (158). The rate of activation over 14 days in culture showed the number of large

oocytes (>50 µm in diameter) was significantly increased in the CTK-treated ovaries compared to the control ovaries (158). This activation in CTK-treated ovaries was counteracted by the application of hydrostatic pressure, which strongly indicates a role for physical forces in follicle activation divorced of disruption of the microenvironment (158). While this body of works strongly implicates physical forces, including increased, in follicle activation it was done without a quantified rigidity gradient in native ovaries. To decipher the rigidity of the ovary there have been multiple recent investigations utilizing different methods. One using shear-wave velocities across *ex vivo* bovine ovaries indicated differences in the viscoelastic properties of the ovary across compartments (155). Shear wave (SW) measurements showed significant variations between the cortex and medulla, as measured along the length (cortex: 2.57 ± 0.53 m/s, medulla: 2.87 ± 0.77 m/s) and width (cortex: 2.99 ± 0.81 m/s, medulla: 3.24 ± 0.97 m/s) and the spatial distribution and magnitude of SW velocity vary between these two anatomical planes overall showing SW velocity being 11.4% and 8.4% higher in the medulla than the cortex, indicating higher rigidity of the medulla, at a resolution of ~1mm with this result running contrary to popular observational data that the ovarian cortex is more rigid than the medulla (155). Additional research in murine models showed two rigidity peaks in murine models with low stiffness at the edge and center of the ovary with an overall rigidity range spanning 0.5–10 kPa, with substantial spatial variation on a microstructural level, in addition to larger-scale differences between the different regions of the ovary. The range of values detected in this murine experiment is consistent with our own gross AFM mapping in higher mammalian ovaries though the distribution of high versus low rigidity is different. This study concluded that higher stiffness regions were dominated by large developmentally advanced follicles, suggesting that these structures should be considered mechanically dominant in the ovary. However, using engineered materials we have been able to

determine that dECM hydrogels retain the significant differences in rigidity between compartments indicating that the composition of the ECM also plays a role in determining the physical properties in higher mammalian species. This conclusion is supported by a higher-resolution rigidity mapping experiment carried out in murine ovaries that showed significant changes in the rigidity of the ovary across the lifespan with older mice having more rigid ovaries compared to those of reproductive in tandem with changes to the amount of COL1 detected (156, 157). In support of our own data showing that ovarian rigidity is in part supported by the ECM these changes in rigidity were reversed when the ovaries were treated with collagenase which strongly indicates that the matrisome is providing the difference in rigidity of ovaries at different ages which is consistent with the AFM carried out in engineered materials derived from bovine dECM as detailed in **Chapter 3** (156, 157). There has been limited research done on the rigidity of human ovaries and the work done thus far has focused on the cortex across reproductive ages finding that the rigidity of this compartment was 3178 Pa (±245) for reproductive-age ovaries and significantly more rigid for prepubertal ($6538\,Pa \pm 351$) and menopausal ($7117\,Pa \pm 714$) ovaries. The next steps forward will be higher-resolution mapping in higher-mammalian species across compartments and using *in vitro* culture to examine if the rigidities observed in the ovary lead to differential effects in follicle activation and folliculogenesis (see future directions below).

We have established a platform for selectively depleting matrisome proteins for future mechanistic studies

In the second half of **Chapter 3,** we described a toolkit for examining the contribution of matrisome proteins to follicle activation and folliculogenesis by selectively depleting the candidate proteins EMILIN1 and AGRN using magnetic assisted protein filtration (MAPF). We demonstrated that selective depletion of EMILIN1 and AGRN did not alter the rigidity of gels or

printed scaffolds in comparison to whole untreated hydrogels and inks. However, while this is true for these two proteins this may not be true for all proteins, and it is likely that some selective depletion of fibrous proteins or structural proteins such as collagens, would affect the rigidity of the resultant biomaterial products. Using human mesenchymal stem cells (hMSCs) cultured on these depleted materials we showed no significant differences in proliferation or cell survival for depleted materials compared to whole materials and that the depleted materials drive gene expression that is reversed with addition of the depleted protein. Together this data paints a picture that we have a novel toolkit for use in deciphering matrisome:follicle interactions *in vitro* by combining our MAPF system with our engineered materials.

Future Directions

The experiments described in **Chapter 2-3** identified significant differences in the distribution of matrisome proteins and rigidity across ovarian compartments. Further, in **Chapter 3** we characterize engineered materials derived from both ovarian compartments using atomic force microscopy (AFM) and compare those rigidities to established *in vitro* culture methods finding significant differences between those methods and rigidities in the ovary. Further, in **Chapter 3** we characterize a novel method for selectively depleting matrisome proteins using magnetic assisted protein filtration (MAPF) and how gene expression, survival, and proliferation human mesenchymal stem cells change when cultured on these materials. However, significant questions remain about the distribution of matrisome proteins, physical cues, and the mechanistic relationship between follicle activation, folliculogenesis, and the matrisome. The following experiments have been designed to further our understanding of how matrisome protein candidates EMILIN1 and AGRN drive follicle dynamics, how physical cues map to ovarian structures, how rigidities found using our AFM experiments drive follicle dynamics in higher mammals, and

finally outline experiments for creating an unbiased high-resolution map of the matrisome in the ovary.

Using compartmental rigidity to explore the contribution of compartment-specific physical cues to follicle dynamics

Previously alginate experiments have shown that changes to rigidity create follicle stage-specific effects on follicle growth and survival (151-154). However, now having quantified the rigidity of the bovine ovarian cortex and medulla we can use these measurements in conjunction with alginate encapsulation to determine if compartment specific rigidities support follicle activation or quiescence. Utilizing alginate, an inert material that has been previously shown to support folliculogenesis we can create gels that have physical properties tuned to their specific compartment as is detailed in **Chapter 3** (151-154, 204). Based on this data we will use alginate gels of 8kPa and 2-4kPa that will represent cortical and medullary rigidity, respectively. Primordial follicles will be cultured in clusters of 10 as previously performed with non-human primate and murine follicles to increase follicle survival and secondary follicles will be cultured individually (41,152). The follicles will be cultured in growth media for 18 days (up until the point where they would normally be removed for in vitro ovulation cultures) and analyzed using standard processes with collection points every other day for assessing follicle survival and growth by using light microscopy to measure follicle and oocyte diameter and formation of an antrum and ELISAs for estradiol secretion into the media (60). These results will indicate if matched micromechanical properties better support follicle quiescence and growth independent of any biochemical support provided by the substrate

High-resolution mapping of the physical properties of the ovary

In **Chapter 3** we quantified the rigidity gradient in low resolution. However, using high-resolution AFM mapping we can identify if these compartmental differences in the micromechanical

properties of the bovine ovary are associated with specific follicle stages or ovarian structures. One half of the ovary will be fixed while the other will be submitted for AFM analysis. AFM analyses will be carried out by adhering the ovarian tissue to a 35mm dishes using AFM safecoat, to minimize artifacts. AFM will be performed using a Piuma nano-indenter equipped with a 25µm probe to allow for greater special resolution. This will provide rigidity as a Young's modulus reading as previously performed to identify tissue rigidity (294-297). We will map the rigidity gradient in 50µm increments in both anterior and axial directions to form a 25X10 grid located at the cortex, mid-medulla, and deep medulla. To correlate the probe reading with ovarian topography, the data from the AFM analysis will be overlaid with H&E staining of the adjacent slice that was fixed after bisecting the ovary. Clear inclusion/exclusion criteria will be established prior to analysis of assay results and will include consideration of the proximity of large antral follicles and vessels to the probe tip. These results will define the physical rigidity across the bovine ovarian compartments and follicle stages allowing us to examine the contribution of follicular compartments and structures to the microenvironment of the ovary.

Exploring the relationship between EMILIN1 and AGRN to follicle activation and folliculogenesis
In **Chapter 3** we established and characterized a toolkit for selectively depleting matrisome proteins from whole dECM prior to 3D-printing or gel casting. We seeded hMSCs onto plates coated with these materials and found that they drove differential gene expression consistent with the literature. We can now leverage this system to look at matrisome:follicle mechanisms. In order to examine the contribution of EMILIN1 we will use the magnet assisted protein filtration (MAPF) method to selectively deplete the candidate from dECM prior to printing scaffolds using the FRESH 3D printing technique. Primordial follicles will be cultured in clusters of 10, as this was found to be beneficial in cultures using alginate beads, in growth media for 18 days (up until the

point where they would normally be removed for *in vitro* ovulation cultures) (232). Rescue experiments will be performed similarly to those in **Chapter 3** with adding a physiological concentration of EMILIN1 or AGRN back into the culture system via growth media supplementation. Assessment of follicle activation will be carried out using antibodies examining DDX4/Laminin (quiescent) and DDX4/ZP3 (activated/growing), granulosa cell proliferation will be determined using an antibody for Ki67 and compared to follicles seeded in un-filtered dECM scaffolds. Specific to EMILIN1 IHC will examine nuclear localization of downstream effector protein SMAD2/3 and ratios of TGFβ/proTGFβ (85,86). This experiment will tell us if EMILIN1 contributes to primordial follicle activation in bovine ovaries and if this contribution is through a TGFβ and SMAD2/3 mediated pathway

For AGRN the above experiment will be modified to examine DAG1 and HIPPO and their contributions to follicle activation and folliculogenesis. To quantify changes to follicle activation we will use IHC-based methods to count the ratio of primordial follicles (DDX4/LMNA) to activated/growing follicles (ZP3/DDX4) over eighteen days in culture and then compared to those grown on scaffolds with and without AGRN (174, 270). We investigate HIPPO pathway dynamics through nuclear localization and phosphorylation of the YAP protein (178, 180-182). We will use qPCR to quantify the expression of pathway-specific genes that are turned on during Yap nuclear localization: CCN2, BIRC6/7 which are only expressed when YAP1 is localized to the nucleus and compare expression with that of follicles cultured in unfiltered gels (178, 180-182). This experiment will tell us is if the HIPPO pathway, mediated by AGRN, contributes to primordial follicle activation and progression of folliculogenesis.

Alternatively, in place of 3D printed scaffolds an encapsulation method could be used such as alginate where the bead is supplemented with either AGRN or EMILIN1 to examine any changes

to follicle activation and folliculogenesis occur independent of any other matrisome-based biochemical cues.

References

1. L.R. Meacham, et al. Standardizing risk assessment for treatment-related gonadal insufficiency and infertility in childhood adolescent and young adult cancer: the pediatric initiative network risk stratification system J. Adolesc. Young Adult., 9 (2020), pp. 662-666

2. G.M. Armuand, et al. Desire for children, difficulties achieving a pregnancy, and infertility distress 3 to 7 years after cancer diagnosis Support Care Cancer, 22 (2014), pp. 2805-2812

3. J. Słowikowska-Hilczer, et al. Fertility outcome and information on fertility issues in individuals with different forms of disorders of sex development: findings from the dsd-LIFE study

4. T. Muka, et al. Association of age at onset of menopause and time since onset of menopause with cardiovascular outcomes, intermediate vascular traits, and all-cause mortality: a systematic review and meta-analysis JAMA Cardiol., 1 (2016), pp. 767-776

5. W. Chemaitilly, et al. Premature ovarian insufficiency in childhood cancer survivors: a report from the St. Jude Lifetime Cohort J. Clin. Endocrinol. Metab., 102 (2017), pp. 2242-2250

6. F. Pacheco, K. Oktay Current success and efficiency of autologous ovarian transplantation: a meta-analysis Reprod. Sci., 24 (2017), pp. 1111-1120

7. J. Donnez, M.-M. Dolmans Fertility preservation in women New Engl. J. Med., 377 (2017), pp. 1657-1665

8. M. Shapira, et al. Evaluation of ovarian tissue transplantation: results from three clinical centers Fertil. Steril., 114 (2020), pp. 388-397

9. Laronda, M. M. Engineering a bioprosthetic ovary for fertility and hormone restoration. *Theriogenology* (2020)

10. Jadoul P, Guilmain A, Squifflet J, Luyckx M, Votino R, Wyns C, et al. Efficacy of ovarian tissue cryopreservation for fertility preservation: lessons learned from 545 cases. Hum Reprod 2017;32:1046e54.

11. Dolmans, M.-M. et al. Reimplantation of cryopreserved ovarian tissue from patients with acute lymphoblastic leukemia is potentially unsafe. Blood 116, (2010) pp. 2908-2914

12. M. Rosendahl, et al. Evidence of residual disease in cryopreserved ovarian cortex from female patients with leukemia Fertil. Steril., 94 (2010), pp. 2186-2190

13. E. Kniazeva, et al. Primordial follicle transplantation within designer biomaterial grafts produce live births in a mouse infertility model Sci. Rep., 5 (2015), p. 17709

14. M. Soares, et al. Eliminating malignant cells from cryopreserved ovarian tissue is possible in leukaemia patients Brit. J. Haematol., 28 (2017), pp. 255-259

15. M.M. Laronda, et al. A bioprosthetic ovary created using 3D printed microporous scaffolds restores ovarian function in sterilized mice Nat. Commun., 8 (2017), p. 15261

16. Kim JY. Control of ovarian primordial follicle activation. Clin Exp Reprod Med. 2012 Mar;39(1):10-4.

17. Pelosi E, Omari S, Michel M, Ding J, Amano T, Forabosco A, Schlessinger D, Ottolenghi C. Constitutively active Foxo3 in oocytes preserves ovarian reserve in mice. Nat Commun. 2013.

18. Gorre N, Adhikari D, Lindkvist R, Brännström M, Liu K, Shen Y. mTORC1 Signaling in oocytes is dispensable for the survival of primordial follicles and for female fertility. PLoS One. 2014 Oct 22;9(10).

19. Rajareddy S, Reddy P, Du C, Liu L, Jagarlamudi K, Tang W, Shen Y, Berthet C, Peng SL, Kaldis P, Liu K. p27kip1 (cyclin-dependent kinase inhibitor 1B) controls ovarian development by suppressing follicle endowment and activation and promoting follicle atresia in mice. Mol Endocrinol. 2007.

20. Choi Y, Qin Y, Berger MF, Ballow DJ, Bulyk ML, Rajkovic A. Microarray analyses of newborn mouse ovaries lacking Nobox. Biol Reprod. 2007.

21. Pangas SA, Choi Y, Ballow DJ, Zhao Y, Westphal H, Matzuk MM, Rajkovic A. Oogenesis requires germ cell-specific transcriptional regulators Sohlh1 and Lhx8. Proc Natl Acad Sci U S A. 2006.

22. Gershon, E., & Dekel, N. (2020). Newly Identified Regulators of Ovarian Folliculogenesis and Ovulation. International journal of molecular sciences, 21(12), p. 4565.

23. Pedersen T, Hannah P (1968) Proposal for a classification of oocytes and follicles in the mouse ovary. J Reprod Fertil 17: pp. 555–557

24. Magoffin DA (2005) Ovarian theca cell. Int J Biochem Cell Biol 37: pp. 1344–1349.

25. Eppig JJ (2001) Review Oocyte control of ovarian follicular development and function in mammals. Reproduction 122(6): pp. 829–838

26. Edson MA, Nagaraja AK, Matzuk MM et al (2009) The mammalian ovary from genesis to revelation. Endocr Rev 30: pp. 624–712.

27. Richards JS, Pangas SA (2010a) Fertility control. Handb Exp Pharmacol pp. 198:3–27.

28. Uda M, Ottolenghi C, Crisponi L et al (2004) Foxl2 disruption causes mouse ovarian failure by pervasive blockage of follicle development. Hum Mol Genet 13: pp. 1171–1181.

29. Zheng W, Nagaraju G, Liu Z, Liu K (2012) Functional roles of the phosphatidylinositol 3-kinases (PI3Ks) signaling in the mammalian ovary. Mol Cell Endocrinol 356: pp. 24–30.

30. Salomon Y, Yanovsky A, Mintz Y et al (1977) Synchronous generation of ovarian hCG binding sites and LH-sensitive adenylate cyclase in immature rats following treatment with pregnant mare serum gonadotropin. J Cyclic Nucleotide Res 3: pp. 163–176.

31. West, E.R., Shea, L.D., and Woodruff, T.K. Engineering the follicle microenvironment.

(2007) Semin Reprod Med 25(4): pp. 287-99.

32. Berkholtz CB, Shea LD & Woodruff TK 2006 Extracellular matrix functions in follicle maturation. Seminars in Reproductive Medicine pp. 262–269.

33. Ford, E. A., Beckett, E. L., Roman, S. D., McLaughlin, E. A., & Sutherland, J. M. (2020). Advances in human primordial follicle activation and premature ovarian insufficiency, Reproduction, 159(1), pp. R15-R29.

34. Fujihara M, Yamamizu K, Comizzoli P, Wildt DE & Songsasen N 2018 Retinoic acid promotes in vitro follicle activation in the cat ovary by regulating expression of matrix metalloproteinase 9. PLoS ONE e0202759.

35. Luti, S, Fiaschi, T, Magherini, F, et al. Follicular microenvironment: Oxidative stress and adiponectin correlated with steroids hormones in women undergoing in vitro fertilization. Mol Reprod Dev. 2021; 88: pp. 175– 184.

36. Teilmann SC (2005) Differential expression and localisation of connexin-37 and connexin-43 in follicles of different stages in the 4-week-old mouse ovary. Mol Cell Endocrinol 234: pp. 27–35.

37. Swartz, M.A., Tschumperlin, D.J., Kamm, R.D., and Drazen, J.M. Mechanical stress is communicated between different cell types to elicit matrix remodeling. (2001) Proc Natl Acad Sci U S A 98(11): pp. 6180-5.

38. Kidder GM, Mhawi AA. Gap junctions and ovarian folliculogenesis. Reproduction. 2002 May;123(5): pp. 613-20.

39. Ackert CL, Gittens JE, O'Brien MJ, Eppig JJ, Kidder GM. Intercellular communication via connexin43 gap junctions is required for ovarian folliculogenesis in the mouse. Dev Biol. 2001 May 15;233(2): pp. 258-70.

40. Gittens JE, Kidder GM. Differential contributions of connexin37 and connexin43 to oogenesis revealed in chimeric reaggregated mouse ovaries. J Cell Sci. 2005 Nov 1;118(Pt 21): pp. 5071-8.

41. M.M. Laronda, et al. Initiation of puberty in mice following decellularized ovary transplant Biomaterials, 50 (2015), pp. 20-29

42. F. Bochner, et al. A novel intravital imaging window for longitudinal microscopy of the mouse ovary Sci. Rep., 5 (2015), p. 12446

43. N.F. Henning, et al. Proteomic analyses of decellularized porcine ovaries identified new matrisome proteins and spatial differences across and within ovarian compartments Sci. Rep., 9 (2019), p. 20001

44. X. Shao, et al. MatrisomeDB: the ECM-protein knowledge database

Nucleic Acids Res., 48 (2019), pp. D1136-D1144

45. J.S. Shah, et al. Biomechanics and mechanical signaling in the ovary: a systematic review J. Assist. Reprod. Genet., 321 (2018), pp. 1-14

46. T.J. Keane, et al. Tissue-specific effects of esophageal extracellular matrix Tissue Eng. A, 21 (2015), pp. 2293-2300

47. Naba A, Clauser KR, Hoersch S, et al. The matrisome: in silico definition and in vivo characterization by proteomics of normal and tumor extracellular matrices. Mol Cell Proteomics. 2012; p. 11.

48. Naba A, Clauser KR, Lamar JM, et al. Extracellular matrix signatures of human mammary carcinoma identify novel metastasis promoters. eLife. 2014

49. aba A, Clauser KR, Whittaker CA, et al. Extracellular matrix signatures of human primary metastatic colon cancers and their metastases to liver. BMC Cancer. 2014;14:518.

50. Hansen KC, Kiemele L, Maller O, et al. An in-solution ultrasonication-assisted digestion method for improved extracellular matrix proteome coverage. Mol Cell Proteomics. 2009;8: pp. 1648–57.

51. Belluoccio D, Wilson R, Thornton DJ, et al. Proteomic analysis of mouse growth plate cartilage. *Proteomics.* 2006;6:6549–6553.

52. Schreiweis MA, Butler JP, Kulkarni NH, et al. A proteomic analysis of adult rat bone reveals the presence of cartilage/chondrocyte markers. *J Cell Biochem.* 2007;101:466–476.

53. Balasubramani M, Schreiber EM, Candiello J, et al. Molecular interactions in the retinal basement membrane system: a proteomic approach. *Matrix Biol.* 2010;29:471–483.

54. Didangelos A, Yin X, Mandal K, et al. Proteomics characterization of extracellular space components in the human aorta. *Mol Cell Proteomics.* 2010;9:2048–2062.

55. O'Brien J, Fornetti J, Schedin P. Isolation of mammary-specific extracellular matrix to assess acute cell-ECM interactions in 3D culture. *J Mammary Gland Biol Neoplasia.* 2010;15:353–364.

56. Wilson R, Diseberg AF, Gordon L, et al. Comprehensive profiling of cartilage extracellular matrix formation and maturation using sequential extraction and label-free quantitative proteomics. *Mol Cell Proteomics.* 2010;9:1296–1313.

57. Didangelos A, Yin X, Mandal K, et al. Extracellular matrix composition and remodeling in human abdominal aortic aneurysms: a proteomics approach. *Mol Cell Proteomics.* 2011;10

58. Barallobre-Barreiro J, Didangelos A, Schoendube FA, et al. Proteomics analysis of cardiac extracellular matrix remodeling in a porcine model of ischemia/reperfusion injury. *Circulation.* 2012;125:789–802.]

59. Booth AJ, Hadley R, Cornett AM, et al. Acellular normal and fibrotic human lung matrices as a culture system for in vitro investigation. *Am J Respir Crit Care Med.* 2012;186:866–876.

60. Önnerfjord P, Khabut A, Reinholt FP, et al. Quantitative proteomic analysis of eight cartilaginous tissues reveals characteristic differences as well as similarities between subgroups. *J Biol Chem.* 2012;287:18913–18924.

61. Decaris ML, Gatmaitan M, FlorCruz S, et al. Proteomic analysis of altered extracellular matrix turnover in bleomycin-induced pulmonary fibrosis. *Mol Cell Proteomics.* 2014;13:1741–1752.

62. Lennon R, Byron A, Humphries JD, et al. Global analysis reveals the complexity of the human glomerular extracellular matrix. *J Am Soc Nephrol.* 2014;25:939–951.

63. Müller C, Khabut A, Dudhia J, et al. Quantitative proteomics at different depths in human articular cartilage reveals unique patterns of protein distribution. *Matrix Biol.* 2014;40:34–45.

64. Uechi G, Sun Z, Schreiber EM, et al. Proteomic view of basement membranes from human retinal blood vessels, inner limiting membranes, and lens capsules. *J Proteome Res.* 2014

65. Hill RC, Calle EA, Dzieciatkowska M, et al. Quantification of extracellular matrix proteins from a rat lung scaffold to provide a molecular readout for tissue engineering. *Mol Cell Proteomics MCP.* 2015;14:961–973.

66. A.E. Jakus, et al. 'Tissue papers' from organ-specific decellularized extracellular matrices Adv. Funct. Mater., 27 (2017), p. 1700992

67. Shridhar A, Amsden BG, Gillies ER, Flynn LE. Investigating the Effects of Tissue-Specific Extracellular Matrix on the Adipogenic and Osteogenic Differentiation of Human Adipose-Derived Stromal Cells Within Composite Hydrogel Scaffolds. Front Bioeng Biotechnol. 2019 Dec 11;7:402..

68. Yuanyuan Zhang, Yujiang He, Shantaram Bharadwaj, Nevin Hammam, Kristen Carnagey, Regina Myers, Anthony Atala, Mark Van Dyke. Tissue-specific extracellular matrix coatings for the promotion of cell proliferation and maintenance of cell phenotype. Biomaterials. 2009 Aug; 30(23-24): 4021–4028.

69. Woodruff TK, Shea LD. A new hypothesis regarding ovarian follicle development: ovarian rigidity as a regulator of selection and health. J Assist Reprod Genet. 2011 Jan;28(1):3-6. doi: 10.1007/s10815-010-9478-4. Epub 2010 Sep 25. PMID: 20872066; PMCID: PMC3045494.

70. T. Wang, et al. Mechanophysical cues in extracellular matrix regulation of cell behavior Chembiochem, 21 (2020), pp. 1254-1264

71. Rodriguez A., Briley S.M., Patton B.K., Tripurani S.K., Rajapakshe K., Coarfa C., Rajkovic A., Andrieux A., Dejean A., Pangas S.A. Loss of the E2 SUMO-conjugating enzyme Ube2i in oocytes during ovarian folliculogenesis causes infertility in mice. Development. 2019;146

72. Brown C., LaRocca J., Pietruska J., Ota M., Anderson L., Smith S.D., Weston P., Rasoulpour T., Hixon M.L. Subfertility caused by altered follicular development and oocyte growth in female mice lacking PKB alpha/Akt1. Biol. Reprod. 2010;82:246–256.

73. Hu L.L., Su T., Luo R.C., Zheng Y.H., Huang J., Zhong Z.S., Nie J., Zheng L.P. Hippo pathway functions as a downstream effector of AKT signaling to regulate the activation of primordial follicles in mice. J. Cell Physiol. 2019;234:1578–1587.

74. Nguyen X.P., Nakamura T., Osuka S., Bayasula B., Nakanishi N., Kasahara Y., Muraoka A., Hayashi S., Nagai T., Murase T., et al. Effect of the Neuropeptide Phoenixin and Its Receptor GPR173 During Folliculogenesis. Reproduction. 2019

75. Arcos A., Paola M., Gianetti D., Acuna D., Velasquez Z.D., Miro M.P., Toro G., Hinrichsen B., Munoz R.I., Lin Y., et al. alpha-SNAP is expressed in mouse ovarian granulosa cells and plays a key role in folliculogenesis and female fertility. Sci. Rep. 2017;7:11765.

76. Mao Z., Yang L., Lu X., Tan A., Wang Y., Ding F., Xiao L., Qi X., Yu Y. C1QTNF3 in the murine ovary and its function in folliculogenesis. Reproduction. 2018;155:333–346.

77. Vitt UA, McGee EA, Hayashi M, Hsueh AJ. In vivo treatment with GDF-9 stimulates primordial and primary follicle progression and theca cell marker CYP17 in ovaries of immature rats. Endocrinology. 2000 Oct;141(10):3814-20. doi: 10.1210/endo.141.10.7732.

78. Devesa, J and Diego C. The Role of Growth Hormone on Ovarian Functioning and Ovarian Angiogenesis. *Front. Endocrinol.* 2019 July.

79. McGee EA, et al. Follicle-Stimulating Hormone Enhances the Development of Preantral Follicles in Juvenile Rats. *Biology of Reproduction.* 57, 990-998 (1997).

80. Yan H, Zhang J, Wen J, et al. CDC42 controls the activation of primordial follicles by regulating PI3K signaling in mouse oocytes. *BMC Biol*. 2018.

81. Gee SH, Montanaro F, Lindenbaum MH, Carbonetto S. Dystroglycan-alpha, a dystrophin-associated glycoprotein, is a functional Agrin receptor. Cell. 1994;77(5):675–686.

82. Ng, K.-M. *et al.* Evidence That Fibulin Family Members Contribute to the Steroid-dependent Extravascular Sequestration of Sex Hormone-binding Globulin. *J Biol Chem* **281**, 15853–15861 (2006).

83. Xie, J. & Haslam, S. Z. Extracellular Matrix Regulates Ovarian Hormone-Dependent Proliferation of Mouse Mammary Epithelial Cells 1. *Endocrinology* **138**, 2466–2473 (1997).

84. Laronda, M. M. *et al.* Alginate encapsulation supports the growth and differentiation of human primordial follicles within ovarian cortical tissue. *J Assist Reprod Gen* **31**, 1013 1028 (2014). PMID: 24845158, PMCID: PMC4130945

85. Granados-Aparici S, Hardy K, Franks S, Sharum IB, Waite SL, Fenwick MA. SMAD3 directly regulates cell cycle genes to maintain arrest in granulosa cells of mouse primordial follicles. Sci Rep. 2019 Apr 24;9(1):6513.

86. Hardy Kate, Mora Jocelyn M., Dunlop Carina, Carzaniga Raffaella, Franks Stephen, Fenwick Mark A. Nuclear exclusion of SMAD2/3 in granulosa cells is associated with primordial follicle activation in the mouse ovary. Journal of Cell Science. 2018;131(17):jcs218123

87. A. Lee, et al. 3D bioprinting of collagen to rebuild components of the human heart Science, 365 (2019), pp. 482-487

88. B. Brown, et al. The basement membrane component of biologic scaffolds derived from extracellular matrix Tissue Eng., 12 (2006), pp. 519-526

89. J.P. Hodde, et al. Glycosaminoglycan content of small intestinal submucosa: a bioscaffold for tissue replacement Tissue Eng., 2 (1996), pp. 209-217

90. T. Lu, et al. Enhanced osteointegration on tantalum-implanted polyetheretherketone surface with bone-like elastic modulus Biomaterials, 51 (2015), pp. 173-183

91. D.E. Koser, et al. CNS cell distribution and axon orientation determine local spinal cord mechanical properties Biophys. J., 108 (2015), pp. 2137-2147

92. M. Saito, K. Marumo Effects of collagen crosslinking on bone material properties in health and disease Calcif. Tissue Int., 97 (2015), pp. 242-261

93. Y.M. Coulson-Thomas, et al. The identification of proteoglycans and glycosaminoglycans in archaeological human bones and teeth PLoS One, 10 (2015), Article e0131105

94. C. Pierret, et al. Developmental cues and persistent neurogenic potential within an in vitro neural niche BMC Dev. Biol., 10 (2010), p. 5

95. J. Massoulié, C.B. Millard Cholinesterases and the basal lamina at vertebrate neuromuscular junctions Curr. Opin. Pharmacol., 9 (2009), pp. 316-325

96. J.R. Sanes The basement membrane/basal lamina of skeletal muscle J. Biol. Chem., 278 (2003), pp. 12601-12604

97. J. Hodde, et al. Fibronectin peptides mediate HMEC adhesion to porcine-derived extracellular matrix Biomaterials, 23 (2002), pp. 1841-1848

98. A. Peloso, et al. The human pancreas as a source of protolerogenic extracellular matrix scaffold for a new-generation bioartificial endocrine pancreas Ann. Surg., 264 (2016), pp. 169-179

99. V.L. Massey, et al. The hepatic 'matrisome' responds dynamically to injury: characterization of transitional changes to the extracellular matrix in mice Hepatology, 65 (2017), pp. 969-982

100. E.C. Opara, et al. Design of a bioartificial pancreas J. Investig. Med., 58 (2010), p. 831

101. K. Hardy, et al. Nuclear exclusion of SMAD2/3 in granulosa cells is associated with primordial follicle activation in the mouse ovary J. Cell Sci., 131 (2018), Article jcs.218123

102. X. Fang, et al. SMAD3 activation: a converging point of dysregulated TGF-beta superfamily signaling and genetic aberrations in granulosa cell tumor development? Biol. Reprod., 95 (2016), p. 105

103. I.B. Sharum, et al. Serine threonine kinase receptor associated protein regulates early follicle development in the mouse ovary Reproduction, 153 (2017), pp. 221-231

104. J.R. Gershlak, et al. Mesenchymal stem cells ability to generate traction stress in response to substrate stiffness is modulated by the changing extracellular matrix composition of the heart during development Biochem. Biophys. Res. Commun., 439 (2013), pp. 161-166

105. J. Gravning, et al. Myocardial connective tissue growth factor (CCN2/CTGF) attenuates left ventricular remodeling after myocardial infarction PLoS One, 7 (2012), Article e52120

106. S.E. Mercer, et al. A dynamic spatiotemporal extracellular matrix facilitates epicardial-mediated vertebrate heart regeneration Dev. Biol., 382 (2013), pp. 457-469

107. B.I. Jugdutt Ventricular remodeling after infarction and the extracellular collagen matrix Circulation, 108 (2003), pp. 1395-1403

108. A.J. Booth, et al. Acellular normal and fibrotic human lung matrices as a culture system for in vitro investigation Am. J. Respir. Crit. Care, 186 (2012), pp. 866-876

109. C.G.M. van Dijk, et al. Extracellular matrix analysis of human renal arteries in both quiescent and active vascular state Int. J. Mol. Sci., 21 (2020), p. 3905

110. J.G. Snedeker, et al. Strain-rate dependent material properties of the porcine and human kidney capsule. J. Biomech., 38 (2005), pp. 1011-1021

111. R.D. Bülow, P. Boor Extracellular matrix in kidney fibrosis: more than just a scaffold J. Histochem. Cytochem., 67 (2019), pp. 643-661

112. A.R. Gillies, R.L. Lieber Structure and function of the skeletal muscle extracellular matrix Muscle Nerve, 44 (2011), pp. 318-331

113. M.D. Boppart, Z.S. Mahmassani Integrin signaling: linking mechanical stimulation to skeletal muscle hypertrophy Am. J. Physiol. Cell Physiol., 317 (2019), pp. C629-C641

114. M. Cescon, et al. Lack of collagen VI promotes neurodegeneration by impairing autophagy and inducing apoptosis during aging Aging Albany, 8 (2016), pp. 1083-1098

115. R.O. Hynes. The extracellular matrix: not just pretty fibrils. Science, 326 (2009), pp. 1216-1219

116 I.D. Campbell, M.J. Humphries. Integrin structure, activation, and interactions. Cold Spring Harb. Perspect. Biol. (2011),

117. T. Rozario, D.W. DeSimone. The extracellular matrix in development and morphogenesis: a dynamic view. Dev. Biol., 341 (2010), pp. 126-140

118. S.A. Wickström, K. Radovanac, R. Fässler. Genetic analyses of integrin signaling. Cold Spring Harb. Perspect. Biol. (2011),

119. Hynes, R. O. & Naba, A. Overview of the Matrisome—An Inventory of Extracellular Matrix Constituents and Functions. Csh Perspect Biol 4, a004903 a004903 (2012).

120. Finch-Edmonson M and Sudol M. Framework to function: Mechanosensitive regulators of gene tracscription. Cellular and Molecular Biology Letters, 2016.

121 Purvis, J. E., and Lahav, G. Encoding and decoding cellular information through signaling dynamics. Cell, 2013.

122. Keane TJ, DeWard A, Londono R, Saldin LT, Castleton AA, Carey L, Nieponice A, Lagasse E, Badylak SF. Tissue-Specific Effects of Esophageal Extracellular Matrix. Tissue Eng Part A. 2015 Sep;21(17-18):2293-300.

123. Bissell MJ, Hall HG, Parry G. How does the extracellular matrix direct gene expression? J Theor Biol, 1982.

124. E. Ouni, et al. Spatiotemporal changes in mechanical matrisome components of the human ovary from prepuberty to menopause Hum. Reprod., 35 (2020), pp. 1391-1410

125. M.P. Kurylo, et al. Effect of proteoglycans at interfaces as related to location, architecture, and mechanical cues Arch. Oral Biol., 63 (2016), pp. 82-92

126. E.H. Ernst, et al. Dormancy and activation of human oocytes from primordial and primary follicles: molecular clues to oocyte regulation Hum. Reprod., 32 (2017), pp. 1684-1700

127. J.M. Muncie, V.M. Weaver The physical and biochemical properties of the extracellular matrix regulate cell fate Curr. Top. Dev. Biol., 130 (2018), pp. 1-37

128. A. Shridhar, et al. Investigating the effects of tissue-Specific extracellular matrix on the adipogenic and osteogenic differentiation of human adipose-derived stromal cells within composite hydrogel scaffolds Front. Bioeng. Biotechnol., 7 (2019), p. 402

129. E. Bassat, et al. The extracellular matrix protein agrin promotes heart regeneration in mice Nature, 547 (2017), pp. 179-184

130. K.-M. Ng, et al. Evidence that fibulin family members contribute to the steroid-dependent extravascular sequestration of sex hormone-binding globulin J. Biol. Chem., 281 (2006), pp. 15853-15861

131. Close S.P.B. Teixeira, et al. Biomaterials for sequestration of growth factors and modulation of cell behavior Adv. Funct. Mater., 30 (2020), p. 1909011

132. Irving-Rodgers, H.F. and Rodgers, R.J. Extracellular matrix of the developing ovarian follicle. (2006) Semin Reprod Med 24(4):195-203.

133. Rodgers, R.J., Irving-Rodgers, H.F., and Russell, D.L. Extracellular matrix of the developing ovarian follicle. (2003) Reproduction 126(4):415-24.

134. Irving-Rodgers, H.F. and Rodgers, R.J. Extracellular matrix in ovarian follicular development and disease. (2005) Cell Tissue Res 322(1):89-98.

135. Rodgers, R.J., Irving-Rodgers, H.F., and van Wezel, I.L. Extracellular matrix in ovarian follicles. (2000) Mol Cell Endocrinol 163(1-2):73-9.135.

136. S. Silber, et al. Cryopreservation and transplantation of ovarian tissue: results from one center in the USA J. Assist. Reprod. Genet., 35 (2018), pp. 2205-2213

137. E. Latorre, et al. Active superelasticity in three-dimensional epithelia of controlled shape Nature, 563 (2018), pp. 203-208

138. J.T. Thorne, et al. Dynamic reciprocity between cells and their microenvironment in reproduction Biol. Reprod., 92 (2015), p. 25

139. M. Finch-Edmondson, M. Sudol Framework to function: mechanosensitive regulators of gene transcription Cell. Mol. Biol. Lett., 21 (2016), p. 28

140. Epstein, N.D. and Davis, J.S. Sensing stretch is fundamental. (2003) Cell 112(2): pp.147-50.

141. Tamada M, Sheetz MP, Sawada Y. Activation of a signaling cascade by cytoskeletal stretch. Dev Cell. 2004;7 (5): pp. 709–718.

142. Jaalouk DE, Lammerding J. Mechanotransduction gone awry. Nat Rev Mol Cell Biol. 2009;10 (1): pp. 63–73

143. Sukharev S, Corey D. Mechanosensitive channels: multiplicity of families and gating paradigms. Sci STKE. 2004;2004(219):re4.

144. Agha R, Ogawa R, Pietramaggiori G, Orgill DP. A review of the role of mechanical forces in cutaneous wound healing. J Surg Res. 2011;171 (2): pp. 700–708

145. Sawada Y, Tamada M, Dubin-Thaler BJ, et al. . Force sensing by mechanical extension of the Src family kinase substrate p130Cas. Cell. 2006;127 (5): pp. 1015–1026

146. Kuo JC. Mechanotransduction at focal adhesions: integrating cytoskeletal mechanics in migrating cells. J Cell Mol Med. 2013;17 (6): pp. 704–712.

147. Ingber DE. Integrins as mechanochemical transducers. Curr Opin Cell Biol. 1991;3 (5):841–848

148. Ingber DE. Cellular mechanotransduction: putting all the pieces together again. FASEB J. 2006;20 (7):811–82

149. Ghosh K, Ingber DE. Micromechanical control of cell and tissue development: implications for tissue engineering. Adv Drug Deliv Rev. 2007;10 (13):1306–1318

150. C.D. Wood, et al. Multi-modal magnetic resonance elastography for noninvasive assessment of ovarian tissue rigidity in vivo Acta Biomater., 13 (2015), pp. 295-300

151. J.E. Hornick, et al. Isolated primate primordial follicles require a rigid physical environment to survive and grow in vitro Hum. Reprod., 27 (2012), pp. 1801-1810

152. J.E. Hornick, et al. Multiple follicle culture supports primary follicle growth through paracrine-acting signals Reproduction, 145 (2013), pp. 19-32

153. A. Shikanov, et al. Interpenetrating fibrin-alginate matrices for in vitro ovarian follicle development Biomaterials, 30 (2009), pp. 5476-5485

154. J. Xu, et al. Fibrin promotes development and function of macaque primary follicles during encapsulated three-dimensional culture Hum. Reprod., 28 (2013), pp. 2187-2200

155. E.S. Gargus, et al. Ultrasound shear wave velocity varies across anatomical region in ex vivo bovine ovaries Tissue Eng. A, 26 (2020), pp. 720-732

156. Parkes, Wendena S et al. "Hyaluronan and Collagen Are Prominent Extracellular Matrix Components in Bovine and Porcine Ovaries." Genes vol. 12,8 1186. 30 Jul. 2021,

157. Amargant, Farners et al. "Ovarian stiffness increases with age in the mammalian ovary and depends on collagen and hyaluronan matrices." Aging cell vol. 19,11 (2020): e13259.

158. G. Nagamatsu, et al. Mechanical stress accompanied with nuclear rotation is involved in the dormant state of mouse oocytes Sci. Adv., 5 (2019), Article eaav9960

159. K. Kawamura, et al. Hippo signaling disruption and Akt stimulation of ovarian follicles for infertility treatment Proc National Acad Sci, 110 (2013), pp. 17474-17479

160. I. Kawashima, K. Kawamura Regulation of follicle growth through hormonal factors and mechanical cues mediated by Hippo signaling pathway Syst. Biol. Reprod. Med., 64 (2017), pp. 3-11

161. K. Hayashi, et al. Environmental factors for establishment of the dormant state in oocytes Develop. Growth Differ., 62 (2020), pp. 150-157

162. Afratis N, Gialeli C, Nikitovic D, Tsegenidis T, Karousou E, Theocharis AD, Pavão MS, Tzanakakis GN, Karamanos NK. Glycosaminoglycans: key players in cancer cell biology and treatment. FEBS J. 2012 Apr;279(7):1177-97.

163. Ouni E, Vertommen D, Chiti MC, Dolmans MM, Amorim CA. A Draft Map of the Human Ovarian Proteome for Tissue Engineering and Clinical Applications. Mol Cell Proteomics. 2019 Mar 15;18(Suppl 1):S159-S173.

164. Ouni E, Bouzin C, Dolmans MM, Marbaix E, Pyr Dit Ruys S, Vertommen D, Amorim CA. Spatiotemporal changes in mechanical matrisome components of the human ovary from prepuberty to menopause. Hum Reprod. 2020 Jun 1;35(6):1391-1410.

165. Zacchigna L, Vecchione C, Notte A, Cordenonsi M, Dupont S, Maretto S, Cifelli G, Ferrari A, Maffei A, Fabbro C et al. Emilin1 links TGF-beta maturation to blood pressure homeostasis. Cell 2006;124:929–942.

166. Zanetti M, Braghetta P, Sabatelli P, Mura I, Doliana R, Colombatti A, Volpin D, Bonaldo P, Bressan GM. EMILIN-1 deficiency induces elastogenesis and vascular cell defects. Mol Cell Biol 2004;24:638–650.

167. Schiavinato A, Keene DR, Wohl AP, Corallo D, Colombatti A, Wagener R, Paulsson M, Bonaldo P, Sengle G. Targeting of EMILIN-1 and EMILIN-2 to fibrillin microfibrils facilitates their incorporation into the extracellular matrix. J Invest Dermatol 2016;136:1150–1160.

168. Knight, P. G., & Glister, C. (2006). TGF-β superfamily members and ovarian follicle development, Reproduction, 132(2), 191-206.

169. John GB, Gallardo TD, Shirley LJ, Castrillon DH. 2008. Foxo3 is a PI3K-dependent molecular switch controlling the initiation of oocyte growth. Dev Biol 321:197–204.

170. Ernst EH, Grondahl ML, Grund S, Hardy K, Heuck A, Sunde L, Franks S, Andersen CY, Villesen P & Lykke-Hartmann K 2017 Dormancy and activation of human oocytes from primordial and primary follicles: molecular clues to oocyte regulation. Human Reproduction 1684–1700.

171. Ernst EH, Franks S, Hardy K, Villesen P & Lykke-Hartmann K 2018 Granulosa cells from human primordial and primary follicles show differential global gene expression profiles. Human Reproduction 666–679.

172. Granados-Aparici, S., Hardy, K., Franks, S. et al. SMAD3 directly regulates cell cycle genes to maintain arrest in granulosa cells of mouse primordial follicles. Sci Rep 9, 6513 (2019).

173. Granados-Aparici S, Hardy K, Franks S, Sharum IB, Waite SL, Fenwick MA. SMAD3 directly regulates cell cycle genes to maintain arrest in granulosa cells of mouse primordial follicles. Sci Rep. 2019 Apr 24;9(1):6513.

174. Sharum, I. B., Granados-Aparici, S., Warrander, F. C., Tournant, F. P. and Fenwick, M. A. (2017). Serine threonine kinase receptor associated protein regulates early follicle development in the mouse ovary. Reproduction 153, 221-231.

175. Zacchigna L, Vecchione C, Notte A, Cordenonsi M, Dupont S, Maretto S, Cifelli G, Ferrari A, Maffei A, Fabbro C, Braghetta P, Marino G, Selvetella G, Aretini A, Colonnese C, Bettarini U, Russo G, Soligo S, Adorno M, Bonaldo P, Volpin D, Piccolo S, Lembo G, Bressan GM. Emilin1 links TGF-beta maturation to blood pressure homeostasis. Cell. 2006 Mar 10;124(5):929-42.

176. Olivieri D, Sykora MM, Sachidanandam R, Mechtler K, Brennecke J. An in vivo RNAi assay identifies major genetic and cellular requirements for primary piRNA biogenesis in Drosophila. EMBO J. 2010 Oct 6;29(19):3301-17.

177. Chakraborty, Sayan, and Wanjin Hong. "Linking Extracellular Matrix Agrin to the Hippo Pathway in Liver Cancer and Beyond." Cancers vol. 10,2 45. 6 Feb. 2018,

178. Chronowska E. High-throughput analysis of ovarian granulosa cell transcriptome. Biomed Res Int. 2014;2014:213570

179. Plewes MR, Hou X, Zhang P, Liang A, Hua G, Wood JR, Cupp AS, Lv X, Wang C, Davis JS. Yes-associated protein 1 is required for proliferation and function of bovine granulosa cells in vitro†. Biol Reprod. 2019 Nov 21;101(5):1001-1017.

180. Hu L.L., Su T., Luo R.C., Zheng Y.H., Huang J., Zhong Z.S., Nie J., Zheng L.P. Hippo pathway functions as a downstream effector of AKT signaling to regulate the activation of primordial follicles in mice. J. Cell. Physiol. 2019;234:1578–1587.

181. Kawamura K, Cheng Y, Suzuki N, Deguchi M, Sato Y, Takae S, Ho CH, Kawamura N, Tamura M, Hashimoto S, Sugishita Y, Morimoto Y, Hosoi Y, Yoshioka N, Ishizuka B, Hsueh AJ. Hippo signaling disruption and Akt stimulation of ovarian follicles for infertility treatment. Proc Natl Acad Sci U S A. 2013 Oct 22;110(43):17474-9.

182. Nagashima T, Kim J, Li Q, Lydon JP, DeMayo FJ, Lyons KM, Matzuk MM. Connective tissue growth factor is required for normal follicle development and ovulation. Mol Endocrinol 2011; 25:1740–1759.

182. Pan D. Hippo signaling in organ size control. Genes Dev. 2007;21:886–897.

183. Halder G, Johnson RL. Hippo signaling: growth control and beyond. Development. 2011;138:9–22.

184. Hergovich A. Mammalian Hippo signalling: a kinase network regulated by protein-protein interactions. Biochem Soc Trans. 2012;40:124–128.

185. Kawamura K, Cheng Y, Suzuki N, et al. Hippo signaling disruption and Akt stimulation of ovarian follicles for infertility treatment. Proc Natl Acad Sci U S A. 2013;110:17474–17479.

186. Johnson R, Halder G. The two faces of Hippo: targeting the Hippo pathway for regenerative medicine and cancer treatment. *Nat Rev Drug Discov.* 2014;13:63–79.

187. Wada K, Itoga K, Okano T, et al. Hippo pathway regulation by cell morphology and stress fibers. *Development.* 2011;138:3907–3914.

188. Liu-Chittenden Y, Huang B, Shim JS, et al. Genetic and pharmacological disruption of the TEAD-YAP complex suppresses the oncogenic activity of YAP. Genes Dev. 2012;26:1300–1305.

189. Irving-Rodgers HF, Rodgers RJ. Extracellular matrix in ovarian follicular development and disease. Cell Tissue Res. 2005;322(1):89–98.

190. McCarthy, K.J. (2015) The basement membrane proteoglycans perlecan and agrin: something old, something new. Curr. Top. Membr., 76, 255–303.

191. Van Haele M, Moya IM, Karaman R, Rens G, Snoeck J, Govaere O, Nevens F, Verslype C, Topal B, Monbaliu D, Halder G, Roskams T. YAP and TAZ Heterogeneity in Primary Liver Cancer: An Analysis of Its Prognostic and Diagnostic Role. Int J Mol Sci. 2019 Feb 1;20(3):638.

192. Xiang C, Li J, Hu L, Huang J, Luo T, Zhong Z, Zheng Y, Zheng L. Hippo signaling pathway reveals a spatio-temporal correlation with the size of primordial follicle pool in mice. Cell Physiol Biochem. 2015;35:957–968.

190. Abir, R., S. Franks, M. A. Mobberley, P. A. Moore, R. A. Margara, and R. M. Winston. Mechanical isolation and in vitro growth of preantral and small antral human follicles. Fertil. Steril. 68:682–688, 1997.

191. Gutierrez, C. G., J. H. Ralph, E. E. Telfer, I. Wilmut, and R. Webb. Growth and antrum formation of bovine preantral follicles in long-term culture in vitro. Biol. Reprod. 62:1322–1328, 2000.

192. Roy, S. K., and B. J. Treacy. Isolation and long-term culture of human preantral follicles. Fertil. Steril. 59:783–790, 1993.

193. Tambe, S. S., and T. D. Nandedkar. Steroidogenesis in sheep ovarian antral follicles in culture: time course study and supplementation with a precursor. Steroids 58:379–383, 1993.

194. Eppig JJ, Pendola FL, Wigglesworth K, Pendola JK. Mouse oocytes regulate metabolic cooperativity between granulosa cells and oocytes: amino acid transport. Biol Reprod. 2005 Aug;73(2):351-7.

195. Su YQ, Sugiura K, Eppig JJ. Mouse oocyte control of granulosa cell development and function: paracrine regulation of cumulus cell metabolism. Semin Reprod Med. 2009 Jan;27(1):32-42.

196. Eppig, J.J. (1991), Intercommunication between mammalian oocytes and companion somatic cells. Bioessays, 13: 569-574.

197. Pangas, S. A., Saudye, H., Shea, L. D., and Woodruff, T. K. (2003). Novel approach for the three-dimensional culture of granulosa cell– oocyte complexes. Tissue Eng. 9, 1013–1021.

198. Kreeger, P. K., Fernandes, N. N., Woodruff, T. K., and Shea, L. D. (2005). Regulation of mouse follicle development by follicle-stimulating hormone in a three-dimensional in vitro culture system is dependent on follicle stage and dose. Biol. Reprod. 73, 942–950.

199. Xu, M., Kreeger, P. K., Shea, L. D., and Woodruff, T. K. (2006a). Tissueengineered follicles produce live, fertile offspring. Tissue Eng. 12, 2739–2746. doi:10.1089/TEN.2006.12.2739

200. Xu, M., West, E., Shea, L. D., and Woodruff, T. K. (2006b). Identification of a stage-specific permissive in vitro-culture environment for follicle growth and oocyte development. Biol. Reprod. 75, 916–923.

201. Xu, M., Banc, A., Woodruff, T. K., and Shea, L. D. (2009a). Secondary follicle growth and oocyte maturation by culture in alginate hydrogel following cryopreservation of the ovary or individual follicles. Biotechnol. Bioeng. 103, 378–386.

202. Xu, M., Barrett, S. L., West-Farrell, E., Kondapalli, L. A., Kiesewette, S. E., Shea, L. D., and Woodruff, T. K. (2009b). In vitro-grown human ovarian follicles from cancer patients support oocyte growth. Hum. Reprod. 24, 2531–2540.

203. Xu, M., West-Farrell, E. R., Stouffer, R. L., Shea, L. D., Woodruff, T. K., and

Zelinski, M. B. (2009c). Encapsulated three-dimensional culture supports development of nonhuman primate secondary follicles. Biol. Reprod. 81, 587–594.

204. Freeman, F.E., Kelly, D.J. Tuning Alginate Bioink Stiffness and Composition for Controlled Growth Factor Delivery and to Spatially Direct MSC Fate within Bioprinted Tissues. Sci Rep 7, 17042 (2017).

205. Malda, J. et al. 25th anniversary article: Engineering hydrogels for biofabrication. Adv Mater 25, 5011–28 (2013).

206. Stevens, M. M. et al. In vivo engineering of organs: the bone bioreactor. Proc Natl Acad Sci USA 102, 11450–5 (2005).

207. Augst, A. D. et al. Alginate hydrogels as biomaterials. Macromol Biosci 6, 623–33 (2006).

208. Badylak SF, Taylor D, Uygun K. Whole-organ tissue engineering: decellularization and recellularization of three-dimensional matrix scaffolds. Annu Rev Biomed Eng. 2011;13:27–53.

209. Crapo PM, Gilbert TW, Badylak SF. An overview of tissue and whole organ decellularization processes. Biomaterials. 2011;32(12):3233–43.

210. Gilbert TW, Sellaro TL, Badylak SF. Decellularization of tissues and organs. Biomaterials. 2006;27(19):3675–83

211. Eivazkhani, F. et al. Evaluating two ovarian decellularization methods in three species. Mater. Sci. Eng. C 102, 670–682 (2019).

212. Alshaikh, A. B. et al. Decellularization of the mouse ovary: Comparison of different scaffold generation protocols for future ovarian bioengineering. J. Ovarian Res. 12, (2019).

213. Liu, W.-Y. et al. Xenogeneic Decellularized Scaffold: A Novel Platform for Ovary Regeneration. Tissue Eng. Part C Methods 23, 61–71 (2017).

214. Hassanpour, A., Talaei-Khozani, T., Kargar-Abarghouei, E., Razban, V. & Vojdani, Z. Decellularized human ovarian scaffold based on a sodium lauryl ester sulfate (SLES)-treated protocol, as a natural three-dimensional scaffold for construction of bioengineered ovaries. Stem Cell Res. Ther. 9, 252 (2018).

215. Pors, S. E. et al. Initial steps in reconstruction of the human ovary: survival of pre-antral stage follicles in a decellularized human ovarian scaffold. Hum. Reprod. 34, 1523–1535 (2019).

216. Alshaikh AB, Padma AM, Dehlin M, Akouri R, Song MJ, Brännström M, et al. Decellularization of the mouse ovary: comparison of different scaffold generation protocols for future ovarian bioengineering. J Ovarian Res. 2019;12(1):58.

217. Mirzaeian L, Eivazkhani F, Hezavehei M, Moini A, Esfandiari F, Valojerdi MR, et al. Optimizing the cell seeding protocol to human decellularized ovarian scaffold: application of dynamic system for bio-engineering. Cell J. 2020;22(2):227–35.

218. Vermeulen, M. *et al.* Generation of Organized Porcine Testicular Organoids in Solubilized Hydrogels from Decellularized Extracellular Matrix. *Int. J. Mol. Sci.* **20**, 5476 (2019).

219. Rezaei Topraggaleh, T., Rezazadeh Valojerdi, M., Montazeri, L. & Baharvand, H. A testis-derived macroporous 3D scaffold as a platform for the generation of mouse testicular organoids. *Biomater. Sci.* **7**, 1422–1436 (2019).

220. Theus A. S., Ning L., Hwang B., Gil C., Chen S., Wombwell A., Mehta R., and Serpooshan V., *Polymers* 12(10), 2262 (2020)

221. Lee S. C., Gillispie G., Prim P., and Lee S. J., *Chem. Rev.* 120, 10834 (2020).

222. Hazur J., Detsch R., Karakaya E., Kaschta J., Tessmar J., Schneidereit D., Friedrich O., Schubert D. W., and Boccaccini A. R., *Biofabrication* 12(4), 045004

223. Lee J., Oh S. J., An S. H., Kim W. D., and Kim S. H., *Biofabrication* 12(3), 035018 (2020).

224. Shiwarski, Daniel J et al. "Emergence of FRESH 3D printing as a platform for advanced tissue biofabrication." APL bioengineering vol. 5,1 010904. 16 Feb. 2021, doi:10.1063/5.0032777

225. Jiménez R: Ovarian Organogenesis in Mammals: Mice Cannot Tell Us Everything. Sex Dev 2009;3:291-301.

226. Adams GP, Pierson RA. Bovine model for study of ovarian follicular dynamics in humans. Theriogenology 1995 43:113–120

227. Chow, E. J. et al. Pregnancy after chemotherapy in male and female survivors of childhood cancer treated between 1970 and 1999: a report from the Childhood Cancer Survivor Study cohort. Lancet Oncol 17(567), 576 (2016).

228. Eddie, S. L., Kim, J. J., Woodruff, T. K. & Burdette, J. E. Microphysiological modeling of the reproductive tract: a fertile endeavor. Exp Biol Med 239(1192), 1202 (2014).

229. Lobo, R. A. Hormone-replacement therapy: current thinking. Nat Rev Endocrinol 13(1), 12 (2016)

230. Mostoufi-Moab, S. et al. Endocrine Abnormalities in Aging Survivors of Childhood Cancer: A Report From the Childhood Cancer Survivor Study. J Clin Oncol 34(1), 13 (2016).

231. Schmidt, P. The 2012 Hormone Therapy Position Statement of The North American Menopause Society. Menopause J North Am Menopause Soc 19(257), 271 (2012).

232. Jorge, S., Chang, S., Barzilai, J. J., Leppert, P. & Segars, J. H. Mechanical signaling in reproductive tissues: mechanisms and importance. Reprod Sci 21(1093), 1107 (2014).

233. Shikanov, A., ith, R., Xu, M., Woodruff, T. K. & Shea, L. D. Hydrogel network design using multifunctional macromers to coordinate tissue maturation in ovarian follicle culture. Biomaterials 32(2524), 2531 (2011).

234. Skory, R., Xu, Y., Shea, L. D. & Woodruff, T. K. Engineering the ovarian cycle using in vitro follicle culture. Hum Reprod 30(1386), 1395 (2015)

235. Baker, B. M. & Chen, C. S. Deconstructing the third dimension – how 3D culture microenvironments alter cellular cues. J Cell Sci 125(3015), 3024 (2012).

236. Tate, C. C. et al. Laminin and fibronectin scaffolds enhance neural stem cell transplantation into the injured brain. J Tissue Eng Regen M 3, 208–217 (2009).

237. Song, J. J. et al. Regeneration and experimental orthotopic transplantation of a bioengineered kidney. Nat Med 19(1), 8 (2013).

238. Mazza, G. et al. Decellularized human liver as a natural 3D-scaffold for liver bioengineering and transplantation. Sci Rep-uk 5, 13079 (2015).

239. Wang, X., Wang, K., Zhang, W., Qiang, M. & Luo, Y. A bilaminated decellularized scaffold for islet transplantation: Structure, properties and functions in diabetic mice. Biomaterials 138, 80–90 (2017).

240. Nelson, C. M. et al. Emergent patterns of growth controlled by multicellular form and mechanics. P Natl Acad Sci Usa 102(11594), 11599 (2005).

241. Wang, L. et al. A two-dimensional electrophoresis reference map of human ovary. J Mol Med 83, 812–821 (2005).

242. Griffin, J., Emery, B. R., Huang, I., Peterson, M. C. & Carrell, D. T. Comparative analysis of follicle morphology and oocyte diameter in four mammalian species (mouse, hamster, pig, and human). J Exp Clin Assisted Reproduction 3, 2 (2006).

243. Foxcroft, G. & Hunter, M. Basic physiology of follicular maturation in the pig. J Reproduction Fertility Suppl 33, 1–19 (1985).

244. Kanitz, W., Brussow, K.-P. & Becker, F. Comparative Aspects of Follicular Development, Follicular and Oocyte Maturation and Ovulation in Cattle and Pigs. Archiv fur Tierzucht 44, 9–23 (2001).

245. Malgorzata, D., Malgorzata, G., Malgorzata, K.-S. & Zbigniew, T. The Primordial to Primary Follicle Transition — A Reliable Marker of Ovarian Function. *Insights from Animal Reproduction* **1**, 18, (2016).

246. Laronda, M. M. et al. Diethylstilbestrol induces vaginal adenosis by disrupting SMAD/RUNX1-mediated cell fate decision in the Müllerian duct epithelium. Dev Biol 381(5), 16 (2013).

247. Cox, J. et al. Accurate Proteome-wide Label-free Quantification by Delayed Normalization and Maximal Peptide Ratio Extraction, Termed MaxLFQ. Mol Cell Proteomics 13, 2513–2526 (2014).

248. Cox, J. & Mann, M. MaxQuant enables high peptide identification rates, individualized p.p.b.-range mass accuracies and proteome-wide protein quantification. Nat Biotechnol 26, 1367–1372 (2008).

249. Krasny, L. et al. Comparative proteomic assessment of matrisome enrichment methodologies. Biochem J 473, 3979–3995 (2016).

250. Buse, E., Zöller, M. & Esch, E. The Macaque Ovary, with Special Reference to the Cynomolgus Macaque (Macaca fascicularis). Toxicol Pathol 36, 24S–66S (2008).

251. Fereydouni, B., Drummer, C., Aeckerle, N., Schlatt, S. & Behr, R. The neonatal marmoset monkey ovary is very primitive exhibiting many oogonia. Reproduction 148(237), 247 (2014).

252. Adams, G. P., Singh, J. & Baerwald, A. R. Large animal models for the study of ovarian follicular dynamics in women. Theriogenology 78, 1733–1748 (2012).

253. Manji, R. A., Lee, W. & Cooper, D. Xenograft bioprosthetic heart valves: Past, present and future. Int J Surg 23, 280–284 (2015).

254. Otterburn, D. & Losken, A. The Use of Porcine Acellular Dermal Material for TRAM Flap Donor-Site Closure. Plast Reconstr Surg 123, 74e–76e (2009).

255. Wang, Y., Chen, S., Shi, J., Li, G. & Dong, N. Mid- to long-term outcome comparison of the Medtronic Hancock II and bi-leaflet mechanical aortic valve replacement in patients younger than 60 years of age: a propensity-matched analysis. Interact Cardiov Th 22, 280–286 (2016).

256. Danussi, C. et al. EMILIN1-$\alpha4/\alpha9$ integrin interaction inhibits dermal fibroblast and keratinocyte proliferation. J Cell Biology 195(131), 145 (2011).

257. Cariño, C. et al. Localization of species conserved zona pellucida antigens in mammalian ovaries. Reprod Biomed Online 4, 116–126 (2002).

258. Berkholtz, C. B., Lai, B. E., Woodruff, T. K. & Shea, L. D. Distribution of extracellular matrix proteins type I collagen, type IV collagen, fibronectin, and laminin in mouse folliculogenesis. Histochem Cell Biol 126(583), 592 (2006).

259. Committee on Adolescent Health Care. Primary Ovarian Insufficiency in Adolescents and Young Women, The Am Col of Obstet and Gynecol. 605 (2014) 193–7.

260. Rocca, W. A. et al. Increased risk of cognitive impairment or dementia in women who underwent oophorectomy before menopause, Neurology. **69** (2007) 1074–1083.

261. Jacobsen, B. K., Knutsen, S. F. & Fraser, G. E. Age at Natural Menopause and Total Mortality and Mortality from Ischemic Heart Disease The Adventist Health Study, J Clin Epidemiol. **52** 303307 (1999).

262. Amagai, Y. et al. Age at menopause and mortality in Japan: the Jichi Medical School Cohort Study. **16**, 161166 (2006).

263. Hong, J. S. et al. Age at menopause and cause-specific mortality in South Korean women: Kangwha Cohort Study, Maturitas. **56** (2007) 411–419.

264. Rocca, W. A. et al. Accelerated Accumulation of Multimorbidity After Bilateral Oophorectomy: A Population-Based Cohort Study, Mayo Clin Proc. **91** (2016) 1577–1589.

265. Corkum KS, Rhee DS, Wafford EQ, Demeestere I, Dasgupta R, Baertschiger R, Malek MM, Aldrink JH, Heaton TE, Weil BR, Madonna M, Lautz TB. Fertility and hormone preservation and restoration for female children and adolescents receiving gonadotoxic cancer treatments: A systematic review, J Pediatr Surg. (2019).

266. Smith RM, Woodruff TK, Shea LD. Designing Follicle–Environment Interactions with Biomaterials. Canc Treat. 156 (2010) 11–24.

267. West ER, Xu M, Woodruff TK, Shea LD. Physical properties of alginate hydrogels and their effects on in vitro follicle development, Biomaterials. 28(30) (2007) 4439–4448.

268. Thomas J. Hinton, Quentin Jallerat, Rachelle N. Palchesko, Joon Hyung Park, Martin S. Grodzicki, Hao-Jan Shue, Mohamed H. Ramadan, Andrew R. Hudson, Adam W. Feinberg. Three-dimensional printing of complex biological structures by freeform reversible embedding of suspended hydrogels, Science Advances 1 (2015).

269. Grosbois J., Demeestere I. Dynamics of pi3k and hippo signaling pathways during in vitro human follicle activation, Hum. Reprod. 33 (2018) 1705–1714.

270. Bonnet A, Lê Cao KA, Sancristobal M, Benne F, Robert-Granié C, Law-So G, et al. . In vivo gene expression in granulosa cells during pig terminal follicular development, Reproduction. 136 (2008) 211–24.

271. B.S. Elkin, E.U. Azeloglu, K.D. Costa, B. Morrison Mechanical heterogeneity of the rat hippocampus measured by atomic force microscope indentation, J. Neurotrauma. 24 (5) (2007) 812–822.

272. M. Lekka, D. Gil, K. Pogoda, J. Dulińska-Litewka, R. Jach, J. Gostek, et al. Cancer cell detection in tissue sections using AFM Arch, Biochem. Biophys. 518 (2) (2012) 151–156.

273. A. Samani, J. Zubovits, D. Plewes Elastic moduli of normal and pathological human breast tissues: an inversion-technique-based investigation of 169 samples, Phys. Med. Biol. 52 (6) (2007) 1565–1576.

274. D. Sicard, L.E. Fredenburgh, D.J. Tschumperlin Measured pulmonary arterial tissue stiffness is highly sensitive to AFM indenter dimensions, J Mech Behav Biomed Mater. 74 (2017) 118–127.

275. A.J. Engler, F. Rehfeldt, S. Sen, D.E. Discher Microtissue elasticity: measurements by atomic force microscopy and its influence on cell differentiation Methods, Cell Biol. 83 (2007), 521–545.

276. J. Swift, I.L. Ivanovska, A. Buxboim, T. Harada, P.C.D.P. Dingal, J. Pinter, et al. Nuclear lamin-A scales with tissue stiffness and enhances matrix-directed differentiation, Science. 341 (6149) (2013).

272. Y. Cheng, Y. Feng, L. Jansson, Y. Sato, M. Deguchi, K. Kawamura, et al. Actin polymerization-enhancing drugs promote ovarian follicle growth mediated by the Hippo signaling effector YAP, Faseb. J. 29 (6) (2015) 2423–2430

273. A. Carracedo, P.P. Pandolfi The PTEN-PI3K pathway: of feedbacks and cross-talks, Oncogene. 27(41) (2008) 5527–5541

274. K. Jagarlamudi, L. Liu, D. Adhikari, P. Reddy, A. Idahl, U. Ottander, et al. Oocyte-specific deletion of Pten in mice reveals a stage-specific function of PTEN/PI3K signaling in oocytes in controlling follicular activation, PLoS One. 4 (7) (2009).

275. P. Reddy, L. Liu, D. Adhikari, K. Jagarlamudi, S. Rajareddy, Y. Shen, et al. Oocyte-specific deletion of pten causes premature activation of the primordial follicle pool, Science. 319 (5863) (2008) 611–613

276. S. Cecconi, A. Mauro, V. Cellini, F. Patacchiola The role of Akt signalling in the mammalian ovary, Int. J. Dev. Biol. 56 (10–12) (2012) 809–817

277. T Hopkins, Victoria L. Bemmer, Stephen Franks, Carina Dunlop, Kate Hardy, Iain E. Dunlop, Micromechanical mapping of the intact ovary interior reveals contrasting mechanical roles for follicles and stroma, Biomaterials. 277 (2021)

278. Rodgers R.J., and Irving-Rodgers H.F.. Morphological classification of bovine ovarian follicles, Reproduction. 139 (2010) 309.

279. S. Franks, J. Stark, K. Hardy Follicle dynamics and anovulation in polycystic ovary syndrome, Hum. Reprod. Update. 14 (4) (2008) 367–378

280. Reindollar RH. Turner syndrome: contemporary thoughts and reproductive issues, Semin Reprod Med. 29(4) (2011) 342–52.

281. Prince, E. et al. Patterning of structurally anisotropic composite hydrogel sheets, Biomacromolecules. 19 (2018) 1276–1284.

282. De France, K. J. et al. Injectable anisotropic nanocomposite hydrogels direct in situ growth and alignment of myotubes, Nano Lett. 17 (2017) 6487–6495.

283. Gladman, A. S., Matsumoto, E. A., Nuzzo, R. G., Mahadevan, L. & Lewis, J. A. Biomimetic 4D printing, Nat. Mater. 15 (2016) 413–418.

284. Norman, J. J. & Desai, T. A. Methods for fabrication of nanoscale topography for tissue engineering scaffolds, Ann. Biomed. Eng. 34 (2006) 89–101.

285. Prozzillo Y, Fattorini G, Santopietro MV, et al. Targeted Protein Degradation Tools: Overview and Future Perspectives, Biology (Basel). 9(12) (2020) 421.

286. Jungbluth, M., Renicke, C. & Taxis, C. Targeted protein depletion in Saccharomyces cerevisiae by activation of a bidirectional degron, BMC Syst Biol. 4 (2010) 176.

287. Deng, W., Bates, J.A., Wei, H. et al. Tunable light and drug induced depletion of target proteins, Nat Commun. 11 (2020) 304.

288. Angel PM, Narmoneva DA, et al. Proteomic Alterations Associated with Biomechanical Dysfunction are Early Processes in the Emilin1 Deficient Mouse Model of Aortic Valve Disease, Ann Biomed Eng. 45(11) (2017) 2548–2562.

289. Datta PK, Moses HL. STRAP and Smad7 synergize in the inhibition of transforming growth factor beta signaling. Mol Cell Biol. 2000 May;20(9):3157-67.

290. Yan X, Liu Z, Chen Y. Regulation of TGF-beta signaling by Smad7. Acta Biochim Biophys Sin (Shanghai). 2009 Apr;41(4):263-72.

291. Cichon, Magdalena A et al. "MYC Is a Crucial Mediator of TGFβ-Induced Invasion in Basal Breast Cancer." Cancer research vol. 76,12 (2016): 3520-30. doi:10.1158/0008-5472.CAN-15-3465

292. Rosairo D, Kuyznierewicz I, Findlay J, Drummond A. Transforming growth factor-beta: its role in ovarian follicle development. Reproduction. 2008 Dec;136(6):799-809.

293. Masanori Shimodaira, Tomohiro Nakayama, Naoyuki Sato, Takahiro Naganuma, Mai Yamaguchi, Noriko Aoi, Mikano Sato, Yoichi Izumi, Masayoshi Soma, Koichi Matsumoto, Association Study of the Elastin Microfibril Interfacer 1 (EMILIN1) Gene in Essential Hypertension, American Journal of Hypertension, Volume 23, Issue 5, May 2010, Pages 547–555

294. Schillers H, Rianna C, Schäpe J, Luque T, Doschke H, Wälte M, Uriarte JJ, Campillo N, Michanetzis GPA, Bobrowska J, Dumitru A, Herruzo ET, Bovio S, Parot P, Galluzzi M, Podestà A, Puricelli L, Scheuring S, Missirlis Y, Garcia R, Odorico M, Teulon JM, Lafont F, Lekka M, Rico F, Rigato A, Pellequer JL, Oberleithner H, Navajas D, Radmacher M. Standardized Nanomechanical Atomic Force Microscopy Procedure (SNAP) for Measuring Soft and Biological Samples. Sci Rep. 2017 Jul 11;7(1):5117.

295. Stylianou A, Kontomaris SV, Grant C, Alexandratou E. Atomic Force Microscopy on Biological Materials Related to Pathological Conditions. Scanning. 2019 May 12;2019:8452851.

296. Liu F, Tschumperlin DJ. Micro-mechanical characterization of lung tissue using atomic force microscopy. J Vis Exp. 2011 Aug 28;(54):2911.

297. Wagh AA, Roan E, Chapman KE, Desai LP, Rendon DA, Eckstein EC, Waters CM. Localized elasticity measured in epithelial cells migrating at a wound edge using atomic force microscopy. Am J Physiol Lung Cell Mol Physiol. 2008 Jul;295(1):L54-60. doi: 10.1152/ajplung.00475.2007.

298. Dennis, J. E. & Charbord, P. Origin and Differentiation of Human and Murine Stroma. Stem Cells 20, 205–214 (2002).

299. Reeves, G. Specific stroma in the cortex and medulla of the ovary. Cell types and vascular supply in relation to follicular apparatus and ovulation. Obstet. Gynecol. 37, 832–44 (1971).

300. Huang, C. T. F., Weitsman, S. R., Dykes, B. N. & Magoffin, D. A. Stem Cell Factor and Insulin-Like Growth Factor-I Stimulate Luteinizing Hormone-Independent Differentiation of Rat Ovarian Theca Cells1. Biol. Reprod. 64, 451–456 (2001).

301. Parrott, J. A. & Skinner, M. K. Kit ligand actions on ovarian stromal cells: Effects on theca cell recruitment and steroid production. Mol. Reprod. Dev. 55, 55–64 (2000).

302. Nilsson, E. E. & Skinner, M. K. Kit ligand and basic fibroblast growth factor interactions in the induction of ovarian primordial to primary follicle transition. Mol. Cell. Endocrinol. 214, 19–25 (2004).

303. Knight, P. G. & Glister, C. TGF- superfamily members and ovarian follicle development. Reproduction 132, 191–206 (2006).

304. Lee, W.-S. et al. Effects of bone morphogenetic protein-7 (BMP-7) on primordial follicular growth in the mouse ovary. Mol. Reprod. Dev. 69, 159–163 (2004).

305. Wagner, M., Yoshihara, M., Douagi, I. et al. Single-cell analysis of human ovarian cortex identifies distinct cell populations but no oogonial stem cells. Nat Commun 11, 1147 (2020).

306. Lu P, Takai K, Weaver VM, Werb Z. Extracellular matrix degradation and remodeling in development and disease. Cold Spring Harb Perspect Biol. 2011;3(12):a005058. Published (2011)

307. Wonil Han, Narendra K. Singh, Joeng Ju Kim, Hyeonji Kim, Byoung Soo Kim, Ju Young Park, Jinah Jang, Dong-Woo Cho, Directed differential behaviors of multipotent adult stem cells from decellularized tissue/organ extracellular matrix bioinks, Biomaterials, Volume 224 (2019).

308. Heeren AM, van Iperen L, Klootwijk DB, de Melo Bernardo A, Roost MS, Gomes Fernandes MM, Louwe LA, Hilders CG, Helmerhorst FM, van der Westerlaken LA, Chuva de Sousa Lopes SM. Development of the follicular basement membrane during human gametogenesis and early folliculogenesis. BMC Dev Biol. 2015 Jan 21;15:4.

309. ten Dijke P, Arthur HM 2007. Extracellular control of TGFbeta signalling in vascular development and disease. Nat Rev Mol Cell Biol 8: 857–869

310. Lonai P 2003. Epithelial mesenchymal interactions, the ECM and limb development. J Anat 202: 43–50

311. Shi Y, Massagué J 2003. Mechanisms of TGF-β signaling from cell membrane to the nucleus. Cell 113: 685–700

312. Hynes RO 2009. The extracellular matrix: Not just pretty fibrils. Science 326: 1216–1219

313. West, E. R., Xu, M., Woodruff, T. K. & Shea, L. D. Physical properties of alginate

hydrogels and their effects on in vitro follicle development. Biomaterials 28, 4439–4448

(2007).

314. West ER, Xu M, Woodruff TK, Shea LD. Physical properties of alginate hydrogels and their effects on in vitro follicle development. Biomaterials. 2007;28(30):4439–4448.

315. Xu M, West E, Shea LD, Woodruff TK. Identification of a stage-specific permissive in vitro culture environment for follicle growth and oocyte development. Biol Reprod. 2006;75(6):916–923.

316. West-Farrell ER, Xu M, Gomberg MA, Chow YH, Woodruff TK, Shea LD. The mouse follicle microenvironment regulates antrum formation and steroid production: alterations in gene expression profiles. Biol Reprod. 2009;80(3):432–439.

317. Alessi DR, James SR, Downes CP, Holmes AB, Gaffney PR, Reese CB, et al.

Characterization of a 3-phosphoinositide-dependent protein kinase which phosphorylates

and activates protein kinase Balpha. Curr Biol 1997;7(4):261-9.

318. Stephens L, Anderson K, Stokoe D, Erdjument-Bromage H, Painter GF, Holmes AB, et al. Protein kinase B kinases that mediate phosphatidylinositol 3,4,5-trisphosphatedependent activation of protein kinase B. Science 1998;279(5351):710-4.

319. Sarbassov DD, Guertin DA, Ali SM, Sabatini DM. Phosphorylation and regulation of Akt/PKB by the rictor-mTOR complex. Science 2005;307(5712):1098-101.

318. Manning BD, Cantley LC. AKT/PKB signaling: navigating downstream. Cell 2007;129(7):1261-74.

319. Andreas, E., Hoelker, M., Neuhoff, C. et al. MicroRNA 17–92 cluster regulates proliferation and differentiation of bovine granulosa cells by targeting PTEN and BMPR2 genes. Cell Tissue Res 366, 219–230 (2016).

320. Lian Liu, Singareddy Rajareddy, Pradeep Reddy, Chun Du, Krishna Jagarlamudi, Yan Shen, David Gunnarsson, Gunnar Selstam, Karin Boman, Kui Liu; Infertility caused by retardation of follicular development in mice with oocyte-specific expression of Foxo3a. Development 1 January 2007; 134 (1): 199–209

321. Gallardo TD, John GB, Bradshaw K, et al. Sequence variation at the human FOXO3 locus: a study of premature ovarian failure and primary amenorrhea. Hum Reprod. 2008;23(1):216-221.

322. Edward D. Tarnawa, Michael D. Baker, Gina M. Aloisio, Bruce R. Carr, Diego H. Castrillon, Gonadal Expression of Foxo1, but Not Foxo3, Is Conserved in Diverse Mammalian Species, Biology of Reproduction, Volume 88, Issue 4, 1 April 2013, 103, 1–11,

323. Stahl M, Dijkers PF, Kops GJ, Lens SM, Coffer PJ, Burgering BM, Medema RH. The forkhead transcription factor FoxO regulates transcription of p27Kip1 and Bim in response to IL-2. J Immunol. 2002 May 15;168(10):5024-31.

324. Li, Jing et al. "Activation of dormant ovarian follicles to generate mature eggs." Proceedings of the National Academy of Sciences of the United States of America vol. 107,22 (2010): 10280-4. doi:10.1073/pnas.1001198107

325. Reddy P, Liu L, Adhikari D, Jagarlamudi K, Rajareddy S, Shen Y, et al. Oocyte-specific deletion of Pten causes premature activation of the primordial follicle pool. Science. 2008 Feb 1;319(5863):611–3..

326. Kim S-Y, Ebbert K, Cordeiro MH, Romero M, Zhu J, Serna VA, et al. Cell Autonomous Phosphoinositide 3-Kinase Activation in Oocytes Disrupts Normal Ovarian Function

Through Promoting Survival and Overgrowth of Ovarian Follicles. Endocrinology. 2015 Apr;156(4):1464–76.

327. Li J, Kawamura K, Cheng Y, Liu S, Klein C, Liu S, et al. Activation of dormant ovarian follicles to generate mature eggs. Proc Natl Acad Sci USA. National Acad Sciences; 2010 Jun 1;107(22):10280–4.

328. Adhikari D, Gorre N, Risal S, Zhao Z, Zhang H, Shen Y, et al. The safe use of a PTEN inhibitor for the activation of dormant mouse primordial follicles and generation of fertilizable eggs. Kim S, editor. PLoS ONE. 2012;7(6):e39034..

329. Hancke K, Walker E, Strauch O, Göbel H, Hanjalic-Beck A, Denschlag D. Ovarian transplantation for fertility preservation in a sheep model: can follicle loss be prevented by antiapoptotic sphingosine-1-phosphate administration? Gynecol Endocrinol. 2009;25(12):839–843.

330. Baird DT. Long-term ovarian function in sheep after ovariectomy and transplantation of autografts stored at -196 C. Endocrinology. 1999;140(1):462–71.

331. Donnez J, Jadoul P, Squifflet J, Van Langendonckt A, Donnez O, Van Eyck AS, et al. Ovarian tissue cryopreservation and transplantation in cancer patients. Best Pract Res Clin Obstet Gynaecol. 2010;24(1):87–100.

332. Van Eyck A-S, Jordan BF, Gallez B, Heilier J-F, Van Langendonckt A, Donnez J. Electron paramagnetic resonance as a tool to evaluate human ovarian tissue reoxygenation after xenografting. Fertil Steril. 2009;92(1):374–81.

333. Terren, C., Nisolle, M., & Munaut, C. (2021). Pharmacological inhibition of the PI3K/PTEN/Akt and mTOR signalling pathways limits follicle activation induced by ovarian cryopreservation and in vitro culture. Journal of ovarian research, 14(1), 95. https://doi.org/10.1186/s13048-021-00846-5

334. Sehgal SN, Baker H, Vezina C. Rapamycin (AY-22,989), a new antifungal antibiotic. II. Fermentation, isolation and characterization. J. Antibiotics. (1975) 28:727–32.

335. Tsang CK, Qi H, Liu LF, Zheng XF. Targeting mammalian target of rapamycin (mTOR) for health and diseases. Drug Discov Today. (2007) 12:112–24.

336. Heitman J, Movva NR, Hall MN. Targets for cell cycle arrest by the immunosuppressant rapamycin in yeast. Science. (1991) 253:905–9.

337. Brown EJ, Albers MW, Shin TB, Ichikawa K, Keith CT, Lane WS, et al. . A mammalian protein targeted by G1-arresting rapamycin-receptor complex. Nature. (1994)

338. Sabatini DM, Erdjument-Bromage H, Lui M, Tempst P, Snyder SH. RAFT1: a mammalian protein that binds to FKBP12 in a rapamycin-dependent fashion and is homologous to yeast TORs. Cell. (1994) 78:35–43.

339. Cafferkey R, Young PR, McLaughlin MM, Bergsma DJ, Koltin Y, Sathe GM, et al. . Dominant missense mutations in a novel yeast protein related to mammalian phosphatidylinositol 3-kinase and VPS34 abrogate rapamycin cytotoxicity. Mol Cell Biol. (1993) 13:6012–23.

340. Lamming DW, Ye L, Katajisto P, Goncalves MD, Saitoh M, Stevens DM, et al. . Rapamycin-induced insulin resistance is mediated by mTORC2 loss and uncoupled from longevity. Science. (2012) 335:1638–43.

341. Saxton RA, Sabatini DM. mTOR signaling in growth, metabolism, and disease. Cell. (2017) 168:960–76.

342. Adhikari D, Flohr G, Gorre N, Shen Y, Yang H, Lundin E, et al. . Disruption of Tsc2 in oocytes leads to overactivation of the entire pool of primordial follicles. Mol Hum Reprod. (2009) 15:765–70.

343. Adhikari D, Zheng W, Shen Y, Gorre N, Hamalainen T, Cooney AJ, et al. . Tsc/mTORC1 signaling in oocytes governs the quiescence and activation of primordial follicles. Hum Mol Genet. (2010) 19:397–410.

344. Pangas SA, Matzuk MM. Genetic models for transforming growth factor beta superfamily signaling in ovarian follicle development. Mol Cell Endocrinol. 2004;225(1–2):83–91

345. Massague J. TGF-beta signal transduction. Annu Rev Biochem. 1998;67:753–791.

346. Shimasaki S, Moore RK, Otsuka F, Erickson GF. The bone morphogenetic protein system in mammalian reproduction. Endocr Rev. 2004;25(1):72–101.

347.Lewis KA, Gray PC, Blount AT, et al. Betaglycan binds inhibin and can mediate functional antagonism of activin signalling. Nature. 2000;404(6776):411–414.

348. Kaivo-Oja N, Jeffery LA, Ritvos O, Mottershead DG. Smad signalling in the ovary. Reprod Biol Endocrinol. 2006;4:21

349. Balemans W, Van Hul W. Extracellular regulation of BMP signaling in vertebrates: a cocktail of modulators. Dev Biol. 2002;250(2):231–250.

350. Tremblay KD, Dunn NR, Robertson EJ. Mouse embryos lacking Smad1 signals display defects in extra-embryonic tissues and germ cell formation. Development. 2001;128:3609–3621.

351. Lechleider RJ, Ryan JL, Garrett L, Eng C, Deng C, Wynshaw-Boris A, Roberts AB. Targeted mutagenesis of Smad1 reveals an essential role in chorioallantoic fusion. Dev Biol. 2001;240:157–167.

352. Weinstein M, Yang X, Li C, Xu X, Gotay J, Deng CX. Failure of egg cylinder elongation and mesoderm induction in mouse embryos lacking the tumor suppressor smad2. Proc Natl Acad Sci U S A. 1998;95:9378–9383.

353. Nomura M, Li E. Smad2 role in mesoderm formation, left-right patterning and craniofacial development. Nature. 1998;393:786–790.

354. Xu J, Oakley J, McGee EA. Stage-specific expression of Smad2 and Smad3 during folliculogenesis. Biol Reprod. 2002;66:1571–1578.

355. Datta PK, Moses HL. STRAP and Smad7 synergize in the inhibition of transforming growth factor beta signaling. Mol Cell Biol. 2000 May;20(9):3157-67.

356. Sharum, I. B., Granados-Aparici, S., Warrander, F. C., Tournant, F. P., & Fenwick, M. A. (2017). Serine threonine kinase receptor associated protein regulates early follicle development in the mouse ovary, Reproduction, 153(2), 221-231

357. Lutz M, Knaus P. Integration of the TGF-beta pathway into the cellular signalling network. Cell Signal. 2002;14(12):977–988.

358. Kulkarni AB, Huh CG, Becker D, et al. Transforming growth factor beta 1 null mutation in mice causes excessive inflammatory response and early death. Proc Natl Acad Sci U S A. 1993;90(2):770–774

359. Ingman WV, Robker RL, Woittiez K, Robertson SA. Null mutation in transforming growth factor beta1 disrupts ovarian function and causes oocyte incompetence and early embryo arrest. Endocrinology. 2006;147(2):835–845.

360. Shimasaki S, Moore RK, Otsuka F, Erickson GF. The bone morphogenetic protein system in mammalian reproduction. Endocr Rev. 2004;25(1):72–101.

361. K.A. Lawson, N.R. Dunn, B.A. Roelen, L.M. Zeinstra, A.M. Davis, C.V. Wright, et al.

Bmp4 is required for the generation of primordial germ cells in the mouse embryo

Genes & Development, 13 (1999), pp. 424-436

362. Y. Ying, G.Q. Zhao Cooperation of endoderm-derived BMP2 and extraembryonic ectoderm-derived BMP4 in primordial germ cell generation in the mouse

Developmental Biology, 232 (2001), pp. 484-492

363. M.K. Skinner Regulation of primordial follicle assembly and development Human Reproduction Update, 11 (2005), pp. 461-471

364. W.-S. Lee, S.-J. Yoon, T.-K. Yoon, K.-Y. Cha, S.-H. Lee, S. Shimasaki, et al. Effects of bone morphogenetic protein-7 (BMP-7) on primordial follicular growth in the mouse ovary Molecular Reproduction and Development, 69 (2004), pp. 159-163

365. McNatty KP, Moore LG, Hudson NL, Quirke LD, Lawrence SB, Reader K, Hanrahan JP, Smith P, Groome NP, Laitinen M, Ritvos O, Juengel JL. The oocyte and its role in regulating ovulation rate: a new paradigm in reproductive biology. Reproduction. 2004;128(4):379–386]

366. Moore RK, Otsuka F, Shimasaki S. Molecular basis of bone morphogenetic protein-15 signaling in granulosa cells. J Biol Chem. 2002;278(1):304–310.

367. Kaivo-Oja N, Mottershead DG, Mazerbourg S, Myllymaa S, Duprat S, Gilchrist RB, Groome NP, Hsueh AJ, Ritvos O. Adenoviral gene transfer allows Smad-responsive gene promoter analyses and delineation of type I receptor usage of transforming growth factor-beta family ligands in cultured human granulosa luteal cells. J Clin Endocrinol Metab. 2005;90(1):271–278.

368 Mazerbourg S, Klein C, Roh J, Kaivo-Oja N, Mottershead DG, Korchynskyi O, Ritvos O, Hsueh AJ. Growth differentiation factor-9 signaling is mediated by the type I receptor, activin receptor-like kinase 5. Mol Endocrinol. 2004;18(3):653–665.

369. Dixit H, et al. Missense mutations in the BMP15 gene are associated with ovarian failure. Hum Genet. 2006;119(4):408–415.

370. Laissue P, et al. Mutations and sequence variants in GDF9 and BMP15 in patients with premature ovarian failure. Eur J Endocrinol. 2006;154(5):739–744.

371. Hoekstra C, et al. Dizygotic twinning. Hum Reprod Update. 2008;14(1):37–47.

372. Pangas, Stephanie A. "Regulation of the ovarian reserve by members of the transforming growth factor beta family." Molecular reproduction and development vol. 79,10 (2012): 666-79.

373. Dong J, Albertini DF, Nishimori K, Kumar TR, Lu N, Matzuk MM. Growth differentiation factor-9 is required during early ovarian folliculogenesis. Nature. 1996;383:531–535.

374. Liu, C., Peng, J., Matzuk, M. et al. Lineage specification of ovarian theca cells requires multicellular interactions via oocyte and granulosa cells. Nat Commun 6, 6934 (2015).

375. Yan C, Wang P, DeMayo J, et al. Synergistic roles of bone morphogenetic protein 15 and growth differentiation factor 9 in ovarian function. Mol Endocrinol. 2001;15(6):854–866

376. Peng J, Li Q, Wigglesworth K, Rangarajan A, Kattamuri C, Peterson RT, Eppig JJ, Thompson TB, Matzuk MM. Growth differentiation factor 9:bone morphogenetic protein 15 heterodimers are potent regulators of ovarian functions. Proc Natl Acad Sci U S A. 2013 Feb 19;110(8):E776-85.

377. Roy, Sambit et al. "Oocyte-Derived Factors (GDF9 and BMP15) and FSH Regulate AMH Expression Via Modulation of H3K27AC in Granulosa Cells." Endocrinology vol. 159,9 (2018): 3433-3445. doi:10.1210/en.2018-00609

378. Munsterberg A, Lovell-Badge R. Expression of the mouse anti-müllerian hormone gene suggests a role in both male and female sexual differentiation. Development. 1991;113(2):613–624.

379. Rosendahl M, Andersen CY, la Cour Freiesleben N, Juul A, Lossl K, Andersen AN. Dynamics and mechanisms of chemotherapy-induced ovarian follicular depletion in women of fertile age. Fertil Steril. 2010;94(1):156-66.

380. Broekmans FJ, Visser JA, Laven JS, Broer SL, Themmen AP, Fauser BC. Anti-Mullerian hormone and ovarian dysfunction. Trends Endocrinol Metab. 2008;19(9):340-7.

381. Baarends WM, Uilenbroek JT, Kramer P, et al. Anti-müllerian hormone and anti-müllerian hormone type II receptor messenger ribonucleic acid expression in rat ovaries during postnatal development, the estrous cycle, and gonadotropin-induced follicle growth. Endocrinology. 1995;136(11):4951–4962.

382. Behringer RR, Finegold MJ, Cate RL. Müllerian-inhibiting substance function during mammalian sexual development. Cell. 1994;79(3):415–425.

383. Durlinger AL, Kramer P, Karels B, et al. Control of primordial follicle recruitment by anti-müllerian hormone in the mouse ovary. Endocrinology. 1999;140(12):5789–5796.

384. Schmidt D, Ovitt CE, Anlag K, et al. The murine winged-helix transcription factor Foxl2 is required for granulosa cell differentiation and ovary maintenance. Development. 2004;131(4):933–942.

385. Carlsson IB, Scott JE, Visser JA, et al. Anti-müllerian hormone inhibits initiation of growth of human primordial ovarian follicles in vitro. Hum Reprod. 2006;21(9):2223–2227.

386. Nilsson, Eric E et al. "Roles of Gremlin 1 and Gremlin 2 in regulating ovarian primordial to primary follicle transition." Reproduction (Cambridge, England) vol. 147,6 (2014): 865-74. doi:10.1530/REP-14-0005

387. Muttukrishna S, Tannetta D, Groome N, Sargent I. Activin and follistatin in female reproduction. Mol Cell Endocrinol. 2004;225(1–2):45–56.

388. Woodruff TK, D'Agostino J, Schwartz NB, Mayo KE. Dynamic changes in inhibin messenger RNAs in rat ovarian follicles during the reproductive cycle. Science. 1988;239(4845):1296–1299.

389. Makanji Y, Zhu J, Mishra R, Holmquist C, Wong WPS, Schwartz NB, et al. Inhibin at 90: from discovery to clinical application, a historical review. Endocrine Reviews. 2014 Oct;35(5):747–94.

390. Nakamura T, Takio K, Eto Y, Shibai H, Titani K, Sugino H. Activin-binding protein from rat ovary is follistatin. Science. 1990 Feb 16;247(4944):836–8.

391. Li R, Phillips DM, Mather JP. Activin promotes ovarian follicle development in vitro.

Endocrinology. 1995 Mar;136(3):849–56.

392. Yokota H, Yamada K, Liu X, Kobayashi J, Abe Y, Mizunuma H, et al. Paradoxical action of activin A on folliculogenesis in immature and adult mice. Endocrinology. 1997 Nov;138(11):4572–6.

393. Mizunuma H, Liu X, Andoh K, Abe Y, Kobayashi J, Yamada K, et al. Activin from secondary follicles causes small preantral follicles to remain dormant at the resting stage. Endocrinology. 1999 Jan;140(1):37–42.

394. Pangas SA, Jorgez CJ, Tran M, Agno J, Li X, Brown CW, et al. Intraovarian activins are required for female fertility. Molecular Endocrinology. 2007 Oct;21(10):2458–71.

395. Findlay JK. An update on the roles of inhibin, activin, and follistatin as local regulators of folliculogenesis. Biol Reprod. 1993;48(l):15–23.

396. Stephanie A. Pangas, Carolina J. Jorgez, Mai Tran, Julio Agno, Xiaohui Li, Chester W. Brown, T. Rajendra Kumar, Martin M. Matzuk, Intraovarian Activins Are Required for Female Fertility, Molecular Endocrinology, Volume 21, Issue 10, 1 October 2007, Pages 2458–2471.

397. Harvey KF, Zhang X, Thomas DM. The Hippo pathway and human cancer. Nat Rev Cancer. 2013;13:246–257.

398. Hong AW, Meng Z, Guan KL. The Hippo pathway in intestinal regeneration and disease. Nat Rev Gastroenterol Hepatol. 2016;13:324–337.

399. Plewes, Michele R et al. "Yes-associated protein 1 is required for proliferation and function of bovine granulosa cells in vitro†." Biology of reproduction vol. 101,5 (2019): 1001-1017.

400. Plouffe SW, Meng Z, Lin KC, Lin B, Hong AW, Chun JV, Guan KL. Characterization of Hippo pathway components by gene inactivation. Mol Cell 2016; 64:993–1008.

401. Papageorgiou, Kyriaki et al. "Interplay Between mTOR and Hippo Signaling in the Ovary: Clinical Choice Guidance Between Different Gonadotropin Preparations for Better IVF." Frontiers in endocrinology vol. 12 702446. 21 Jul. 2021.

402. Melody Devos, Johanne Grosbois, Isabelle Demeestere, Interaction between PI3K/AKT and Hippo pathways during in vitro follicular activation and response to fragmentation and chemotherapy exposure using a mouse immature ovary model, Biology of Reproduction, Volume 102, Issue 3, March 2020, Pages 717–729.

403. Maas, Kristi et al. "Hippo signaling in the ovary and polycystic ovarian syndrome." Journal of assisted reproduction and genetics vol. 35,10 (2018): 1763-1771.

404. Nao Suzuki, Nobuhito Yoshioka, Seido Takae, Yodo Sugishita, Midori Tamura, Shu Hashimoto, Yoshiharu Morimoto, Kazuhiro Kawamura, Successful fertility preservation following ovarian tissue vitrification in patients with primary ovarian insufficiency, Human Reproduction, Volume 30, Issue 3, March 2015.

405. Kreimendahl F, Kniebs C, Tavares Sobreiro AM, Schmitz-Rode T, Jockenhoevel S, Thiebes AL. FRESH bioprinting technology for tissue engineering - the influence of printing process and bioink composition on cell behavior and vascularization. J Appl Biomater Funct Mater. 2021

Appendix A: Supplemental Figures and Tables

Chapter 2

Supplemental Figure 1
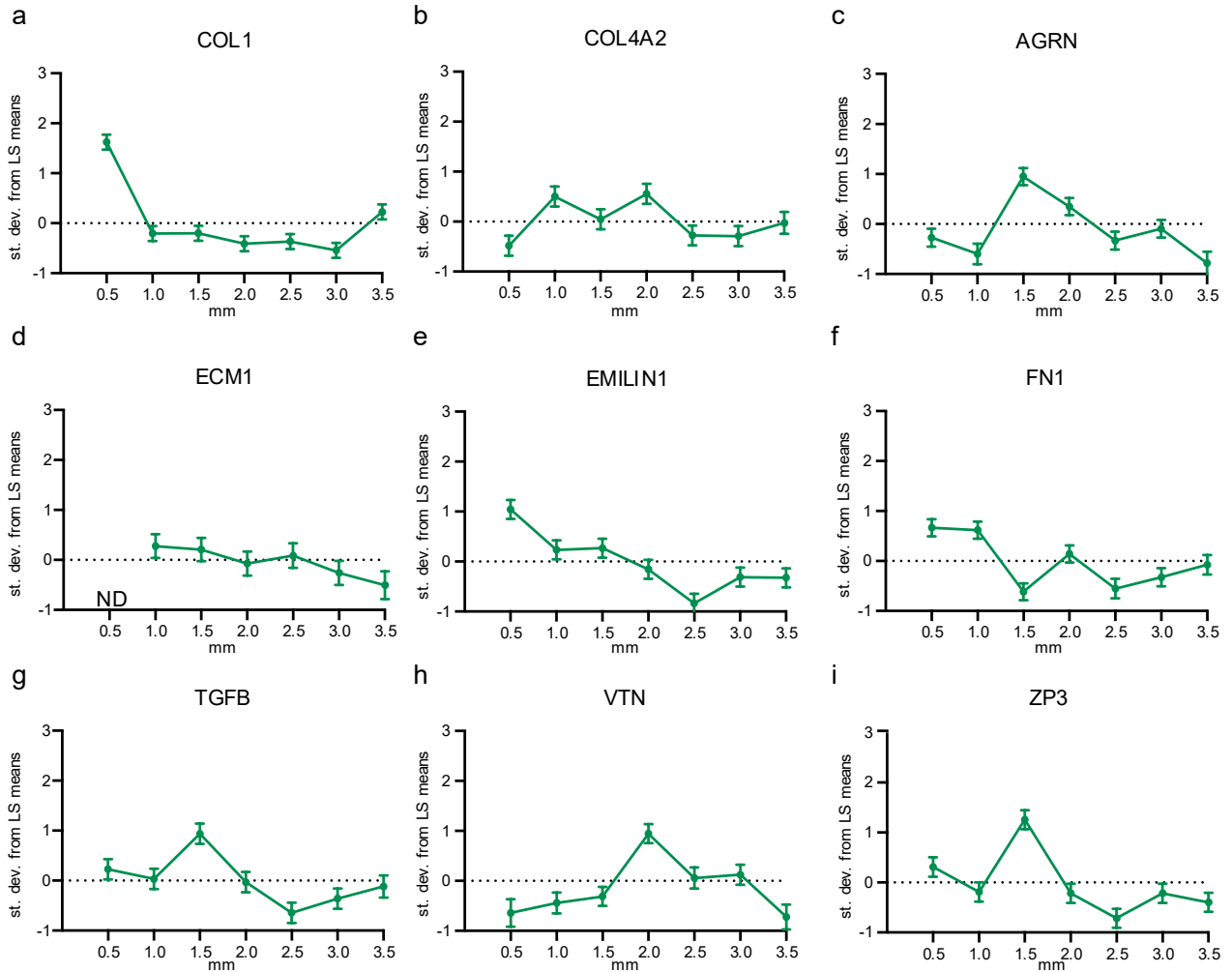
Peptide reads represented by standard deviations from LS Means for (a) COL1, (b) COL4A2, (c) AGR (d) ECM1, (e) EMILIN1, (f) FN1, (g) TGFB, (h) VTN, (i) ZP3. These are represented across depths 0.5 3.5 mm. ND, not detected; bars represented as mean, SEM.

Supplemental Figure 2
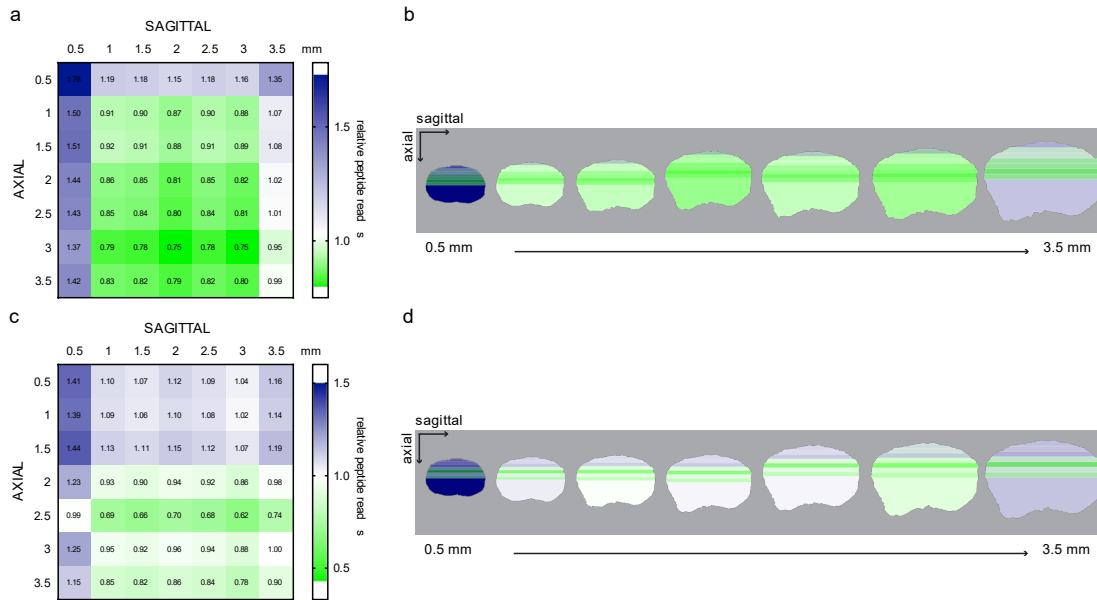
a

b

c

d

Heatmaps of (a,b) COL1A2 and (c,d) EMILIN1 expression at sagittal and axial intersections (a,c) relative to univeral m
of peptide reads. (b,d) Schematic representation of expression at axial depth slices (top to bottom) visualized on each
sagittal slice (left to right).

Supplemental Table 1: Antibodies used for iPCR and IHC

Target	Manufacturer	SKU	Use
AGRN	Abcam	ab85174	iPCR
AGRN	Lifespan Biosciences	LS-G81348-20	IHC
COL1	Abcam	ab90395	iPCR
COL1	EMD Millipore	234138-1MG	IHC
COL4	EMD MIllipore	CC083	IHC
COL4A2	Abclonal	A7657	iPCR
ECM1	Abcam	ab234976	iPCR & IHC
EMILIN1	Fisher Scientific	PA551745	iPCR
EMILIN1	ABNova	H00011117P01	IHC
FN1	Abcam	ab23750	iPCR & IHC
LMNA	Proteintech	10298-1-AP	iPCR & IHC
TGFB	Abcam	ab92486	iPCR & IHC
VTN	Abcam	ab140016	iPCR & IHC
ZP3	Fisher Scientific	50-561-353	iPCR & IHC

Supplemental Table 2: Primers used for qPCR

Target	Manufacturer	SKU
AGRN	Bio-Rad	qBtaCID0012730
COL1A1	Bio-Rad	qSscCED10042976
COL1A2	Bio-Rad	qSscCED0020342
EMILIN1	Bio-Rad	qSscCED0008548
COL4	Bio-Rad	qSscCID0013145
FN1	Bio-Rad	qSscCID0003939
ECM1	Bio-Rad	qSscCID0013839
VTN	Bio-Rad	qSscCED0021774
ZP3	Bio-Rad	qSscCID0013229
TGFB	Bio-Rad	qSscCID0018090
LMNA	Bio-Rad	qSscCID0012088

Supplemental Table 3: Matrisome proteins identified in the ovary

Protein ID	Previously identified in ovary	Characterized in ovary	Role in ovary
COL1A2	[1] (h)	[2–4] (m), [5] (h), [6] (b)	major structural component of organ
COL2A1	*	[7] (r)	in theca and GC
COL3A1	[8] (b)	[5] (h)	inner layers of capsular stroma
COL4A1	[1] (h), [9,10] (b)	[5] (h), [3,4] (m), [6] (b)	basal lamina component
COL4A2	[1] (h), [9,10] (b)	[5] (h), [3,4] (m), [6] (b)	basal lamina component
COL5A1	[11] (h culture, *mRNA*)	none	unknown
COL5A2	[12] (b GC and theca, *mRNA*)	none	unknown
COL6A2	[1,13] (h), [14] (mo), [15] (m)	[16] (h, *undefined subunit of α6*),	localized to theca
COL6A5	*	[16] (h, *undefined subunit of α6*)	localized to theca
COL14A1	[1] (h), [14] (mo)	none	unknown
AEBP1	none	none	unknown
AGRN	none	none	unknown
DPT	[17] (h, *"faint" mRNA*)	none	unknown
ECM1	[18] (p), [19] (h)	[19] (h)	downregulated in insulin resistant PCOS, potential antral arrest

Protein ID	Previously identified in ovary	Characterized in ovary	Role in ovary
EFEMP1	[18] (p)	[20] (h)	increased tumor angiogenesis, tumor progression
EMILIN1	[1,13] (h)	none	unknown
EMILIN3	none	none	unknown
FBN1	[1] (h), [8] (b)	[21] (fetal b, h), [22] (p), [23,24] (b), [24] (h)	TGFB regulation, structural component of elastin fibers and microfibrils, CC apoptosis
FN1	[1] (h), [18] (p)	[3,4,25] (m), [6] (b)	luteinization and CC expansion
IGFBP7	*	[26,27] (r)	steroidogenesis
LAMB1	[1] (h)	[28] (p), [19] (h), [3,4] (m)	cell proliferation, migration, downregulated in PCOS,
LAMC1	[1] (h)	[28] (p), [19] (h), [3,4] (m)	associated with premature ovarian failure, cell proliferation, migration
LTBP1	*	[29,30] (m), [23] (b)	modulation of TGFB1
MFAP2	[1] (h)	none	unknown
MFGE8	*	[31–33] (m)	phagocytosis of apoptotic GC, gonadogenesis
SRPX2	[18] (p)	none	unknown
TGFB1	[1] (h), [18] (p), [8] (b)	[34] (r), [35] (m), [36] (p)	cell growth, proliferation, inflammation, differentiation, apoptosis
VTN	[1] (h), [18] (p)	[37,38](h), [39,40] (h cells), [41] (p),	IGF binding, integrin binding and adhesion, cancer progression and metastasis
VWA1	*	[42] (m), [43–47](h)	interacts with ERK5-PI3K/Akt axis, increased expression in PCOS, cancer, and during pregnancy, stimulates platelet aggregation
ZP2	*	[48] (h, CHO), [49–52] (h), [53] (c), [54] (mo), [55] (m, mo,h), [56,57] (m)	oocyte maturation, fertilization
ZP3	*	[48] (h, CHO), [49–52] (h), [53] (c), [54] (mo), [55] (m, mo,h), [56,57] (m)	oocyte maturation, fertilization

Protein ID	Previously identified in ovary	Characterized in ovary	Role in ovary
ZP4	[14] (mo)	[48] (h, CHO), [49–52] (h), [53] (c), [54] (mo), [55] (m, mo,h), [56,57] (m)	oocyte maturation, fertilization
A2M	[1] (h), [18] (p)	[58–60] (h serum), [61] (r)	expressed in GC, increased in women with inflammatory conditions including neoplastic lesions, reduced expression in ovarian cancer
AMBP	[18] (p)	[62] (h)	interacts with ITIH family genes in solid tumor cancers
CTSD	*	[63,64] (h)	lysosome activation in late corpus luteum, oxidative stress in ovarian cancer
HRG	[14] (mo)	[65] (h), [66] (p), [67] (h follicle, embryo) [68] (h cells)	*in vitro* maturation, cancer cell invasion
ITIH1	[1] (h), [18] (p), [69] (b FF)	[62] (h)	solid tumor cancer progression, covalent linkage to hyaluronan for ECM stability
ITIH2	[1] (h), [18] (p), [69] (b FF)	[62] (h)	solid tumor cancer progression, covalent linkage to hyaluronan for ECM stability
KNG1	*	[70] (b), [71] (h serum, cells)	ovulation, stimulated by progesterone
LOX	*	[72] (p GC), [73] (h FF, h GC, r), [74] (h FF), [75] (h GC), [76–78] (m), [77] (b), [79] (r)	follicle development, angiogenesis in GC, TGFB, estrogenesis
SERPINA1	[1] (h), [18] (p)	[80] (m), [81] (h FF), [82] (h GC)	plasminogen activator inhibitor, upregulated in PCOS reducing plasmin levels
SERPINA3	[1] (h)	[80] (m)	plasminogen activator inhibitor
SERPINC1	[1] (h), [18] (p)	[80] (m), [83] (r serum)	plasminogen activator inhibitor
SERPIND1	[1] (h), [18] (p)	[80] (m)	plasminogen activator inhibitor
TGM2	[14] (mo), [84] (b, *mRNA*)	none	unknown
Protein ID	Previously identified in ovary	Characterized in ovary	Role in ovary
ANXA1	[1,13] (h), [14] (mo), [18] (p)	none	implicated in both cancer and PCOS, target of GNRH in gonadotrope cells, CL regression
ANXA2	[1,13] (h), [14] (mo)	none	unknown

Protein ID	Previously identified in ovary	Characterized in ovary	Role in ovary
ANXA4	[1,13] (h), [14] (mo)	none	unknown
ANXA5	[1,13] (h), [14] (mo), [85] (h blood)	[86] (r)	in GC after hCG
ANXA7	none	none	unknown
ANXA11	[13] (h)	none	unknown
GPC1	none	none	unknown
LGALS1	[14] (m)	[87] (b), [88,89] (m), [90] (h cells), [91] (b), [92] (p gc)	lutealization, regression of CL
SDC2	[93] (o CC, *mRNA*)	[94] (h)	confined to stroma of normal and benign tissue
BGN	[15] (m, *mRNA*)	none	unknown
DCN	[1] (h); [14] (mo), [18] (p), [8] (b)	[95] (m), [72] (p GC)	signaling molecule in ovarian ECM
FMOD	[1] (h); [14] (mo)	none	unknown
LUM	[1] (h); [14] (mo), [18] (p), [96] (b)	[97] (fetal b), [98] (CHO)	stromal expansion, cell migration, expression in CC
PRELP	[1] (h), [14] (mo),	none	unknown
VCAN	[18] (p)	[99] (h serum), [100–102] (h CC), [103] (m, r)	binds hyaluronan, decreased in PCOS, CC, oocyte competency, development quality of oocytes

Abbreviations: b, bovine; c, canine; CC, cumulus cells; CHO, Chinese hamster ovarian cells; CL, corpus luteum; GC, granulosa cell; FF, follicular fluid; h, human; m, mouse; mo, monkey; o, ovine; p, porcine; PCOS, polycystic ovarian syndrome; r, rat; *, *see characterization*;

Supplemental table 3 References:

1. Ouni, E., Vertommen, D., Chiti, M., Dolmans, M.-M. & Amorim, C. A draft map of the human ovarian proteome for tissue engineering and clinical applications. *Mol Cell Proteomics* **18,** mcp.RA117.000469 (2018).

2. Marongiu, M. *et al.* Novel action of FOXL2 as mediator of Col1a2 gene autoregulation. *Dev Biol* **416,** 200 211 (2016).

3. Berkholtz, C. B., Lai, B. E., Woodruff, T. K. & Shea, L. D. Distribution of extracellular matrix proteins type I collagen, type IV collagen, fibronectin, and laminin in mouse folliculogenesis. *Histochem Cell Biol* **126,** 583–592 (2006).

4. Berkholtz, C., Shea, L. & Woodruff, T. Extracellular Matrix Functions in Follicle Maturation. *Semin Reprod Med* **24,** 262–269 (2006).

5. LIND, A. -K. *et al.* Collagens in the human ovary and their changes in the perifollicular stroma during ovulation. *Acta Obstet Gyn Scan* **85,** 1476–1484 (2006).

6. Figueiredo, J. R. *et al.* Extracellular matrix proteins and basement membrane: Their identification in bovine ovaries and significance for the attachment of cultured preantral follicles. *Theriogenology* **43,** 845–858 (1995).

7. Saha, S. *et al.* Localization and Thyroid Hormone Influenced Expression of Collagen II in Ovarian Tissue. *Cell Physiol Biochem* **19,** 67–76 (2007).

8. Hatzirodos, N. *et al.* Transcript abundance of stromal and thecal cell related genes during bovine ovarian development. *Plos One* **14,** e0213575 (2019).

9. Matti, N., Irving-Rodgers, H. F., Hatzirodos, N., Sullivan, T. R. & Rodgers, R. J. Differential expression of focimatrix and steroidogenic enzymes before size deviation during waves of follicular development in bovine ovarian follicles. *Mol Cell Endocrinol* **321,** 207 214 (2010).

10. Irving-Rodgers, H. F. *et al.* Dynamics of extracellular matrix in ovarian follicles and corpora lutea of mice. *Cell Tissue Res* **339,** 613 624 (2009).

11. Kranc, W. *et al.* Genes responsible for proliferation, differentiation, and junction adhesion are significantly up-regulated in human ovarian granulosa cells during a long-term primary in vitro culture. *Histochem Cell Biol* **151,** 125–143 (2019).

12. Hatzirodos, N., Hummitzsch, K., Irving-Rodgers, H. F. & Rodgers, R. J. Transcriptome Comparisons Identify New Cell Markers for Theca Interna and Granulosa Cells from Small and Large Antral Ovarian Follicles. *Plos One* **10,** e0119800 (2015).

13. Wang, L. *et al.* A two-dimensional electrophoresis reference map of human ovary. *J Mol Med* **83,** 812–821 (2005).

14. He, H. *et al.* Unravelling the proteome of adult rhesus monkey ovaries. *Mol Biosyst* **10,** 653 10 (2013).

15. Oksjoki, S., Sallinen, S., Vuorio, E. & Anttila, L. Cyclic expression of mRNA transcripts for connective tissue components in the mouse ovary. *Mhr Basic Sci Reproductive Medicine* **5,** 803–808 (1999).

16. Iwahashi, M., Muragaki, Y., Ooshima, A. & Nakano, R. Type VI collagen expression during growth of human ovarian follicles. *Fertil Steril* **74,** 343 347 (2000).

17. Li, X. *et al.* Dermatopontin is expressed in human liver and is downregulated in hepatocellular carcinoma. *Biochem Mosc* **74,** 979–985 (2009).

18. Hou, L., Wang, J., Wang, Y., Hua, X. & Wu, J. Compared proteomic analysis of 8- and 32-week-old postnatal porcine ovaries. *Cell Biochem Funct* **36,** 34–42 (2018).

19. Hassani, F. *et al.* Downregulation of Extracellular Matrix and Cell Adhesion Molecules in Cumulus Cells of Infertile Polycystic Ovary Syndrome Women with and without Insulin Resistance. *Cell J* **21,** 35–42

20. Chen, J., Wei, D., Zhao, Y., Liu, X. & Zhang, J. Overexpression of EFEMP1 Correlates with Tumor Progression and Poor Prognosis in Human Ovarian Carcinoma. *Plos One* **8,** e78783 (2013).

21. Bastian, N. A. *et al.* Regulation of fibrillins and modulators of TGFβ in fetal bovine and human ovaries. *Reproduction* **152,** 127–137 (2016).

22. Zhai, B. *et al.* BMP15 Prevents Cumulus Cell Apoptosis Through CCL2 and FBN1 in Porcine Ovaries. *Cell Physiol Biochem* **32,** 264–278 (2013).

23. Prodoehl, M. J. *et al.* Fibrillins and latent TGFβ binding proteins in bovine ovaries of offspring following high or low protein diets during pregnancy of dams. *Mol Cell Endocrinol* **307,** 133 141 (2009).

24. Prodoehl, M. J. *et al.* Genetic and gene expression analyses of the polycystic ovary syndrome candidate gene fibrillin-3 and other fibrillin family members in human ovaries. *Mol Hum Reprod* **15,** 829–41 (2009).

25. Kitasaka, H. *et al.* Inductions of granulosa cell luteinization and cumulus expansion are dependent on the fibronectin-integrin pathway during ovulation process in mice. *Plos One* **13,** e0192458 (2018).

26. TAMURA, K., YOSHIE, M., HASHIMOTO, K. & TACHIKAWA, E. Inhibitory effect of insulin-like growth factor-binding protein-7 (IGFBP7) on in vitro angiogenesis of vascular endothelial cells in the rat corpus luteum. *J Reprod Develop* **60,** 447–453 (2014).

27. Tamura, K., Matsushita, M., Endo, A., Kutsukake, M. & Kogo, H. Effect of Insulin-Like Growth Factor-Binding Protein 7 on Steroidogenesis in Granulosa Cells Derived from Equine Chorionic Gonadotropin-Primed Immature Rat Ovaries. *Biol Reprod* **77,** 485–491 (2007).

28. Ożegowska, K. *et al.* Genes Involved in the Processes of Cell Proliferation, Migration, Adhesion, and Tissue Development as New Potential Markers of Porcine Granulosa Cellular Processes In Vitro: A Microarray Approach. *Dna Cell Biol* **38,** 549–560 (2019).

29. Faraoni, E. Y. *et al.* Sex differences in the development of prolactinoma in mice overexpressing hCGβ: role of TGFβ1. *J Endocrinol* **232,** 535–546 (2017).

30. Dietzel, E. *et al.* Latent TGF-β binding protein-1 deficiency decreases female fertility. *Biochem Bioph Res Co* **482,** 1387–1392 (2017).

31. Kanai, Y. *et al.* Identification of a stromal cell type characterized by the secretion of a soluble integrin-binding protein, MFG-E8, in mouse early gonadogenesis. *Mech Develop* **96,** 223–227 (2000).

32. Mizukami, T. *et al.* Five azacytidine, a DNA methyltransferase inhibitor, specifically inhibits testicular cord formation and Sertoli cell differentiation in vitro. *Mol Reprod Dev* **75,** 1002–1010 (2008).

33. Naka, M. *et al.* Phagocytosis mechanism of apoptotic granulosa cells regulated by milk-fat globule-EGF factor 8. *Med Mol Morphol* **42,** 143–149 (2009).

34. Rosairo, D., Kuyznierewicz, I., Findlay, J. & Drummond, A. Transforming growth factor-β: its role in ovarian follicle development. *Reproduction* **136,** 799–809 (2008).

35. Pangas, S. A. Regulation of the ovarian reserve by members of the transforming growth factor beta family. *Mol Reprod Dev* **79,** 666–679 (2012).

36. Jackowska, M. *et al.* Differential expression of GDF9, TGFB1, TGFB2 and TGFB3 in porcine oocytes isolated from follicles of different size before and after culture in vitro. *Acta Vet Hung* **61,** 99–115 (2013).

37. Younis, A. J. *et al.* Extracellular-like matrices and leukaemia inhibitory factor for in vitro culture of human primordial follicles. *Reproduction Fertility Dev* **29,** 1982 (2017).

38. Carreiras, F. *et al.* Expression and Localization of αv Integrins and Their Ligand Vitronectin in Normal Ovarian Epithelium and in Ovarian Carcinoma. *Gynecol Oncol* **62,** 260–267 (1996).

39. Cruet, S., Salamanca, C., Mitchell, G. W. E. & Auersperg, N. αvβ3 and Vitronectin Expression by Normal Ovarian Surface Epithelial Cells: Role in Cell Adhesion and Cell Proliferation. *Gynecol Oncol* **75,** 254–260 (1999).

40. Jones, J. I., Doerr, M. E. & Clemmons, D. R. Cell migration: Interactions among integrins,

IGFs and IGFBPs. *Prog Growth Factor Res* **6,** 319–327 (1995).

41. Mazerbourg, S., Zapf, J., Bar, R. S., Brigstock, D. R. & Monget, P. Insulin-Like Growth Factor (IGF)-Binding Protein-4 Proteolytic Degradation in Bovine, Equine, and Porcine Preovulatory Follicles: Regulation by IGFs and Heparin-Binding Domain-Containing Peptides. *Biol Reprod* **63,** 390–400 (2000).

42. Jia, Y. *et al.* Thiophenol-formaldehyde triazole causes apoptosis induction in ovary cancer cells and prevents tumor growth formation in mice model. *Eur J Med Chem* **172,** 62–70 (2019).

43. Nayaker, B. S. *et al.* Polycystic ovarian syndrome-associated cardiovascular complications: An overview of the association between the biochemical markers and potential strategies for their prevention and elimination. *Diabetes Metabolic Syndrome Clin Res Rev* **11,** S841–S851 (2017).

44. Cheng, Z. *et al.* Extracellular signal-regulated kinase 5 associates with casein kinase II to regulate GPIb-IX-mediated platelet activation via the PTEN/PI3K/Akt pathway. *J Thromb Haemost* **15,** 1679–1688 (2017).

45. Aziz, M. *et al.* Polycystic ovary syndrome: cardiovascular risk factors according to specific phenotypes. *Acta Obstet Gyn Scan* **94,** 1082–1089 (2015).

46. Shan, Y. *et al.* Coagulation and Fibrinolytic Indices During the First Trimester of Pregnancy in Women With Polycystic Ovary Syndrome. *Reprod Sci* **20,** 1390–1397 (2013).

47. Koiou, E. *et al.* Plasma Von Willebrand factor antigen levels are elevated in the classic phenotypes of polycystic ovary syndrome. *Hormones* **11,** 77–85 (2012).

48. Zhou, Z. *et al.* Novel mutations in ZP1, ZP2, and ZP3 cause female infertility due to abnormal zona pellucida formation. *Hum Genet* **138,** 327–337 (2019).

49. Canosa, S. *et al.* Zona pellucida gene mRNA expression in human oocytes is related to oocyte maturity, zona inner layer retardance and fertilization competence. *Mhr Basic Sci Reproductive Medicine* **23,** 292–303 (2017).

50. Gook, D. A., Edgar, D. H., Borg, J. & Martic, M. Detection of zona pellucida proteins during human folliculogenesis. *Hum Reprod* **23,** 394–402 (2008).

51. Kiefer, S. & Saling, P. Proteolytic Processing of Human Zona Pellucida Proteins1. *Biol Reprod* **66,** 407–414 (2002).

52. Greve, J. M., Salzmann, G. S., Roller, R. J. & Wassarman, P. M. Biosynthesis of the major zona pellucida glycoprotein secreted by oocytes during mammalian oogenesis. *Cell* **31,** 749–759 (1982).

53. Kempisty, B. *et al.* Expression and cellular distribution of zona pellucida glycoproteins in canine oocytes before and after in vitro maturation. *Zygote* **23,** 863–873 (2015).

54. Konrad, L. *et al.* Quantification of ZP1, ZP2 and ZP3 mRNA of marmoset monkey (Callithrix jacchus) oocytes from periantral and antral follicles. *Andrologia* **44,** 349–353 (2012).

55. Cariño, C. *et al.* Localization of species conserved zona pellucida antigens in mammalian ovaries. *Reprod Biomed Online* **4,** 116–126 (2002).

56. El-Mestrah, M., Castle, P. E., Borossa, G. & Kan, F. Subcellular Distribution of ZP1, ZP2, and ZP3 Glycoproteins During Folliculogenesis and Demonstration of Their Topographical Disposition Within the Zona Matrix of Mouse Ovarian Oocytes. *Biol Reprod* **66,** 866–876 (2002).

57. Rankin, T., Soyal, S. & Dean, J. The mouse zona pellucida: folliculogenesis, fertility and pre-implantation development. *Mol Cell Endocrinol* **163,** 21–25 (2000).

58. Haoula, Z. *et al.* Validation of proteomic biomarkers previously found to be differentially expressed in women with Polycystic Ovary Syndrome: a cross-sectional study. *Gynecol Endocrinol* **30,** 213–216 (2014).

59. Šunderić, M., Malenković, V. & Nedić, O. Complexes between insulin-like growth factor binding proteins and alpha-2-macroglobulin in patients with tumor. *Exp Mol Pathol* **98,** 173–177 (2015).

60. ZBROJA-SONTAG, W. Defense Proteins and Immune Complexes in the Blood Serum of Women With Inflammatory and Neoplastic Lesions of the Ovary. *Am J Reprod Immunol* **4,** 11–20 (1983).

61. jee, Fey, G. & Richards, J. Stat 5b and the orphan nuclear receptors regulate expression of the alpha2-macroglobulin (alpha2M) gene in rat ovarian granulosa cells. *Mol Endocrinol Baltim Md* **12,** 1393–409 (1998).

62. Hamm, A. *et al.* Frequent expression loss of Inter-alpha-trypsin inhibitor heavy chain (ITIH) genes in multiple human solid tumors: A systematic expression analysis. *Bmc Cancer* **8,** 25 (2008).

63. Falfushynska, H., Gnatyshyna, L., Deneha, H., Osadchuk, O. & Stoliar, O. MANIFESTATIONS OF OXIDATIVE STRESS AND MOLECULAR DAMAGES IN OVARIAN CANCER TISSUE. *Ukrainian Biochem J* **87,** 93–102 (2015).

64. ABOELENAIN, M. *et al.* Status of autophagy, lysosome activity and apoptosis during corpus luteum regression in cattle. *J Reprod Develop* **61,** 229–236 (2015).

65. Kakoly, N., Earnest, A., Moran, L. J., Teede, H. J. & Joham, A. E. Group-based developmental BMI trajectories, polycystic ovary syndrome, and gestational diabetes: a community-based longitudinal study. *Bmc Med* **15,** 195 (2017).

66. Cai, L. *et al.* The effects of human recombinant granulocyte-colony stimulating factor treatment during in vitro maturation of porcine oocyte on subsequent embryonic development.

Theriogenology **84,** 1075–1087 (2015).

67. Nordqvist, S. *et al.* The Presence of Histidine-Rich Glycoprotein in the Female Reproductive Tract and in Embryos. *Reprod Sci* **17,** 941–947 (2010).

68. Xu, F. *et al.* The outcome of heregulin-induced activation of ovarian cancer cells depends on the relative levels of HER-2 and HER-3 expression. *Clin Cancer Res Official J Am Assoc Cancer Res* **5,** 3653–60 (1999).

69. Zachut, M., Sood, P., Levin, Y. & Moallem, U. Proteomic analysis of preovulatory follicular fluid reveals differentially abundant proteins in less fertile dairy cows. *J Proteomics* **139,** 122–129 (2016).

70. Ilha, G. *et al.* Characterization of the kallikrein–kinin system during the bovine ovulation process. *Peptides* **32,** 2122–2126 (2011).

71. Zheng, Q. *et al.* Novel Serum Biomarkers Detected by Protein Array in Polycystic Ovary Syndrome with Low Progesterone Level. *Cell Physiol Biochem* **46,** 2297–2310 (2018).

72. Chermuła, B. *et al.* New Gene Markers of Angiogenesis and Blood Vessels Development in Porcine Ovarian Granulosa Cells during Short-Term Primary Culture In Vitro. *Biomed Res Int* **2019,** 1 12 (2019).

73. Zhang, C., Ma, J., Wang, W., Sun, Y. & Sun, K. Lysyl oxidase blockade ameliorates anovulation in polycystic ovary syndrome. *Hum Reprod* **33,** 2096–2106 (2018).

74. Chang, H.-M. *et al.* Activin A-induced increase in LOX activity in human granulosa–lutein cells is mediated by CTGF. *Reproduction* **152,** 293–301 (2016).

75. Fang, Y. *et al.* Transforming growth factor-β1 increases lysyl oxidase expression by downregulating MIR29A in human granulosa lutein cells. *Reproduction* **152,** 205–213 (2016).

76. Weitzel, J., Vernunft, A., Krüger, B., Plinski, C. & Viergutz, T. LOX-1 regulates estrogenesis via intracellular calcium release from bovine granulosa cells. *Cytom Part A* **85,** 88–93 (2014).

77. Weitzel, J. M., Vernunft, A., Krüger, B., Plinski, C. & Viergutz, T. Inactivation of the LOX-1 Pathway Promotes the Golgi Apparatus during Cell Differentiation of Mural Granulosa Cells. *J Cell Physiol* **229,** 1946–1951 (2014).

78. Löhrke, B. *et al.* Lectin-like oxidized low-density lipoprotein receptor-1 (LOX-1) activity decreases estrogenesis in ovarian granulosa cells. *Cytom Part A* **79A,** 669–671 (2011).

79. Harlow, C. R., Rae, M., Davidson, L., Trackman, P. C. & Hillier, S. G. Lysyl oxidase gene expression and enzyme activity in the rat ovary: regulation by follicle-stimulating hormone, androgen, and transforming growth factor-beta superfamily members in vitro. *Endocrinology* **144,** 154–62 (2003).

80. Burchall, G. F. *et al.* Expression of the plasminogen system in the physiological mouse ovary and in the pathological polycystic ovary syndrome (PCOS) state. *Reprod Biol Endocrin* **17,** 33 (2019).

81. Patil, K. *et al.* Quantitative mass spectrometric analysis to unravel glycoproteomic signature of follicular fluid in women with polycystic ovary syndrome. *Plos One* **14,** e0214742 (2019).

82. Kaur, S. *et al.* Differential Gene Expression in Granulosa Cells from Polycystic Ovary Syndrome Patients with and without Insulin Resistance: Identification of Susceptibility Gene Sets through Network Analysis. *J Clin Endocrinol Metabolism* **97,** E2016–E2021 (2012).

83. Huang, Y. *et al.* Discovery of serum biomarkers implicated in the onset and progression of serous ovarian cancer in a rat model using iTRAQ technique. *Eur J Obstet Gyn R B* **165,** 96–103 (2012).

84. Douville, G. & Sirard, M.-A. Changes in granulosa cells gene expression associated with growth, plateau and atretic phases in medium bovine follicles. *J Ovarian Res* **7,** 50 (2014).

85. Matsuzaki, S. *et al.* Anti-glypican-1 antibody-drug conjugate exhibits potent preclinical antitumor activity against glypican-1 positive uterine cervical cancer. *Int J Cancer* **142,** 1056–1066 (2018).

86. TUNGK, D. *et al.* Effects of gonadotropin-releasing hormone agonist on human chorionic gonadotropin activity in granulosa cells of immature female rats. *J Reprod Develop* **64,** 2017–142 (2017).

87. Hatzirodos, N. *et al.* Transcript abundance of stromal and thecal cell related genes during bovine ovarian development. *Plos One* **14,** e0213575 16 (2019).

88. Nio-Kobayashi, J. & Iwanaga, T. Differential Cellular Localization of Galectin-1 and Galectin-3 in the Regressing Corpus Luteum of Mice and Their Possible Contribution to Luteal Cell Elimination. *J Histochem Cytochem* **58,** 741–749 (2010).

89. Nio, J. & Iwanaga, T. Galectins in the Mouse Ovary: Concomitant Expression of Galectin-3 and Progesterone Degradation Enzyme (20α-HSD) in the Corpus Luteum. *J Histochem Cytochem* **55,** 423–432 (2007).

90. Chen, L. *et al.* Clinical implication of the serum galectin-1 expression in epithelial ovarian cancer patients. *J Ovarian Res* **8,** 78 (2015).

91. SANO, M., HASHI, K., NIO-KOYASHI, J. & OKUDA, K. The luteotrophic function of galectin-1 by binding to the glycans on vascular endothelial growth factor receptor-2 in bovine luteal cells. *J Reprod Develop* **61,** 439–448 (2015).

92. Walzel, H. *et al.* Effects of galectin-1 on regulation of progesterone production in granulosa

cells from pig ovaries in vitro. *Glycobiology* **14,** 871–881 (2004).

93. Dhali, A. *et al.* Temporal expression of cumulus cell marker genes during in vitro maturation and oocyte developmental competence. *J Assist Reprod Gen* **34,** 1493–1500 (2017).

94. Davies, J. E. *et al.* Distribution and Clinical Significance of Heparan Sulfate Proteoglycans in Ovarian Cancer. *Clin Cancer Res* **10,** 5178–5186 (2004).

95. Adam, M. *et al.* Decorin is a part of the ovarian extracellular matrix in primates and may act as a signaling molecule. *Hum Reprod* **27,** 3249–3258 (2012).

96. Bunel, A. *et al.* Individual bovine in vitro embryo production and cumulus cell transcriptomic analysis to distinguish cumulus-oocyte complexes with high or low developmental potential. *Theriogenology* **83,** 228–237 (2015).

97. Hartanti, M. *et al.* Morphometric and gene expression analyses of stromal expansion during development of the bovine fetal ovary. *Reproduction Fertility Dev* **31,** 482 (2018).

98. Zeltz, C. *et al.* Lumican inhibits cell migration through α2β1 integrin. *Exp Cell Res* **316,** 2922–2931 (2010).

99. Özler, S. *et al.* Role of Versican and ADAMTS-1 in Polycystic Ovary Syndrome. *J Clin Res Pediatr E* **9,** 24–30 (2017).

100. Ocampo, A. *et al.* Assessment of Prostaglandin-Endoperoxide Synthase 2 and Versican gene expression profile from the cumulus cells: association with better in vitro fertilization outcomes. *J Ovarian Res* **11,** 84 (2018).

101. Liu, Q. *et al.* Analyzing the Transcriptome Profile of Human Cumulus Cells Related to Embryo Quality via RNA Sequencing. *Biomed Res Int* **2018,** 1–8 (2018).

102. Adriaenssens, T. *et al.* Cumulus cell gene expression is associated with oocyte developmental quality and influenced by patient and treatment characteristics. *Hum Reprod* **25,** 1259–1270 (2010).

103. Russell, D. L., Ochsner, S. A., Hsieh, M., Mulders, S. & Richards, J. S. Hormone-regulated expression and localization of versican in the rodent ovary. *Endocrinology* **144,** 1020–31 (2003).

Chapter 3

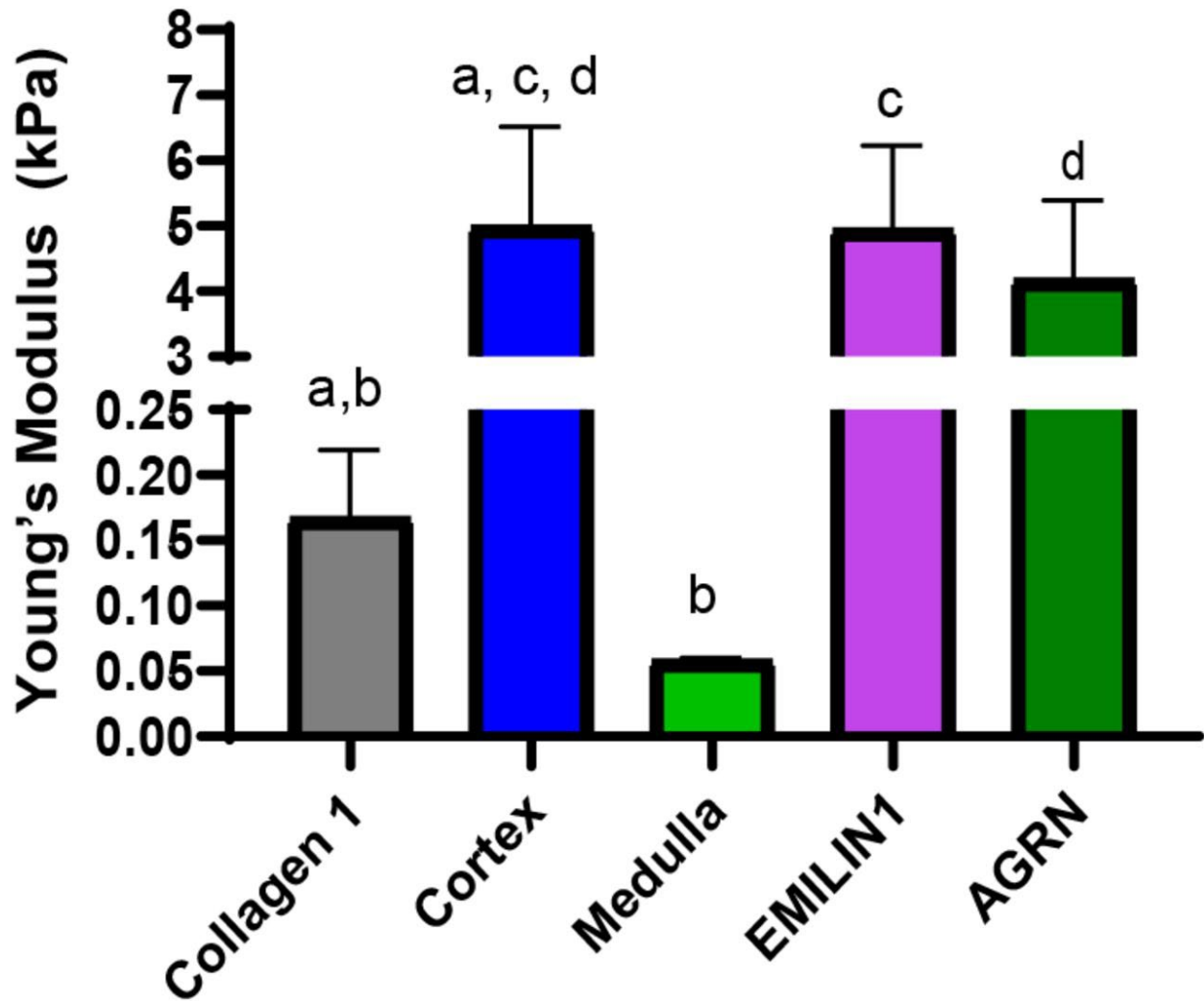Supplemental Figure 1
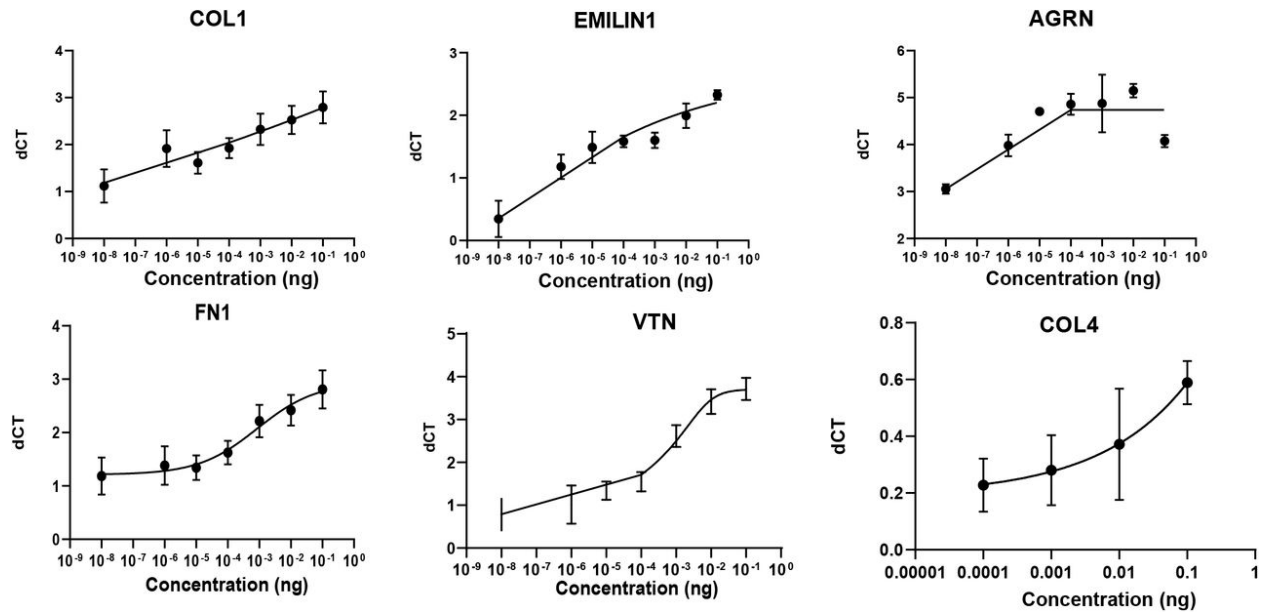
Standard curves used for interpolation of concentrations of protein. Bars represented as mean, SEM; N = 3 biological replicates, 2 technical replicates.

Supplemental Figure 2

Combined AFM data for FRESH printed scaffolds including collagen 1 only scaffold control. Bars equal to mean and standard error, P-values for relationships: a=0.0196, b=0.0782, c=0.9825, d=0.96933.

Supplemental Table 1

Target	Manufacturer	SKU	Use
AGRN	Abcam	ab85174	iPCR/MAPF
AGRN	LifeSpan Biosciences	LS-G81348-20	Protein Std
COL1	Abcam	ab90395	iPCR/MAPF
COL1	EMD Millipore	234138-1MG	Protein Std
EMILIN1	Fisher Scientific	PA551745	iPCR/MAPF
EMILIN1	Novus Biologicals	H00011117-P01	Protein Std
COL4A2	Abclonal	A7657	iPCR
FN1	Abcam	ab23750	iPCR
VTN	Abcam	ab140016	iPCR

Appendix B Curriculum Vitae

Nathaniel Henning

3849 N Lakewood Ave, Chicago, IL, 60613

651-353-4978

nathaniel.henning@northwestern.edu

Education

PhD   Life Sciences, expected graduation 2022

Northwestern University- Feinberg School of Medicine, Chicago, IL

B.S.   Biology, 2016

Hamline University, Saint Paul, MN

B.A.   Chemistry, 2016

Hamline University, Saint Paul, MN

Research Experience

Driskill Graduate Program (PhD student)   Spring   2017-Present

Monica Laronda, PhD, Northwestern University – Stanley Manne Children's Research Institute, Chicago, IL

Undergraduate Research Technician   Fall 2015 – Spring 2016

Nevin D. Young, PhD University of Minnesota, Saint Paul, MN

REU Research Fellow   Summer 2015

Richard Vierstra, PhD, University of Wisconsin- Madison, Madison, WI

Project title: "Developing Reverse Genetic Tools to Study SUMOylation in *Zea mays"*

Hamline University SCUR Research Fellow   Summer 2014

Nevin D. Young, PhD, through Hamline at the University of Minnesota, St Paul, MN

Project title: "Characterization of CP43 and PIF1 GWAS Selected Candidate Genes in *Medicago truncatula* and their Contribution to Rhizobia Symbiosis and Phenotypes of Interest Using an hpRNA Based RNAi Platform"

Honors, Grants, and Awards

Illinois Symposium on Reproductive Sciences Poster Award   2021

Illinois Society for the Study of Reproduction

Illinois Society for the Prevention of Blindness Research Grant   2020-2021

$3,500 Grant, Duration: Two years

Illinois Society for the Prevention of Blindness, Chicago, IL

Marie J.C. Hendrix Outstanding Graduate Student Award   2019

$5,000 Award, Duration: One Year

Lurie Children's Hospital, Chicago, IL

Manne Research Institute Training Program Travel Award   2019

$1,500 One-time travel Award

Stanley Manne Research Institute, Chicago, IL

Constance Campbell Travel Award   2018

$500 One-time Travel Award

Northwestern University, Center for Reproductive Sciences, Chicago, IL

Presidential Poster Presentation Award   2018

Endocrine Society

Teaching/Mentorship Experience

Emerging Research in Reproductive Science and Medicine TA   2019, 2022

Northwestern University, Masters in Reproductive Sciences Program

DGP STAMP Mentor for first year students   2019

Northwestern University, Driskill Graduate program

Outreach

Lurie Children's Hospital Research Fund Ball   2019
Stanley Manne Research Institute, Chicago, IL

Fertility & Hormone Preservation & Restoration Annual Luncheon   2019
Lurie Children's Hospital Fertility & Hormone Preservation & Restoration Program, Chicago, IL

Society for the Study of Reproduction Volunteer   2019
Society for the Study of Reproduction Conference, San Jose, CA

March for Science Booth Volunteer   2017
Northwestern University, Laronda Lab

Presentations

National/International

1. "Defining the contributions of the matrisome to the physical properties of the bovine ovary to support the design of an engineered ovarian environment;" TERMIS World Congress, Maastricht, Netherlands, 2021.

Poster Presentation

2. "Mapping the physical properties and the contributions of matrisome proteins to ovarian folliculogenesis within an engineered microenvironment;" Biofabrication Conference, Adelaide, Australia, 2021.

Poster Presentation

3. "Investigating the influence of physical properties and matrisome composition of the ovarian microenvironment on folliculogenesis" Oncofertility Consortium Conference, Chicago, 2019.

The Oncofertility consortium is a unique meeting covering oncofertility topics with a focus on trainees, and also expert lead talks given by both clinicians, bench scientists, and patient advocates.

Poster Presentation

4. "Spatially mapping matrisome protein abundance across ovarian compartments: identification of glycoproteins that may affect folliculogenesis" Society for the Study of Reproduction Conference, San Jose, 2019

Poster Presentation, Funded by Travel Award.

5. "Mapping Extracellular Matrix Protein Composition Across Ovarian Compartments and Remodeling during Folliculogenesis" Society for the Study of Reproduction Conference, New Orleans, 2018.

Selected for Flash Talk and Poster Presentation, *Funded by Travel Award*

6. "Mapping Extracellular Matrix Protein Composition Across Ovarian Compartments and Remodeling during Folliculogenesis" Endocrine Society Conference, Chicago, 2018.

Poster Presentation, ***Presidential Poster Prize Winner***

7. "Defining and Mapping the Distribution of the Extracellular Matrix in the Porcine Ovary" Oncofertility Consortium Conference, Chicago, 2017.

Poster Presentation

8. "Characterization of CP43 and PIF1 GWAS Selected Candidate Genes in Medicago truncatula and their Contribution to Rhizobia Symbiosis and Phenotypes of Interest Using an hpRNA Based RNAi Platform"; National Conference for Undergraduate Research, Spokane, WA, 2015.

Poster Presentation

Local

9. "Assessing the contributions of the matrisome to the physical properties of the bovine ovary and integration into an engineered ovarian environment;" Illinois Symposium on Reproductive Sciences, Urbana-Champaign, Illinois, 2021

Poster Presentation, ***First place Poster Award***

10. "Investigating the influence of physical properties and matrisome composition of the ovarian microenvironment on folliculogenesis" Reproductive Research Updates – Center for Reproductive Sciences, Northwestern University, 2019.

Advertised Hour-long Talk.

11. "Investigating the influence of physical properties and matrisome composition of the ovarian microenvironment on folliculogenesis" Illinois Symposium on Reproductive Sciences, Chicago, 2019

Local trainee run symposium that focuses on providing trainees opportunities to present their research in reproductive sciences.

Podium talk

12. "Mapping the Porcine Ovarian Matrisome and Defining Geographical Differences" Reproductive Research Updates – Center for Reproductive Sciences, Northwestern University, 2019.

Advertised Hour-long Talk.

13. "Mapping Extracellular Matrix Protein Composition Across Ovarian Compartments and Remodeling during Folliculogenesis" Illinois Symposium on Reproductive Sciences, Carbondale, 2018

14. "Defining Compartmental Differences in the Ovarian Matrisome" Reproductive Science and Medicine Summit, Chicago, 2018.

15**. "**Mapping Extracellular Matrix Protein Composition Across Ovarian Compartments and Remodeling during Folliculogenesis" Reproductive Research Updates – Center for Reproductive Sciences, Northwestern University, 2018.

Advertised Hour-long Talk.

16. "Differentiation and Characterization of Granulosa-like cells derived from iPSCs" Poster Presentation at the Regenerative Biology and Stem Cells Retreat, Chicago, 2017

Publications:

1. **N Henning**, LeDuc, R.D., Even, K.A. *et al.* Proteomic analyses of decellularized porcine ovaries identified new matrisome proteins and spatial differences across and within ovarian compartments. *Scientific Reports* **9,** 20001 (2019). https://doi.org/10.1038/s41598-019-56454-3

Altmetric (2/24/2022): 92, 97th percentile of articles, 23 Citations, FCR 5.18, RCR 2.21

2. **N Henning**, Monica M. Laronda. The matrisome contributes to the increased rigidity of the bovine ovarian cortex and provides a source of new bioengineering tools to investigate ovarian biology. *bioRxiv* 2021.10.06.463107; https://doi.org/10.1101/2021.10.06.463107.

*Pre-Print – in revisions

3. **N Henning**, Jakus AE, Laronda MM. Building Organs Using Tissue-Specific Microenvironments: Perspectives from a Bioprosthetic Ovary. *Trends Biotechnol*. 2021 Feb 13:S0167-7799(21)00014-7. doi: 10.1016/j.tibtech.2021.01.008.

Altmetric (2/24/2022): 2, 50th percentile of articles, 1 Citation

4. M. Bhattachryya, P Madden, **N Henning,** S Gregory, M Aid, AJ. Martinot, DH Barouch, P Penaloza-MacMaster. Regulation of CD4 T cells and their effects on immunopathological inflammation following viral infection. *Immunology. 2017;152(2):328-343. doi:10.1111/imm.12771*

Altmetric (2/24/2022): 4, 67th percentile of articles, 10 Citations, FCR 1.53, RCR 0.35